Cellular reproduction and extracellular polymer formation in the development of biofilms
by Michael Gerald Trulear

A thesis submitted in partial fulfillment of the requirements for the degree of Doctor of Philosophy in Civil Engineering
Montana State University

Abstract:
Bacteria exhibit a tendency for attaching to and colonizing surfaces which are submerged in aquatic environments. Attachment is mediated by extracellular polymer material which is formed by the bacteria and extends from the cell to the attachment surface. The attached cells reproduce and form additional extracellular polymer increasing the mass of the deposit. The cellular-extracellular matrix is termed a biofilm.

The purpose of this study was to investigate the kinetics and stoichiometry of cellular reproduction and extracellular formation in the development of biofilms.

Experiments were conducted using pure cultures of Ps. aeruginosa with glucose and inorganic nutrients providing the necessary requirements for microbial growth. Both attached growth biofilm reactors ' and dispersed growth chemostat reactors were used as experimental systems.

Rate and stoichiometric expressions which describe cellular re-' production and extracellular polymer formation in biofilms are presented. These expressions are compared with corresponding expressions describing the same processes in dispersed growth chemostat reactors.

Results indicate that the rate and extent of cellular reproduction and extracellular polymer formation depend on Ps.. aeruginosa growth rate. At low growth rate, extracellular polymer formation exceeds cellular reproduction, whereas at high growth rate, the rate and extent of cellular reproduction exceed extracellular polymer formation.

CELLULAR REPRODUCTION AND EXTRACELLULAR POLYMER FORMATION IN THE DEVELOPMENT OF BIOFILMS

by

Michael Gerald Trulear

A thesis submitted in partial fulfillment
of the requirements for the degree

of

Doctor of Philosophy

in

Civil Engineering

MONTANA STATE UNIVERSITY
Bozeman, Montana

May 1983

APPROVAL

of a thesis submitted by

Michael G. Trulear

This thesis has been read by each member of the thesis committee and has been found to be satisfactory regarding content, English usage, format, citations, bibliographic style, and consistency, and is ready for submission to the College of Graduate Studies.

30 April 1983
Date

W. G. Chanaclin
Chairperson, Graduate Committee

Approved for the Major Department

May 1, 1983
Date

Theodore J. Williams
Head, Major Department

Approved for the College of Graduate Studies

5-17-83
Date

Graduate Dean

STATEMENT OF PERMISSION TO USE

In presenting this thesis in partial fulfillment of the requirements for a doctoral degree at Montana State University, I agree that the Library shall make it available to borrowers under rules of the Library. I further agree that copying of this thesis is allowable only for scholarly purposes, consistent with "fair use" as prescribed in the U.S. Copyright Law. Requests for extensive copying or reproduction of this thesis should be referred to University Microfilms International, 300 North Zeeb Road, Ann Arbor, Michigan 48106, to whom I have granted "the exclusive right to reproduce and distribute copies of the dissertation in and from microfilm and the right to reproduce and distribute by abstract in any format."

Signature Michael G. Trenbar

Date May 12, 1983

ACKNOWLEDGMENTS

The author is particularly indebted to the following:

Bill Characklis and family for providing the love, support, guidance, and enthusiasm which made my graduate experience a particularly productive and enjoyable period of my life.

Ted Williams for his concern, advice, and outstanding administrative qualities.

Gordon McFeters for serving on my thesis committee and for his contributions to my graduate program.

The "slime gang" for being the best group of people a person could ever hope to work with.

Ginger Bruvold for diligently typing this manuscript and acting as my long distance personal secretary.

The people in the Civil Engineering Department whom I have not mentioned but who made my stay in Bozeman a thoroughly enjoyable one.

Ed Teft and Calgon Corporation for providing financial support through the Calgon Graduate Research Fellowship.

TABLE OF CONTENTS

TABLE OF CONTENTS--Continued

TABLE OF CONTENTS--Continued

LIST OF TABLES

LIST OF FIGURES

LIST OF FIGURES--Continued

LIST OF ELECTRON PHOTOMICROGRAPHS

ABSTRACT

Bacteria exhibit a tendency for attaching to and colonizing surfaces which are submerged in aquatic environments. Attachment is mediated by extracellular polymer material which is formed by the bacteria and extends from the cell to the attachment surface. The attached cells reproduce and form additional extracellular polymer increasing the mass of the deposit. The cellular-extracellular matrix is termed a biofilm.

The purpose of this study was to investigate the kinetics and stoichiometry of cellular reproduction and extracellular formation in the development of biofilms.

Experiments were conducted using pure cultures of Ps. aeruginosa with glucose and inorganic nutrients providing the necessary requirements for microbial growth. Both attached growth biofilm reactors and dispersed growth chemostat reactors were used as experimental systems.

Rate and stoichiometric expressions which describe cellular reproduction and extracellular polymer formation in biofilms are presented. These expressions are compared with corresponding expressions describing the same processes in dispersed growth chemostat reactors.

Results indicate that the rate and extent of cellular reproduction and extracellular polymer formation depend on Ps. aeruginosa growth rate. At low growth rate, extracellular polymer formation exceeds cellular reproduction, whereas at high growth rate, the rate and extent of cellular reproduction exceed extracellular polymer formation.

INTRODUCTION

Microorganisms, primarily bacteria, exhibit a dramatic tendency for attaching to and colonizing surfaces which are submerged in aquatic environments. Attachment is mediated by means of extracellular polymer fibers, primarily polysaccharidic in composition, which are produced by the cell and extend from the cell to form a tangled matrix termed a glycocalyx (Costerton et al., 1978). The attached cells reproduce and form additional glycocalyx material. The microorganism-glycocalyx consortium is termed a biofilm.

Biofilms have been used beneficially by engineers for many years as exemplified by fixed-film wastewater treatment processes (e.g., trickling filters and rotating biological contactors; Grady, 1982). Biofilms also play a major positive role in stream purification processes. In fact, microbial activity in natural waters has been found predominantly at surfaces (Marshall, 1976; Geesey et al., 1978; Geesey, 1982). However, biofilms can be quite troublesome in many engineering systems. For example, biofilms in water distribution and heat transfer equipment can cause substantial energy losses resulting from increased fluid frictional resistance and increased heat transfer resistance (Picologlou et al., 1979; Characklis et al., 1981). Biofilms can also play a significant role in the initiation and perpetuation of conditions favorable for corrosion processes (Iverson, 1972).

In the last decade, biofilms have been recognized as major

determinants in various animal and human disease states. Examples of biofilm-associated diseases include cystic fibrosis, pneumonia, intestinal disorders, and dental caries (Costerton et al., 1981).

The Problem

The most common method of controlling biofilm development in engineering systems is through periodic chlorination. In disease states, the method of control commonly involves the application of antibiotics. In both systems, the effectiveness of the control procedures can be significantly reduced by the protective and highly adsorptive nature of the extracellular glycocalyx material (Costerton and Geesey, 1979) which in some biofilm systems can account for up to 90% of the total biofilm volume (Characklis, 1981). To further complicate control methods, the concentration at which chlorine and antibiotics can be applied are usually set at relatively low levels due to environmental and ecological considerations in the former and to human physiological considerations in the latter.

A priori, an understanding of the rate and extent of extracellular polymer formation in biofilm systems appears of fundamental importance. Such an understanding is presently lacking. The rate and extent of biofilm extracellular polymer formation have not been measured. This investigation stems from the apparent need for a fundamental understanding of the rate and stoichiometry of extracellular polymer formation in biofilms.

Research Goal

The goal of this research was to obtain a fundamental understanding of the rate and stoichiometry of polymer formation in biofilms. To accomplish this goal, the following objectives and tasks were established.

Objectives

1. Determine the kinetics and stoichiometry of cellular reproduction and extracellular polymer formation in dispersed growth chemostat reactors and in attached growth biofilm reactors.
2. Determine the applicability of kinetics and stoichiometry determined from a dispersed growth environment for an attached growth environment.

Tasks

1. Determine rate and stoichiometric expressions which describe cellular reproduction and extracellular polymer formation by Pseudomonas aeruginosa in pure culture chemostat and biofilm reactors.
2. Develop and test mathematical models which describe Pseudomonas aeruginosa cellular reproduction and extracellular polymer formation in pure culture chemostat and biofilm reactors.

LITERATURE REVIEW

Cellular Reproduction and Extracellular Polymer Formation

The individual processes of cellular reproduction and extracellular polymer formation have not been quantitatively studied in biofilms. Previous biofilm studies (Kornegay and Andrews, 1967; Lamotta, 1976 a; Zelver, 1979; Trulear and Characklis, 1982) have investigated "total" biofilm production, however these studies did not distinguish between the fundamental processes of reproduction and polymer formation which occur within the biofilm.

This section will discuss literature concerning cellular reproduction and extracellular polymer formation. The literature reviewed is necessarily from dispersed growth studies since results concerning biofilm cellular reproduction and extracellular polymer formation are not available.

Cellular Reproduction

Bacterial cells reproduce by binary fission. For a given set of environmental conditions (e.g., temperature and pH) the rate of reproduction due to binary fission depends on the concentration of nutrients which are available for growth. If all required nutrients are supplied in excess except one, the growth limiting nutrient, the rate of cellular reproduction can be empirically related to the concentration of the limiting nutrient. The equation most widely used to describe this

relation was originally proposed by Monod (1949) to describe the growth of Escherichia coli on glucose. The Monod equation is written as follows:

$$\mu = \frac{\mu_{max}\, s}{k_s + s} \qquad (1)$$

where

μ	=	cellular specific growth rate	(t^{-1})
μ_{max}	=	maximum cellular specific growth rate	(t^{-1})
s	=	concentration of the limiting nutrient, commonly referred to as the substrate	$(M_s L^{-3})$
k_s	=	saturation coefficient, numerically equal to the substrate concentration at $\mu = 1/2\ \mu_{max}$	$(M_s L^{-3})$

The maximum specific growth rate, μ_{max}, is a measure of the maximum rate at which an organism can reproduce under saturating conditions of the substrate (Monod, 1949; Stanier et al., 1976). The saturation coefficient, k_s, is a measure of the affinity which an organism's enzymes exhibit for a particular substrate (Monod, 1949; Shehata and Marr, 1971). k_s values can also be indicative of extracellular diffusional resistances (Characklis, 1978; Harremoës, 1978). Typical values of μ_{max} and k_s are given in Table 1.

The hyperbolic form of the Monod equation (Figure 13) is identical to the Michaelis-Menten equation (1913) for enzyme-catalyzed reactions and to the Langmuir adsorption isotherm (1918) describing adsorption kinetics.

TABLE 1

Typical Values for the Maximum Specific Growth Rate, μ_{max}, and the Saturation Constant, k_s.

Bacterial Species	Substrate	μ_{max} (h^{-1})	k_s (mg/l)	Temperature (°C)	Reference
Escherichia coli	glucose	1.35	4.0	37°C	Monod (1949)
Escherichia coli	glucose	0.78	0.1	30°C	Shehata & Marr (1971)
Escherichia coli	glucose	0.53	-	37°C	Clarke et al. (1968)
Pseudomonas aeruginosa	glucose	0.37	2.8	25°C	Dharmarajan (1981)
Pseudomonas sp.	glucose	0.38	2.0	20°C	Jenkins (1980)
Pseudomonas sp.	lactate	0.55	-	28°C	Matin et al. (1976)

Extracellular Polymer Formation

The formation of extracellular polymer has long been recognized as an important process in the normal metabolism of many bacteria. Traditionally, two types of extracellular polymer have been distinguished depending on the spatial association of the polymer with the cell (Brock, 1978). Extracellular polymer which remains in a rather compact layer attached to the cell is referred to as a capsule. Conversely, extracellular polymer which does not exhibit a close association with the cell and can exist as a rather dispersed accumulation is referred to as a slime layer. In recent years with the emergence of an increased level of interest in the development of attached microbial growths (biofilms), the capsule-slime layer component of these deposits has been termed the glycocalyx (Costerton, 1978).

Bacterial extracellular polymers are almost universally composed of polysaccharide subunits, primarily mannans, glucans, and uronic acid (Stainier et al., 1976; Costerton, 1979). The ratio of these subunits and the extent of group substitutions within the subunits can vary widely depending on the type(s) of bacteria present (Geesey, 1981).

Most bacterial extracellular polymers are synthesized at the level of the cell membrane and involve successive transfers of nucleotide-sugar precursors (e.g., UDP-glucose and UDP-galactose) from within the cell via membrane-bound lipid carriers (Stanier et al., 1976; Costerton, 1981). The polysaccharide chain is then assembled by polymerases which are attached to outer portions of the cell membrane.

Extracellular polymer formation is greatest if excess carbon is supplied to cultures which are either nitrogen- or phosphorous-limited.

Several investigators (Tam and Finn, 1977; Williams and Wimpenny, 1977; Mian et al., 1978; Williams, 1978) have used nitrogen limitation to enhance polymer formation in dispersed growth cultures. Characklis and Dydek (1976) found that the amount of biofilm increased with increasing carbon to nitrogen ratio, indicating the importance of extracellular polymer in the overall composition of biofilms.

Numerous equations have been proposed to describe the kinetics of extracellular polymer formation. The majority of these equations are empirical and were originally developed in conjunction with the fermentation industry for the description of various microbial fermentation products. The empirical relation used most widely to describe microbial polymer formation is the equation originally developed by Ludedeking and Piret (1959) to describe the formation of lactic acid by Lactobacillus delbrueckii:

$$R_p = k\mu x + k'x \qquad (2)$$

R_p	=	$k\mu x$	+	$k'x$
rate of polymer formation		rate of growth-associated polymer formation		rate of nongrowth-associated polymer formation

where

R_p	=	rate of extracellular polymer formation	$(M_p L^{-3} t^{-1})$
k	=	growth-associated polymer formation rate coefficient	$(M_p M_x^{-1})$
μ	=	cellular specific growth rate	(t^{-1})
x	=	cell concentration	$(M_x L^{-3})$
k'	=	nongrowth-associated polymer formation rate coefficient	$(M_p M_x^{-1} t^{-1})$

A review of literature concerning extracellular polymer formation by various bacterial species reveals that, depending on the particular organism, only one of three different forms of the Luedeking-Piret equation are applicable:

case (1) : polymer formation is growth- and nongrowth-associated, i.e., $k \neq 0$, $k' \neq 0$

case (2) : polymer formation is growth-associated, i.e., $k \neq 0$, $k' = 0$

case (3) : polymer formation is nongrowth-associated, i.e., $k = 0$, $k' \neq 0$

Table 2 presents a summary of the above cases for different bacterial species.

Few investigators have presented interpretations of the Luedeking-Piret growth- and nongrowth-associated coefficients and, due to the empirical nature of the Luedeking-Piret equation, it is not clear whether interpretations are warranted. Luedeking and Piret (1959) state that for the case of growth- and nongrowth-association observed in their study (the formation of lactic acid by Lactobacillus delbrueckii), "one can speculate that the cell dissimilates glucose to lactic acid in order to obtain energy required to form new bacterial protoplasm, and at the same time does it as a normal metabolic activity irrespective of growth." Roels and Kossen (1978) have generalized the original interpretation by Luedeking and Piret and conclude that the growth and nongrowth coefficients are indicative of "energy-pathway" associated product formation. The growth-associated coefficient, k, is related to biosynthetic energy requirements, the nongrowth-associated coefficient,

TABLE 2

Growth Association of Luedeking Piret Polymer Formation Rate Coefficients

Bacterial Species	Polysaccharide Polymer	Growth Association	Reference
Pseudomonas aeruginosa	-	growth and nongrowth	Mian *et al.* (1978)
Xanthamonas campestris	xanthan gum	growth and nongrowth	Moraine and Rogovin (1971), results reprinted in Weiss and Ollis (1980)
Azotobacter vinelandii	alginic acid	growth	Deavin *et al.* (1977), results reprinted in Klimek and Ollis (1980)
Pseudomonas sp.	-	nongrowth	Williams (1974), results reprinted in Klimek and Ollis (1980)
Methylomonas mucosa	-	nongrowth	Tam and Finn (1977)

k', is related to maintenance energy requirements.

Biofilm Accumulation

The accumulation of biofilm on a surface exposed to a fluid flow is the net result of several processes including the following:

1. Adsorption of organic molecules to the surface
2. Transport of microbial cells to the surface
3. Microorganism attachment to the surface
4. Microbial metabolism (cellular reproduction and extracellular polymer formation) at the surface resulting in the production of biofilm
5. Partial detachment of the biofilm due to fluid shear stress

Biofilm accumulation is not a sequence of the above rate processes occurring individually but rather the net result of these processes occurring simultaneously. At specific times in the overall development, certain rate processes contribute more than others.

Adsorption of Organic Molecules to the Surface

Adsorption of an organic monolayer occurs within minutes after exposure of an initially "clean" surface to an aqueous environment containing dissolved organics. This adsorption changes the properties of the wetted surface and actually conditions the surface for subsequent attachment and colonization (Loeb and Neihof, 1975; Baier and Depalma, 1977). The organic molecules involved in this initial adsorption are usually negatively charged (polyanionic) polysaccharides or glycoproteins (Baier, 1975).

Transport of Microbial Cells to the Surface

The transport of microbial cells from the bulk to the surface depends on the fluid flow regime (Characklis, 1981). In turbulent flow, turbulent downsweeps are suspected to be the primary transport mechanism. In laminar flow, chemotaxis and sedimentation may be important.

Microorganism Attachment to the Surface

Observations by Zobell (1943), and later by Marshall et al. (1971), on the adhesion of bacterial cells to surfaces suggests the existence of a two-stage adhesion process: 1) reversible adhesion followed by 2) an irreversible adhesion. Reversible adhesion is characterized by an initially weak adhesion of a cell which can still exhibit Brownian motion but is readily removed by mild rinsing. The adhesive forces which hold the cell at the wall during reversible adhesion probably include the following: a) electrostatic, b) London-van der waals, c) interfacial tension, and d) covalent bonding (Characklis, 1981). Conversely, irreversible adhesion is a more permanent bonding to the surface mediated by the production of extracellular polymers, i.e., glycocalyx material (Corpe, 1970; Fletcher and Floodgate, 1973; Marshall, 1976).

Biofilm Production Due to Microbial Metabolism

The attached microbial cells assimilate nutrients from the bulk fluid and through processes of microbial metabolism, reproduce and form additional extracellular polymers. The combined result of these processes is the production of biofilm. The rate and extent of biofilm production depends on the concentration of nutrients in the bulk fluid

and on their subsequent diffusion into the biofilm (Trulear and Characklis, 1982).

Literature concerning biofilm production (Kornegay and Andrews, 1967; Lamotta, 1976a; Zelver, 1979; Trulear and Characklis, 1982) has not distinguished between reproduction and polymer formation processes. Three of these studies (Kornegay and Andrews, 1967; Lamotta, 1976a; Trulear and Characklis, 1982) have developed models to describe biofilm production. However, all three models are based on Monod-type saturation kinetics which treat the biofilm as if it were composed entirely of microorganisms. Kinetic coefficients obtained from these studies are shown in Table 3. Figure 1 depicts the typical experimental progression reported.

The references cited above are only a small fraction of the literature concerning biofilm kinetics. However these references are the only studies which have explicitly studied biofilm production. Other literature on biofilm kinetics (Sanders, 1966; Maier, 1966; Tomlinson and Snaddon, 1966; Sanders et al., 1970; Atkinson and Daoud, 1970; Atkinson and Davies, 1974; Williamson and McCarty, 1976; Lamotta 1976a and 1976b; Harris and Hansford, 1976; Harremoës, 1978; Rittmann and McCarty, 1978; Rittmann and McCarty, 1981) have been primarily concerned with modeling substrate removal. The majority of these studies have also largely ignored the internal structure of the biofilm. To this author's knowledge, only two groups of investigators (Atkinson and co-workers, and Rittmann and McCarty, 1981) have included internal structure in their modeling and only to the extent of recognizing that a certain fraction

TABLE 3

Typical Coefficients from Biofilm Production Models Utilizing Saturation Kinetics

Influent Glucose Concentration, s_i (mg/l)	Glucose Loading Rate, R_L (mg/m^2 min)	Maximum Specific Production Rate, $r_{p_{max}}$ (t^{-1})	Saturation Constant, k_p (mg/l)	Temperature (°C)	Reference
5.8-130.4	1.7-37.2	0.10-0.52	0.5-69.8	30	Trulear and Characklis (1982)
59.2-577.0	37.6-376.0	0.28	121.0	25	Kornegay and Andrews (1967)
2.2-40.5	1.5-27.0	0.19[a]	7.8[a]	22	Lamotta (1976a)

[a] values based on influent glucose concentration

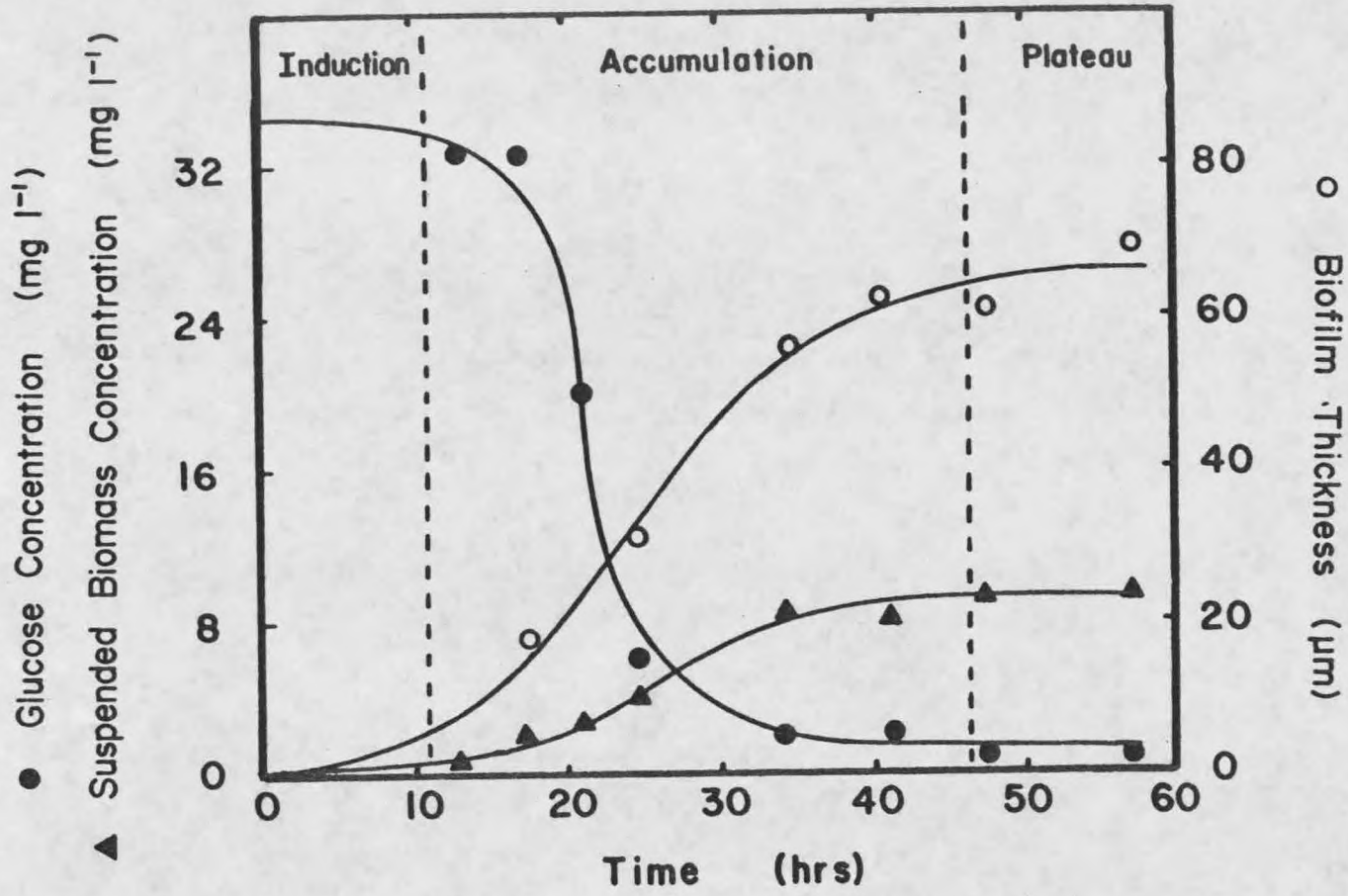

Figure 1. Typical Experimental Progression (From Trulear and Characklis, 1982).

of the biofilm, the cellular component, is actually responsible for utilizing substrate.

Biofilm Detachment

At any point in the development of a biofilm, external portions of biofilm are sheared away into the fluid flow. Detachment due to fluid shear is a continuous removal process and is highly dependent on hydrodynamic conditions. Trulear and Characklis (1982) have investigated the rate of biofilm detachment due to fluid shear and report that detachment rate increases with increasing biofilm mass and with increasing fluid velocity.

In addition to shearing, sloughing can also significantly contribute to biofilm detachment. Sloughing refers to a random, massive removal of biofilm attributed to nutrient/oxygen depletion deep within biofilms (Howell and Atkinson, 1976). Sloughing is more frequently witnessed with thicker, less dense biofilms which develop under low fluid shear conditions.

Biofilm Properties

Physical properties of biofilms which have been measured include biofilm thickness and biofilm mass density. In turbulent flow systems, wet thickness (Th) seldom exceeds 1000 μm and is usually considerably less (Zelver, 1979; Trulear and Characklis, 1982). Biofilm mass density (ρ) reflects dry mass per unit wet biofilm volume and measured values in turbulent flow systems range from 10 to 65 mg/cm^3 (Trulear and Characklis, 1982).

Chemical properties of biofilms which have been measured include inorganic composition (reviewed by Characklis, 1981), protein to polysaccharide ratio (Bryers, 1980), and carbon to nitrogen and carbon to phosphorous ratios (reviewed by Characklis, 1981).

Biological properties of biofilms which have been measured indicate that a wide variety of microorganisms, primarily different species of bacteria and algae, are found in naturally occurring biofilms (Haack and McFeters, 1982). There is evidence which suggests organism succession occurs so that at different stages of biofilm development, different groups of microorganisms may predominate (Marshall, 1976; Corpe, 1978).

The available information on biofilm structure suggest that biofilms may be primarily composed of extracellular polymer material (glycocalyx) and that only a small fraction of the biofilm volume is composed of cellular material (Characklis 1981). Unfortunately, the majority of the evidence supporting this assertion is based on electron microscope photomicrographs (Fletcher and Floodgate, 1973; Costerton, 1981). Due to the extremely high degree of biofilm hydration (85-96% water according to Characklis, 1981) interpretations from observations using electron microscopy must be viewed with caution (Geesey, 1982).

Pseudomonas aeruginosa

Ps. aeruginosa is a polymer-forming bacterium which is ubiquitous in nature and is the cause of many infections and disease states (e.g., cystic fibrosis and various bladder infections) in humans (Costerton, 1979). The primary mode of growth of Ps. aeruginosa in nature and

disease is in polymer-enclosed microcolonies attached to a wide variety of surfaces. The polymer-enclosed, attached mode of growth purportedly protects Ps. aeruginosa (and other biofilm organisms) from the bactericidal activity of bacteriophages and amoebae which are so numerous in natural systems and from antibiotics and host defense mechanisms in diseased systems (Costerton, 1979).

Ps. aeruginosa can be considered a classic biofilm organism and for this reason is the bacterial species used in this study.

Relevant characteristics describing Ps. aeruginosa are as follows:

a) gram stain: negative (Buchanan et al., 1974)

b) morphology: rod shaped, typically 0.5 - 0.8 μm by 1.5 - 3.0 μm (Buchanan et al., 1974)

c) metabolism: chemoorganotroph (Buchanan et al., 1974)

d) respiration: strict aerobe (Buchanan et al., 1974)

e) motility: polar monotrichous flagellation (Buchanan et al., 1974)

f) polymer composition: primarily mannuronic and glucuronic acids (Evans and Linker 1973, Mian et al., 1978)

EXPERIMENTAL METHODS

Experimental Systems

Chemostat and annular reactor (AR) systems were used for this research. Components of the chemostat system include four chemostat reactors, sterile substrate feed apparatus, temperature control, and air supply. Components of the annular reactor system include two AR's, sterile dilution water and substrate feed apparatus, temperature control, and air supply. Figures 2 and 3 are schematic diagrams of the chemostat and AR systems.

Chemostat System

Chemostats. The chemostats were 1000 cm^3 Berzelius Pyrex beakers equipped with side arms and rubber stopppers. Figure 4 illustrates details of the chemostats. Stainless steel baffles and magnetic stirring disks provided complete mixing of the liquid solution. A polypropylene scraping disk in each chemostat provided a method of removing attached microorganisms from the inner surfaces of the glass to prevent wall growth. Anti-backflow cylinders on the influent and effluent lines were used to prevent contamination of the substrate feed solution and chemostat due to the backflow of microorganisms. Table 4 presents relevant characteristics and dimensions of the chemostats.

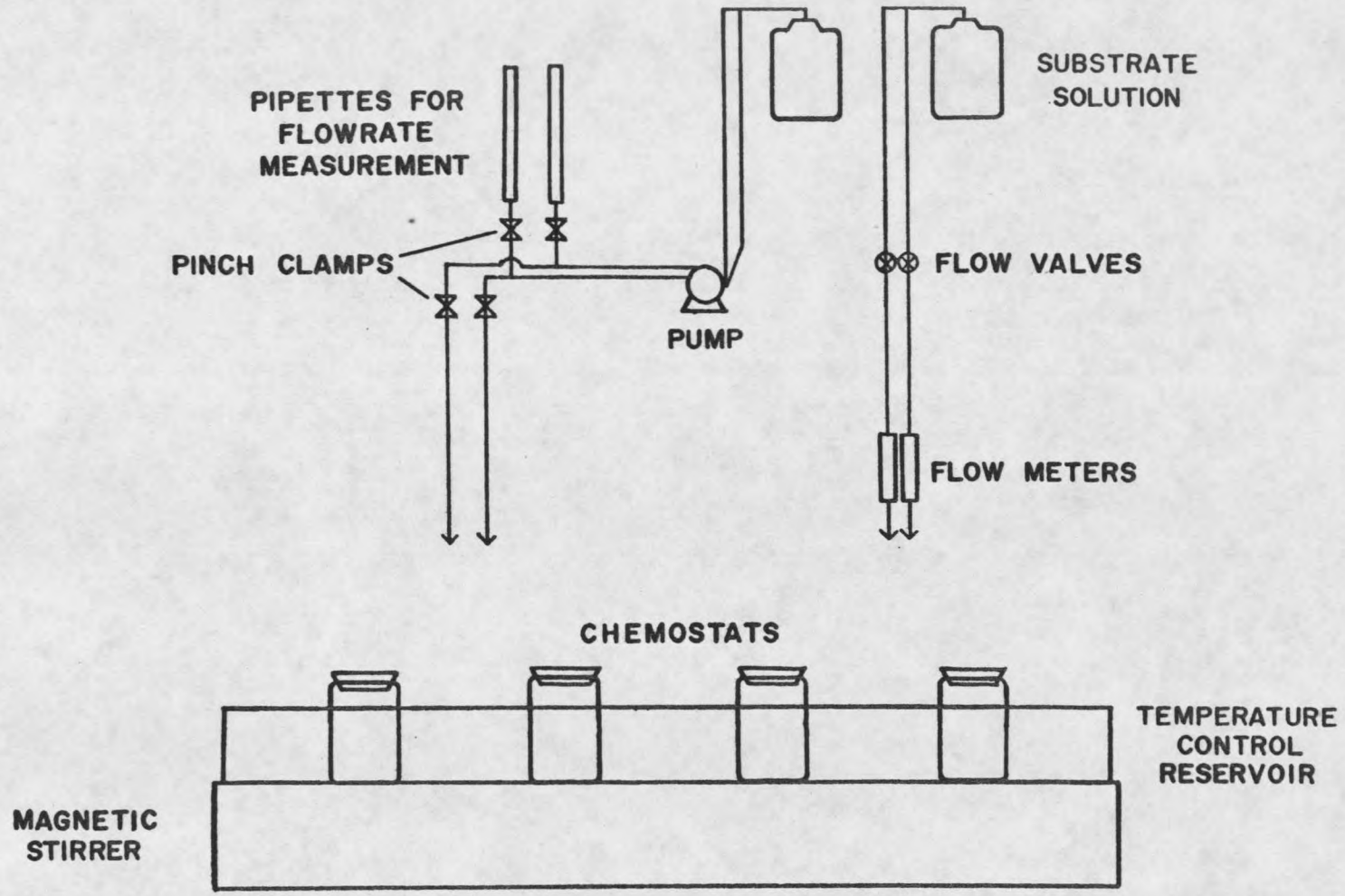

Figure 2. Schematic Diagram of Chemostat System.

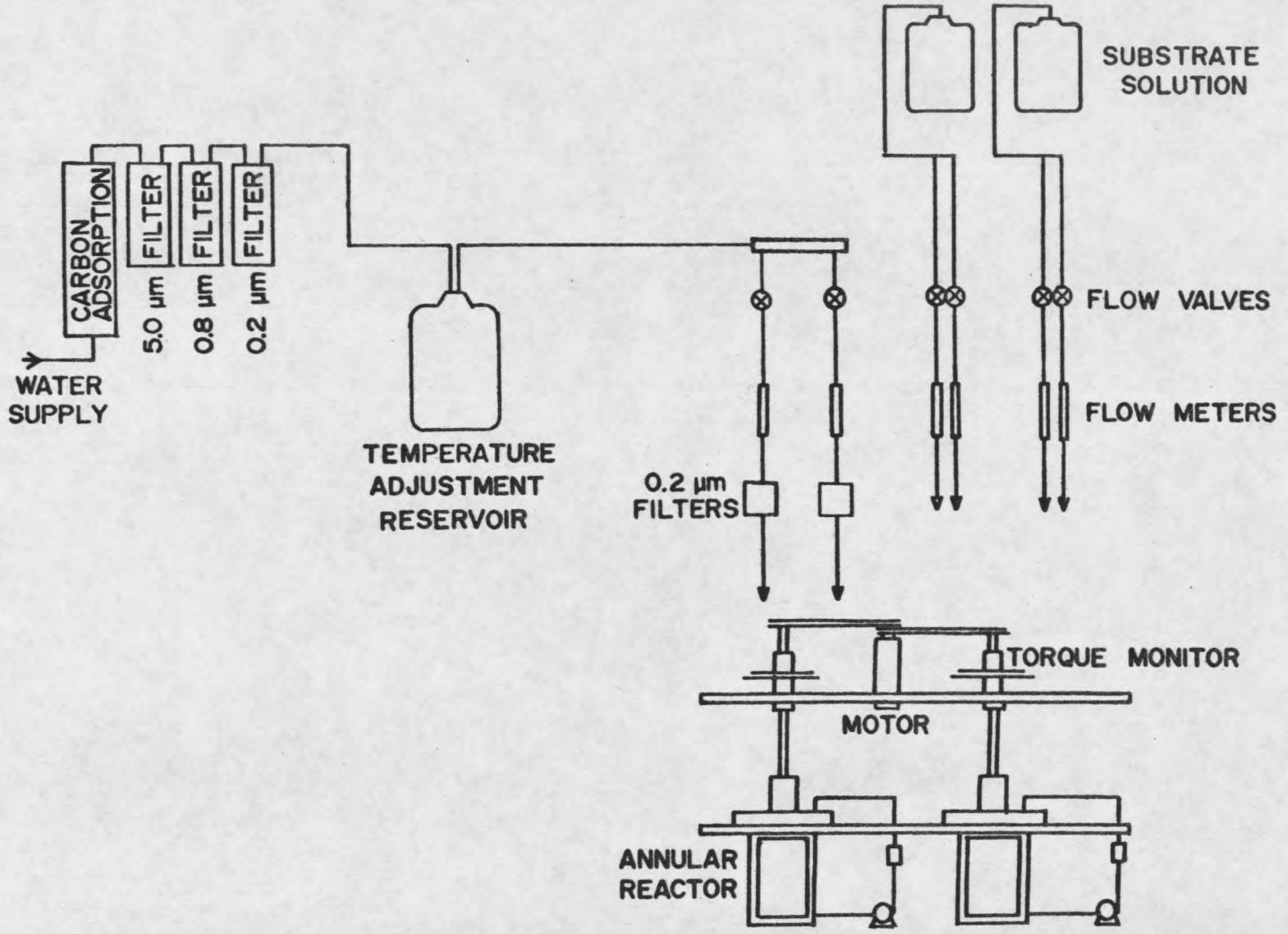

Figure 3. Schematic Diagram of Annular Reactor System.

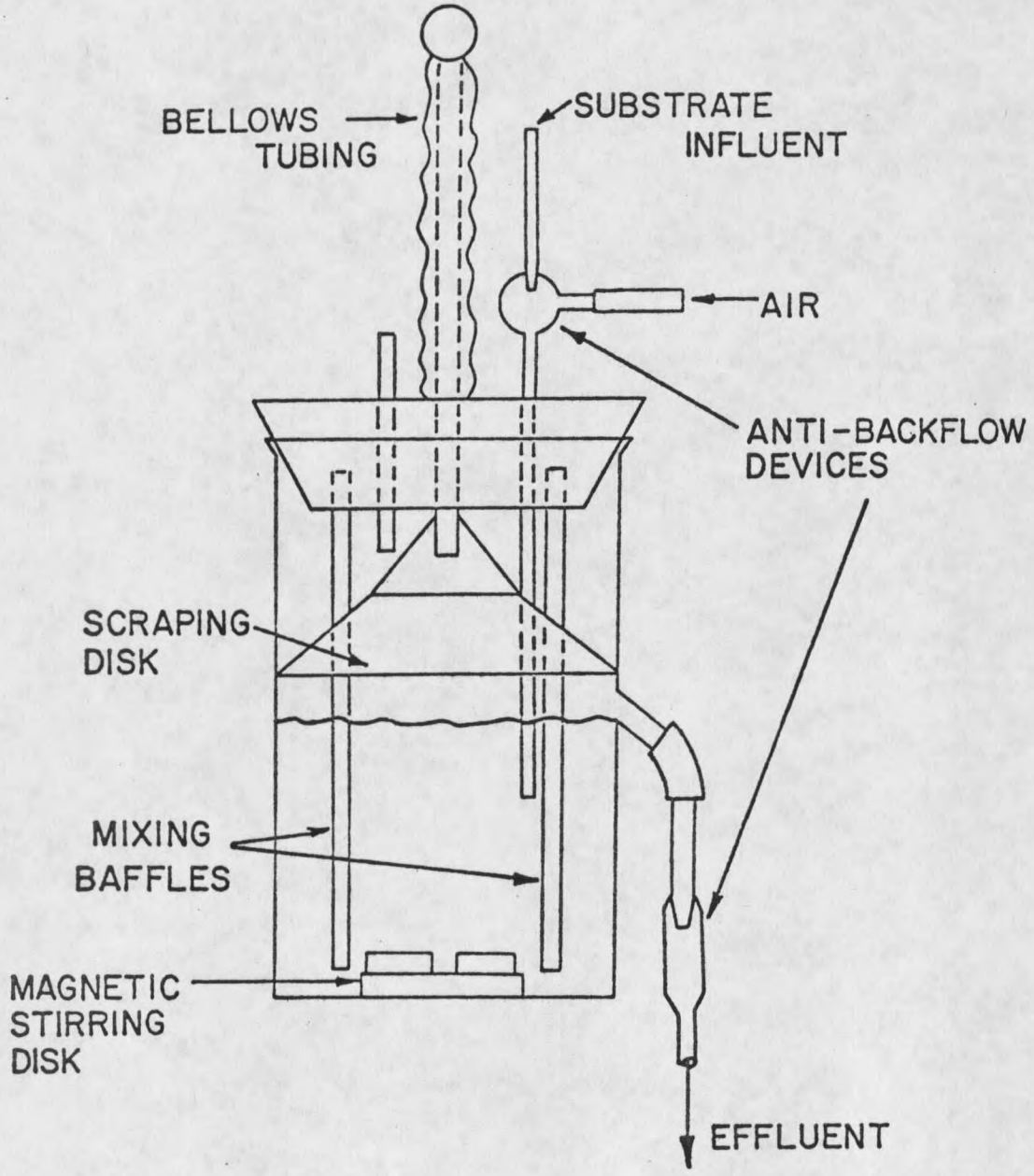

Figure 4. Chemostat Reactor.

TABLE 4

Relevant Characteristics and Dimensions of

The Chemostat Reactors

Liquid Volume	500 cm^3
Height (scraping disk plunger not included)	18.5 cm^2
Diameter	8.8 cm
Dilution Rate	0.025 - 0.40 h^{-1}
Substrate Solution Volumetric Flowrate	0.21 - 3.33 cm^3/min
Mean Residence Time	40.0 - 2.5 h

Substrate feed. Sterile substrate solution was continuously fed to the chemostats by gravity flow for flowrates less than 1.0 cm^3/min or by a peristaltic pump (Buchler Instruments Co., Fort Lee, NJ, Model No. 2-6100) for flowrates greater than 1.0 cm^3/min. Gravity flowrates were controlled to within ±0.05 cm^3/min of the desired flowrate with Dial-A-Flo@ valves (Sorenson Research Co., Salt Lake City, Utah, Cat. No. DAF-30) and monitored with in-line flow meters (Gilmont Instruments Inc., Great Neck, NY, Size No. 11). Pumped flowrates were controlled to within ±0.05 cm^3/min of the desired flowrate and monitored with in-line 5 cm^3 pipettes.

Temperature. Chemostat temperature was controlled at 25 ± 1°C by a temperature controller (Yellow Springs Instrument Co., Yellow Springs, Ohio, Model No. 74) activating a 120 volt immersion heater. The heater and the temperature controller thermister were both located in the chemostat temperature control reservoir.

Air supply. Chemostat liquid solutions were continuously aerated (approximately 0.14 m^3/hr) with filtered laboratory air fed into the reactors through the influent anti-backflow cylinders.

Annular Reactor System

Annular reactors. The AR's were constructed of acrylic plastic and consist of two concentric cylinders, a stationary outer cylinder and a rotating inner cylinder. Figure 5 illustrates details of the reactors. Rotational velocity was controlled by a fractional horsepower gear motor (Model No. NSH-11D3 with Series 200 Speed Controller,

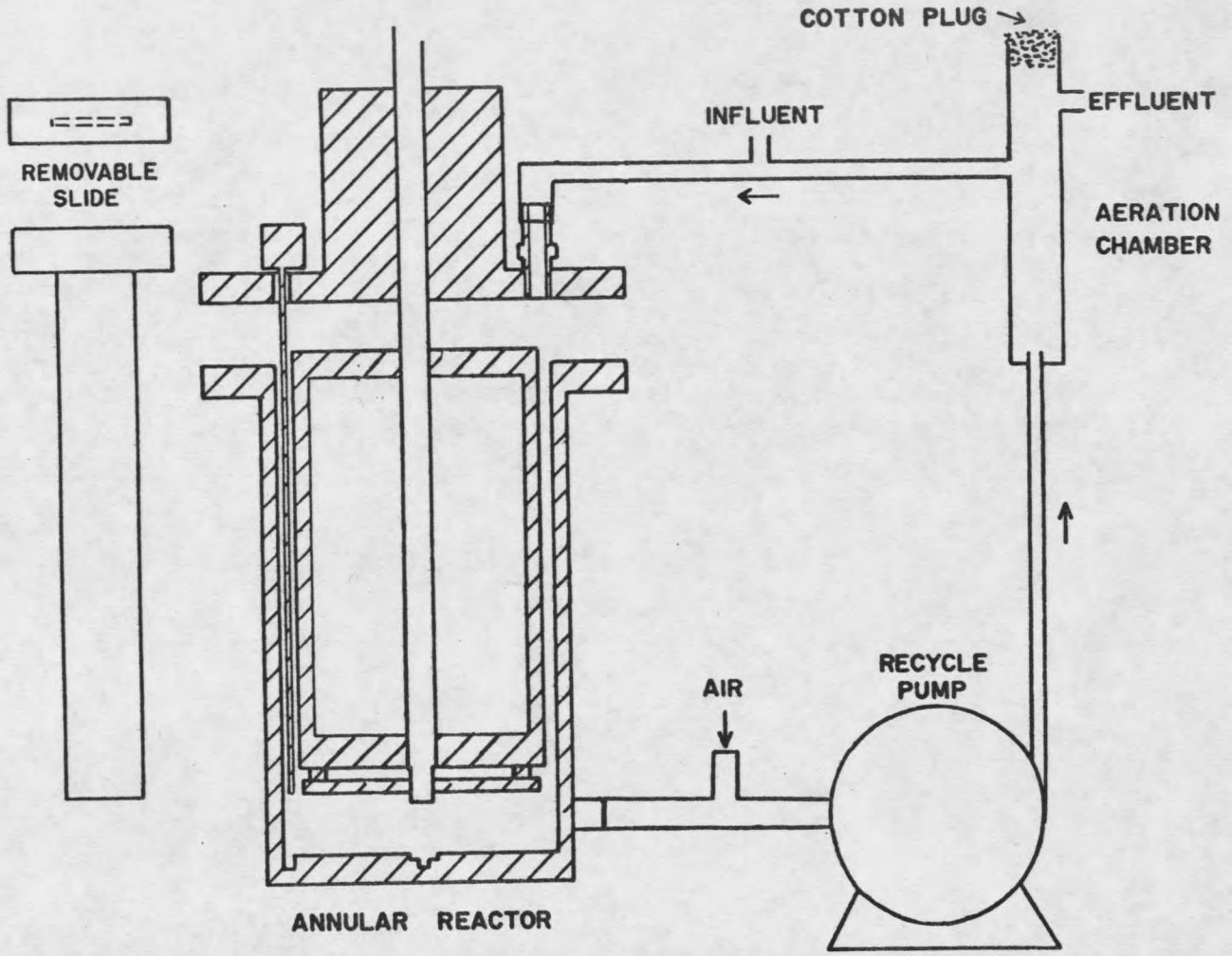

Figure 5. Annular Reactor.

Bodine Electric Co., Chicago, IL) and continuously monitored by a tachometer/torque transducer unit (submitted for United States Patent, Patent Application Serial No. 388,972) mounted on the shaft between the rotating cylinder and the motor drive pulley assembly. The tachometer/torque transducer unit also continuously monitored changes in fluid frictional resistance caused by biofilm development. Rotational velocity and torque were continuously displayed and recorded by an Apple Computer-CRT monitor system (Apple Computer Inc., Cupertino, CA, Model II Plus, and Montgomery Ward, Chicago, IL, Model No. GGY12310-A). Each AR contained four thin removable slides which were used for biofilm sampling and thickness measurements. The slides fit next to the inside walls of the outer cylinders.

The AR's were completely mixed (see mixing study in Appendix B) by virtue of the recirculating action of a peristaltic pump (Cole-Parmer Instrument Co., Chicago IL, Model No. WZ1R057) which was used to pump AR liquid solution from the bottom to the top of each AR at volumetric flowrates approximately 10 times greater than the overall volumetric flowrate through each AR. Table 5 presents relevant characteristics and dimensions of the AR's. Advantages of the AR configuration include the following:

1. No concentration gradients exist in the bulk fluid due to complete mixing. This simplifies mathematical descriptions and sampling.
2. Fluid shear stress at the wall can be varied independently of mean residence time.
3. High surface area to volume ratio.

TABLE 5

Relevant Characteristics and Dimensions

of The Annular Reactors

Reactor	
Liquid Volume	675 cm^3
Total Wetted Surface Area (including aeration chamber and recycle tubing)	1860 cm^2
Inner Cylinder Wetted Surface Area	734 cm^2
Outer Cylinder Wetted Surface Area	920 cm^2
Diameter of Inner Cylinder	10.2 cm
Width of Annular Gap	0.6 cm
Wetted Height of Inner Cylinder	17.8 cm
Wetted Height of Outer Cylinder	20.0 cm
Volumetric Flowrate (dilution water plus substrate solution)	67.5 cm^3/min
Mean residence Time	10 min
Removable Slide	
Wetted Surface Area	38.7 cm^2
Height	24.5 cm
Width	1.9 cm

Dilution water and substrate feed. Treated dilution water was continuously fed into the AR's using reduced tap water line pressure (AW Cash Valve Mfg. Corp., Decatur, IL, Type A-315 Pressure Regulator). Dilution water flowrates were controlled at 66.5 ± 2.5 cm^3/min using needle valves (Whitey Co., Oakland, CA, Model No. ORM2) and monitored with in-line flow meters (Gilmont Instruments Inc., Great Neck, NY, Size No. 13).

Sterile substrate solution was continuously fed to the AR's by gravity flow. Flowrates were controlled at 0.5 ± 0.05 cm^3/min with Dial-A-Flo@ valves (Sorenson Research Co., Salt Lake City, Utah, Cat. No. DAF-30) and monitored with in-line flow meters (Gilmont Instruments Inc., Great Neck, NY, Size No. 11).

Dilution water treatment. Bozeman City tap water was the source of the dilution water. Dilution water treatment consisted of passage through a carbon adsorption column for the removal of residual chlorine and soluble organics followed by filtration using a four filter filtration cascade (5.0 μm, 0.8 μm, 0.2 μm, 0.2 μm; Gelman Sciences, Inc., Ann Arbor, MI, Product Nos., 12585, 12623, 12580, and 12112, respectively) for the removal of particulate and suspended cellular material.

Temperature. Dilution water passed through a Pyrex glass temperature adjustment reservoir (volume 9500 cm^3) before entering the AR's. Reactor temperatures were controlled at 25 ± 1°C by a temperature controller (Yellow Springs Instruments Co., Yellow Springs, OH, Model No. 74) activating a 120 volt immersion heater. The heater was

located in the temperature adjustment reservoir and the temperature controller thermister was located in the dilution water distribution manifold directly upstream of the AR's.

Air supply. AR liquid solutions were continuously aerated with filtered laboratory air (approximately 0.10 m^3/hr) in a small aeration chamber in each AR recycle loop. This effectively maintained AR dissolved oxygen (DO) concentrations near saturation. DO concentrations were monitored by periodically determining the DO concentration of AR effluent samples using a dissolved oxygen probe and meter (Yellow Springs Instrument Co., Yellow Springs, OH, Model No. 54).

Substrate Solution Composition and Preparation

The substrate solution used for the chemostat and AR experiments consisted of glucose as the sole carbon and energy source with micronutrients and phosphate buffer added as shown in Table 6. The concentration of micronutrients are in the same proportions as used by Jenkins et al. (1979). The 0.008 M phosphate buffer used in the chemostat experiments was sufficient to maintain chemostat pH at 7.0 ± 0.1. The 0.004 M phosphate buffer used in the AR experiments was sufficient to maintain AR pH at 6.9 ± 0.1. A lower buffer concentration was used in the AR experiments to conserve buffer, since the mass flow of substrate solution in the AR experiments was significantly greater than in the chemostat experiments (high AR dilution rate).

Substrate solutions were prepared with deionized water and sterilized by autoclaving. In the AR experiments, glucose and micro-

TABLE 6

Substrate Solution Composition

Constituent	Influent Concentration	
	Chemostat	AR
Glucose	10.0 mg/l	10.0 mg/l
NH_4Cl	3.6	3.6
$MgSO_4 \cdot 7H_2O$	1.0	1.0
$CaCl_2$	0.1	0.1
$FeCl_3 \cdot 6H_2O$	0.02	0.02
Vitamin B_{12}	0.05 ug/l	0.05 ug/l
Na_2HPO_4 (Buffer)	0.004 M	0.002 M
KH_2PO_4 (Buffer)	0.004 M	0.002 M

Note: For glucose concentrations other than 10 mg/l the concentration of micronutrients were adjusted proportionally.

AR influent concentration represents influent concentration after combination with dilution water.

nutrient solutions were prepared and fed to the reactors separately. The solutions were combined with dilution water in the AR's to obtain the desired influent concentration.

Experimental Procedures

Cleaning and Sterilization

Standard cleaning and sterilization procedures were established for each experimental system to ensure uniform conditions for experimental start-up.

Chemostat system. The chemostat system cleaning and sterilization procedure was as follows:

1. Following an experiment, disassemble chemostats and soak in a warm soap solution for a minimum of 5 minutes.
2. Scrub all surfaces with a soft bristle brush and rinse thoroughly.
3. Assemble chemostats.
4. Preceding an experiment, prepare substrate feed solutions, fill each chemostat with 300 cm^3 of substrate solution, autoclave feed solutions and chemostats.
5. Flush substrate solution feed lines with a concentrated chlorine solution (approximately 5,000 mg/1) for a minimum of 30 minutes and thoroughly rinse with sterile substrate solution immediately following substrate solution autoclaving.
6. Connect substrate solution feed lines to chemostats and allow solutions to cool prior to initiating experimental start-up.

Annular reactor system. The AR system cleaning and sterilization procedure was as follows:

1. Following an experiment, operate each AR in a batch mode for 10 minutes with an initial chlorine concentration of 1750 mg/l.
2. Disassemble the reactors and soak in a warm soap solution for a minimum of 5 minutes.
3. Scrub all surfaces with a soft bristle brush and rinse.
4. Assemble reactors.
5. Preceding an experiment, remove the dilution water filter capsules located directly downstream of the dilution water flowmeters (see Figure 3 for details) and autoclave.
6. Connect the dilution water feed lines (without the above filter capsules) to the AR's, pour 25 cm^3 of bleach (50,000 mg/l) into the AR temperature adjustment reservoir and start dilution water flow.
7. Connect substrate solution feed lines to the AR's and allow a concentrated chlorine solution (approximately 5,000 mg/l) to flow through the lines into the reactors.
8. After allowing a minimum of 8 hours for residual chlorine to be flushed from the dilution water feed lines, insert the autoclaved filter capsules and continue dilution water flow.
9. Prepare substrate feed solutions and autoclave.
10. Immediately following autoclaving, disconnect chlorine solutions from substrate solution feedlines and replace

with autoclaved substrate solutions.

11. Initiate experimental start-up.

Experimental Start-Up

Chemostats. Experiments were run in duplicate and were started by inoculating each chemostat with a loopful of Ps. aeruginosa and operating the chemostats in a batch mode for 12 hours. This usually resulted in a concentrated suspension of organisms in each chemostat after the 12 hour period. Substrate solution flow was then started at the desired dilution rate. The chemostats were operated in the continuous flow mode for at least six mean residence times prior to sampling to allow the cultures to reach steady state conditions.

Annular reactors. Experiments were run in duplicate and were started by pumping organisms from a steady state chemostat culture of Ps. aeruginosa (chemostat dilution rate = 0.075 h^{-1}) into the AR's for a period of either 12 (experiment 1) or 18 (experiments 2-8) hours. This provided a defined microbial culture for AR initial attachment and colonization. Organism flowrates were maintained at 0.313 ± 0.025 cm^3/min per AR using a peristaltic pump (Buchler Instruments Co., Fort Lee, NJ, Model No. 2-6100). Substrate solution and dilution water were fed into the AR's throughout each experiment, including the 12 or 18 hour initiation period.

Sampling

Chemostats. Samples were collected directly from the effluent anti-backflow cylinders, prepared, and stored as follows:

a) carbon samples - filtered (Nuclepore Corp., Pleasanton, CA, No. 111107, average pore size 0.45 μm) and unfiltered samples (10 cm^3 each) were frozen until analysis.

b) epiflourescence - 5 cm^3 samples were fixed with a filtered formalin solution (Hobbie et al., 1977), homogenized (Dupont Co., Instrument Products, Newtown, CN, Sorvall Omni-Mixer), and refrigerated until analysis.

c) glucose samples - 5 cm^3 samples were filtered (Nuclepore Corp., Pleasanton, CA. No., 111107, average pore size 0.45 μm) and frozen until analysis.

d) suspended solids - 50 cm^3 samples were filtered (Nuclepore Corp., Pleasanton, CA, No. 111107, average pore size 0.45 μm), dried, and weighed.

e) scanning electron-microscopy (SEM) - 25 cm^3 samples were filtered onto Millipore membranes (Millipore Corp., Bedford, MA, No. GVWP 04700, average pore size 0.22 μm), 0.25 cm x 1.8 cm sample sections were cut out of the filters, fixed, and prepared immediately.

f) transmission electron microscopy (TEM) - 100 cm^3 samples were centrifuged into pellets at 3000g for 10 minutes, fixed and prepared immediately.

Annular reactors. Solution samples were collected directly from the AR effluent lines. The samples were prepared and stored as discussed above. Biofilm samples were obtained from the AR removable slides following biofilm thickness measurements. Biofilm was scraped from the slides (except for SEM and TEM samples) using a rubber policeman into 35 cm^3 of filtered (Millipore Corp., Bedford, MA, 0.22 μm, Type GS filter), carbon free (Barnstead Co., Boston, MA, Combination Exchange Cartridge, Cat., No. D8922), deionized water. The resulting solution was homogenized (Dupont Co., Instrument Products, Newtown, CN, Sorvall Omni-Mixer) and subsamples were prepared and stored as follows:

a) carbon samples - 10 cm^3 samples were frozen until analysis.

b) epiflourescence - 5 cm^3 samples were fixed with a filtered formalin solution (Hobbie et al., 1977) and refrigerated until analysis.

c) mass density - 10 cm^3 samples were filtered (Nuclepore Corp., Pleasanton, CA, No. 111107, average pore size 0.45 μm), dried, and weighed.

Biofilm samples for SEM and TEM observation were collected by removing 0.25 cm x 1.8 cm pre-etched sections of unscraped slide, fixing and preparing immediately. Slide sections to be used for TEM samples were precoated with a layer of embedding resin to facilitate thin sectioning.

Experiment Contamination Monitoring

A loopful of reactor solution was streaked on a glucose-micro-nutrient (GMN) agar plate and on a trypticase soy-yeast extract (TSY)

agar plate (see Appendix C for agar recipes) during each experimental sampling period to check for contamination. When contaminant colonies were detected during an experiment, sampling from the contaminated reactor(s) was discontinued. Contaminated chemostat experiments were repeated whereas contaminated AR experiments were repeated only if contamination occurred in the early stages of the experiment.

Analytical Methods

Biofilm Measurements

Biofilm thickness. The thickness of microbial film was determined with the stage micrometer of a microscope (Bausch and Lomb, Inc., Rochester, NY, Dynazoom Microscope) in a method adapted from that of Sanders (1964). A removable slide was withdrawn from an AR and placed on the microscope stage. The 10x objective (100x total magnification) was lowered until the biofilm surface was in focus and the fine adjustment dial setting of the stage micrometer was recorded. The objective was then lowered further until the inert plastic growth surface was in focus (Figure 6). The difference in fine adjustment settings was compared with a calibration curve (Figure 7) and the thickness determined. The reported biofilm thickness was the mean of 3 or 4 measurements along the slide from top to bottom.

Biofilm mass density. The biofilm mass density was determined by filtering a known volume of biofilm through a predried (103°C for 1 hour), preweighed, Nuclepore membrane (Nuclepore Corp., Pleasanton, CA, No. 111107, average pore size 0.45 μm). After filtration the

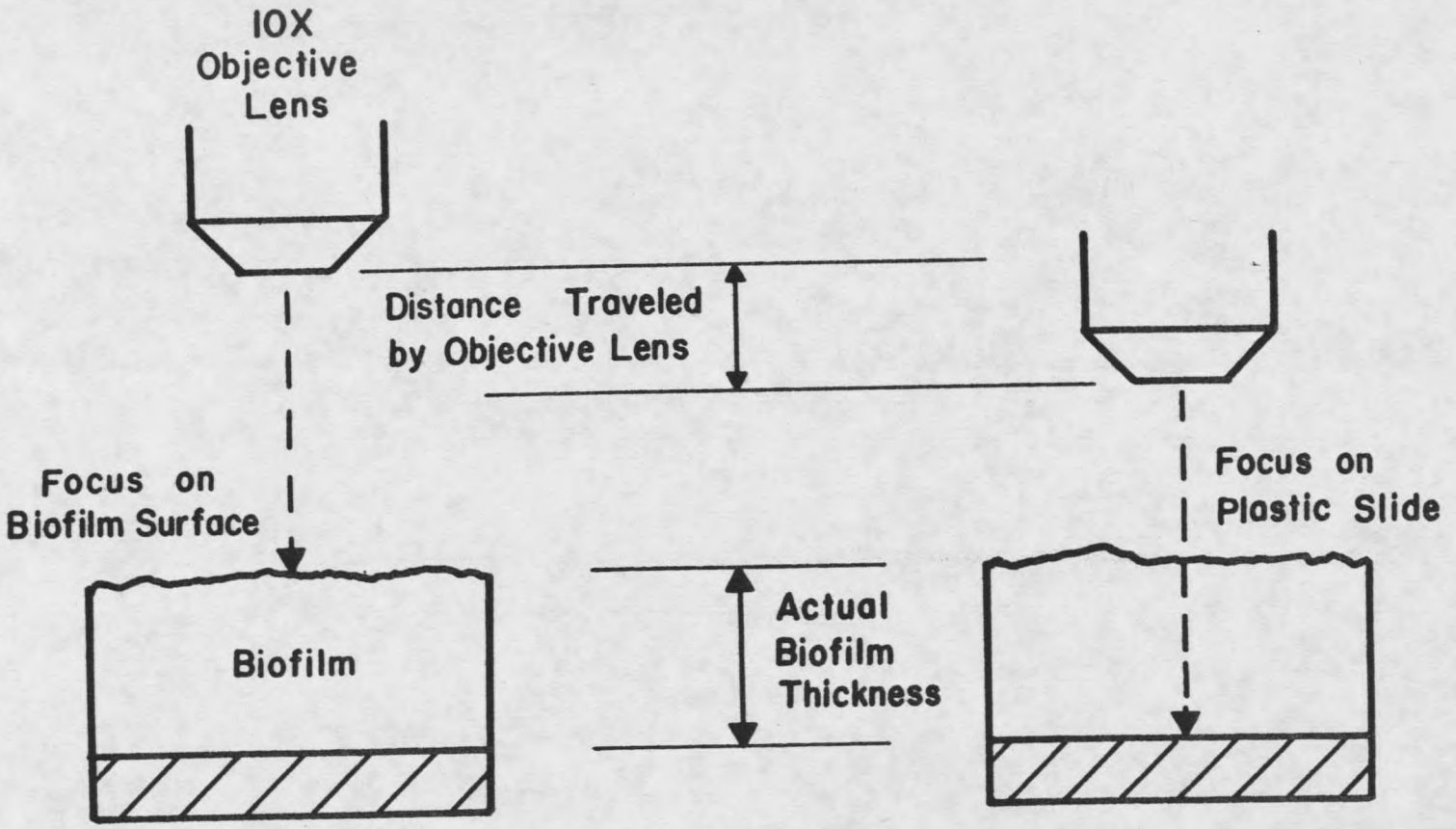

Figure 6. Representation of Biofilm Thickness Measurement.

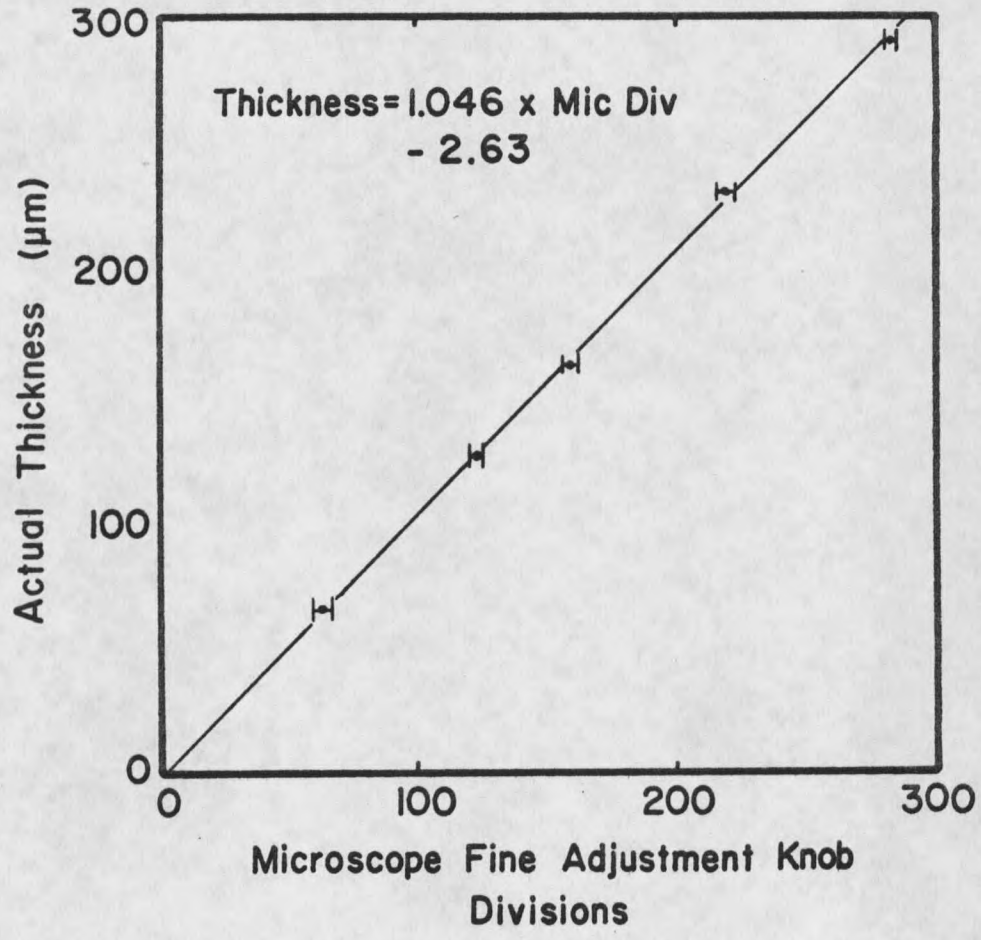

Figure 7. Calibration Curve for Film Thickness Measurement. Each Point is an Average of Repeated Measurements on a Metal Shim With the Actual Thickness Determined With a Vernier Micrometer.

filters were dried at 103°C for 1 hour and weighed (Mettler Instruments Corp., Hightstown, NJ, Type H6 Digital Balance). The biofilm mass density, which has units of dry mass per unit wet volume, was then calculated.

Carbon Measurements

Carbon was used as the basis for the material balance relations which were used in this study. The carbon concentrations which were measured are as follows: glucose carbon, liquid phase cellular carbon, liquid phase polymer carbon, biofilm cellular carbon, and biofilm polymer carbon.

Glucose carbon concentration. Glucose carbon concentration, s, was determined by measuring glucose concentation using a modified version of the Sigma 510 Glucose Analysis Procedure (Sigma Chemical Co., St. Louis, MO) and multiplying the concentration by 0.4 mg glucose carbon/mg glucose. Procedure modifications involved adjusting sample volumes depending on the concentration of glucose anticipated (see Appendix D).

Liquid phase cellular carbon concentration. The concentration of liquid phase cellular carbon, x, was determined by enumerating the total number of cells per reactor liquid volume using epifluorescence microscopy (Leitz Wetzlar, Rockleigh, NJ, Ortholux II Universal Microscope) according to the methods of Hobbie et al. (1977), estimating the average volume per cell in each epi-illuminated microscope field, and multiplying the above quantities by the following values: 1.07

gm cell/cm^3 cell (Doetsch et al., 1973), 0.22 dry cell weight/wet cell weight (Luria, 1960), and 0.5 gm cell carbon/gm cell dry weight (Doetsch et al., 1973, and Luria, 1960).

Liquid phase polymer carbon concentration. The concentration of liquid phase polymer carbon, p, was determined by measuring the total organic carbon concentration (TOC) of a reactor liquid sample, TOC_{soln}, and performing the following calculation:

$$p = TOC_{soln} - s - x$$

TOC determinations were made using the ampule analysis module of an Oceanography International Carbon Analyzer (Oceanography International Corp., College Station, TX, Total Carbon System, Cat. No. 0524B).

Biofilm cellular carbon density. The density of biofilm cellular carbon, x_b, was determined by enumerating the total number of cells per biofilm volume using epifluorescence microscopy and performing calculations analogous to those presented above for x.

Biofilm polymer carbon density. The density of biofilm polymer carbon, p_b, was determined by measuring the TOC of a known volume of biofilm, TOC_b, and performing the following calculation:

$$p_b = TOC_b - x_b$$

Suspended Solids Concentration

Suspended solids concentration was determined by filtering either 50 or 100 cm^3 samples of reactor effluent through predried (103°C for 1 hour), preweighed, Nuclepore membranes (Nuclepore Corp.,

Pleasanton, CA, No. 111107, average pore size 0.45 μm). After filtration the filters were dried at 103°C for 1 hour and weighed (Mettler Instruments Corp., Hightstown, NJ, Type H6 Digital Balance).

Electron Microscopy

Samples for scanning electron microscopy (SEM) were prepared by 30 minute fixation in a 0.5% glutaraldehyde-0.067 M cacodylate buffer solution followed by dehydration in a series of EtOH solutions (30%, 50%, 70%, 90%, 10 minutes each, 100% for 1 minute twice). Dehydration was completed by critical point drying in 100% EtOH. Samples were coated with gold in a Pelco sputter coater operated at 20mA for 3-4 minutes and examined at 40kv in a JEM-100CX electron microscope with an ASID-4D scanning attachment.

Samples for transmission electron microscopy (TEM) were prepared by first prefixing in a prefixative solution of 0.5% glutaraldehyde in 0.1 M cacodylate buffer containing 0.15% ruthenium red for 30 minutes. Chemostat samples were then recentrifuged (3000g for 10 minutes) and the resulting pellet suspended in 2% purified agar. Samples (chemostat and biofilm) were then trimmed to approximately $4mm^2$ sections and fixed for 2 hours in a fixative solution (5% glutaraldehyde in 0.1 M cacodylate buffer containing 0.05% ruthenium red. The samples were washed 5 times (10 minutes/wash) in 0.1 M cacodylate buffer with 0.05% ruthenium red followed by postfixation for 3 hours in 0.1 M cacodylate buffer with 0.05% ruthenium red and 2% osmium tetroxide. The samples were washed again as described above and then dehydrated in a series of EtOH solutions (30%, 50%,

70%, for 30 minutes each, 90% for 10 minutes, and 100% for 1 minute twice). The samples were rinsed twice in 100% propylene oxide (20 minutes each) and then soaked in graded (2:1, 1:2) propylene oxide-Spurr's resin mixtures for several hours each. The samples were placed in embedding molds which contained pure Spurr's resin and hardened at 60°C for approximately 8 hours. The resulting resin blocks were trimmed with razor blades and thin sectioned on a Reichert OMU2 ultramicrotome. The thin sections were picked up on copper grids, stained with uranyl acetate and lead citrate, and examined under a Zeiss EM95-2 electron microscope.

Organism

The Ps. aeruginosa strain used for this study was obtained from Prof. Nels Nelson, Dept. of Microbiology, Montana State University, Bozeman, MT.

Identification

Ps. aeruginosa identification was based on either the API 20E system for the identification of Enterobacteriaceae and other gram-negative bacteria (see Appendix E for details) or on colony morphology and odor after growth on TSY agar.

Storage

Ps. aeruginosa was stored initially in a refrigerator on TSY plates and replated every 2 to 3 weeks to maintain viability. Later the organism was stored at approximately -10°C in a 20% skim milk suspending medium.

RESULTS

Comprehensive listings of raw data for all chemostat and AR experiments can be found in Appendices F and G. Experimental conditions and summaries of experimental results are given in Tables 7 and 8.

Chemostat Experiments

Cellular reproduction and extracellular polymer formation have been observed in dispersed growth chemostat reactors by varying chemostat dilution rate, D, and measuring changes in the following:

1. steady state cellular carbon concentration, $\bar{x}$
2. steady state polymer carbon concentration, $\bar{p}$
3. steady state glucose carbon concentration, $\bar{s}$

The effect of dilution rate on $\bar{x}$, $\bar{p}$, and $\bar{s}$ is shown in Figure 8.

$\bar{x}$ increases with increasing D at low dilution rates, reaches a maximum at D = 0.15 h^{-1} and then gradually decreases to approximately zero at D = 0.40 h^{-1}. The initial increase in $\bar{x}$ is apparently due to the increase in cellular growth rate which results from the increased mass of glucose pumped into the reactor as D increases. However once D exceeds 0.15 h^{-1} the effect of cell washout becomes increasingly important and results in essentially all of the cells being washed out of the reactor at D = 0.40 h^{-1}.

$\bar{p}$ decreases with increasing D throughout the entire range of dilution rate and also reaches a minimum value at D = 0.4 h^{-1}. This

TABLE 7

Experimental Conditions and Summary of Chemostat Experimental Results

Exp #	D (h^{-1})	s_i (mg/l)	$\bar{s}$ (mg/l)	$\bar{x}$ (mg/l)	$\bar{p}$ (mg/l)	$\frac{D\,\bar{p}}{\bar{x}}$ (mg/mg h)	$\frac{D\,(s_i - \bar{s})}{\bar{x}}$ (mg/mg h)
1	0.075	38.3±0.0	0.8±0.3	8.6±0.3	6.3±1.5	0.054±0.011	0.33±0.008
2	0.250	36.5±0.7	7.5±0.8	7.8±0.2	3.0±0.2	0.095±0.004	0.94±0.021
3	0.150	39.1±1.2	0.3±0.0	10.9±1.7	6.0±0.4	0.083±0.008	0.54±0.067
4	0.100	39.3±4.1	0.4±0.0	9.6±0.1	6.9±0.3	0.072±0.001	0.41±0.037
5	0.050	32.0±2.5	0.2±0.0	8.7±2.1	7.2±0.2	0.043±0.009	0.19±0.031
6	0.350	36.0±1.0	28.6±0.8	2.0±0.1	2.1±0.8	0.36±0.16	1.3±0.41
7	0.400	36.5±1.2	33.2±0.3	0.9±0.3	0.1±0.1	0.018±0.025	1.4±0.21
8	0.025	36.7±0.5	0.1±0.0	4.9±1.2	7.8±4.6	0.038±0.014	0.19±0.045

values represent mean ± standard deviation of two samples, one sample from each of two chemostats

TABLE 8

Experimental Conditions and Summary of Annular Reactor Experimental Results

Exp #	# of reactors	s_i (mg/l)	$x^*_{b,max}$ (mg/m^2)	$p^*_{b,max}$ (mg/m^2)
1	1	1.9	53.4	161.8
2	1	3.0	152.9	139.8
3	1	3.5	9.3	146.2
4	2	16.9 ± 1.4	588.2 ± 190.8	485.5 ± 19.5
5	1	16.5	426.1	10.3
6	2	9.6 ± 0.4	330.4 ± 3.0	351.4 ± 130.0
7	1	4.6	67.3	218.1
8	1	3.7	-	-

Values represent either one sample from one AR; or the mean ± standard deviation of two samples, one sample from each of two AR's.

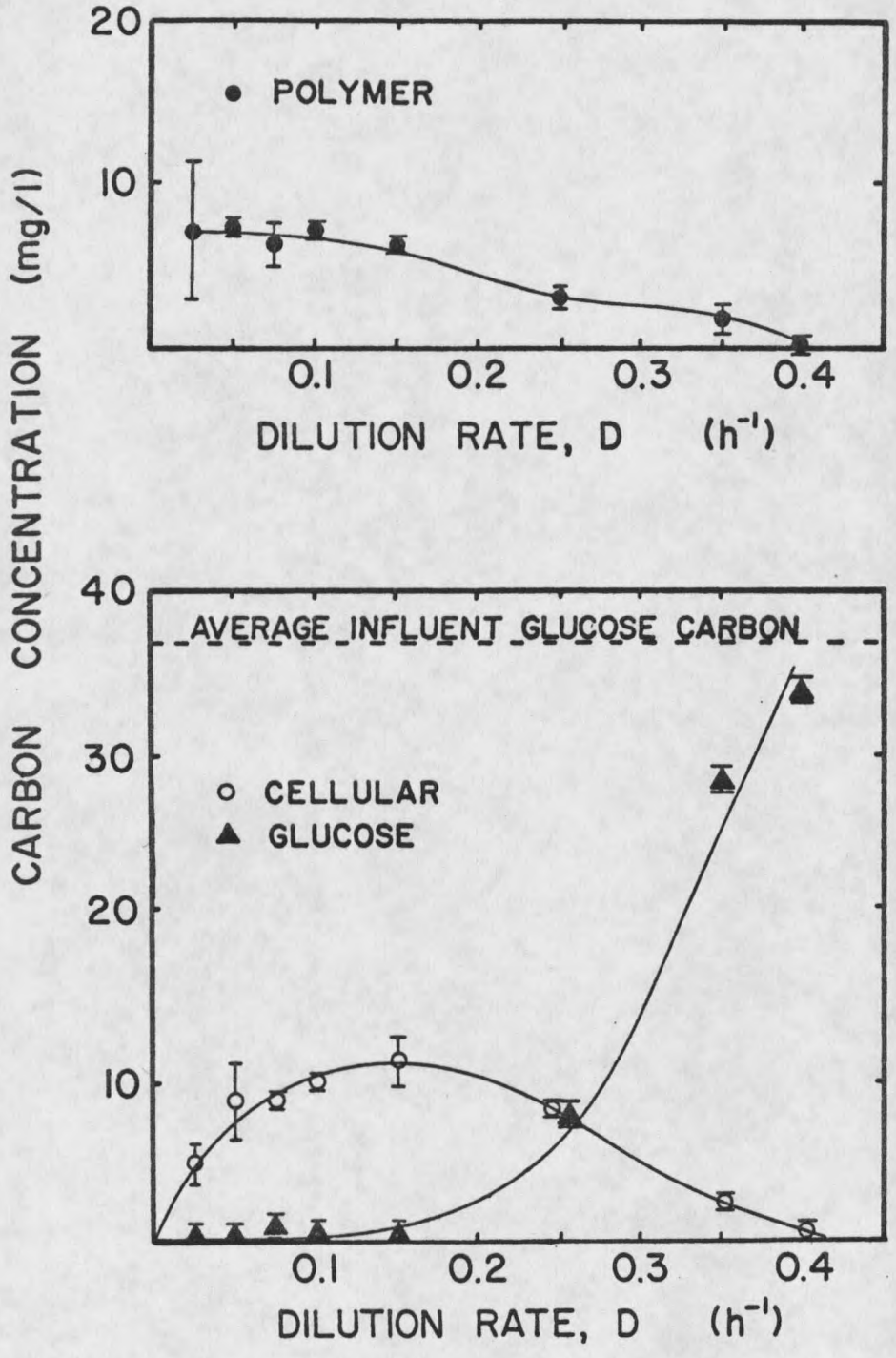

Figure 8. Steady State Cellular, Polymer, and Glucose Carbon Concentration as a Function of Chemostat Dilution Rate (Each Point Represents Mean ± Standard Deviation of Two Samples, One Sample From Each of Two Chemostats).

suggests that the quantity of polymer produced depends on both the quantity of cells present and the growth rate of the cells present.

$\bar{s}$ remains essentially constant at low dilution rates, however once D exceeds approximately 0.15 h^{-1} glucose concentration increases rapidly and approaches the average influent glucose carbon concentration. The increase in $\bar{s}$ once D exceeds 0.15 h^{-1} is attributed to the corresponding decrease in $\bar{x}$.

Annular Reactor Experiments

Cellular reproduction and extracellular polymer formation have been observed in the attached growth annular reactors by varying influent glucose carbon concentration, s_i, and measuring changes in the following:

1. biofilm cellular carbon areal density, x_b^*
2. biofilm polymer carbon areal density, p_b^*
3. biofilm thickness, Th
4. cellular carbon concentration, x
5. polymer carbon concentration, p
6. glucose carbon concentration, s

Figures 9 and 10 illustrate the variations observed in x_b^*, p_b^*, Th, x, p, and s during a typical AR experiment.

Biofilm cellular and polymer carbon increase with time (Figure 9) due to the processes of reproduction and polymer formation which occur at the reactor surface. Glucose is removed from the liquid phase (Figure 10) to support these processes and once the availability of glucose is reduced, cellular and polymer carbon areal densities approach steady state values. Biofilm thickness increases as a direct result of the accumulation of cells and polymer at the surface (Figure 9).

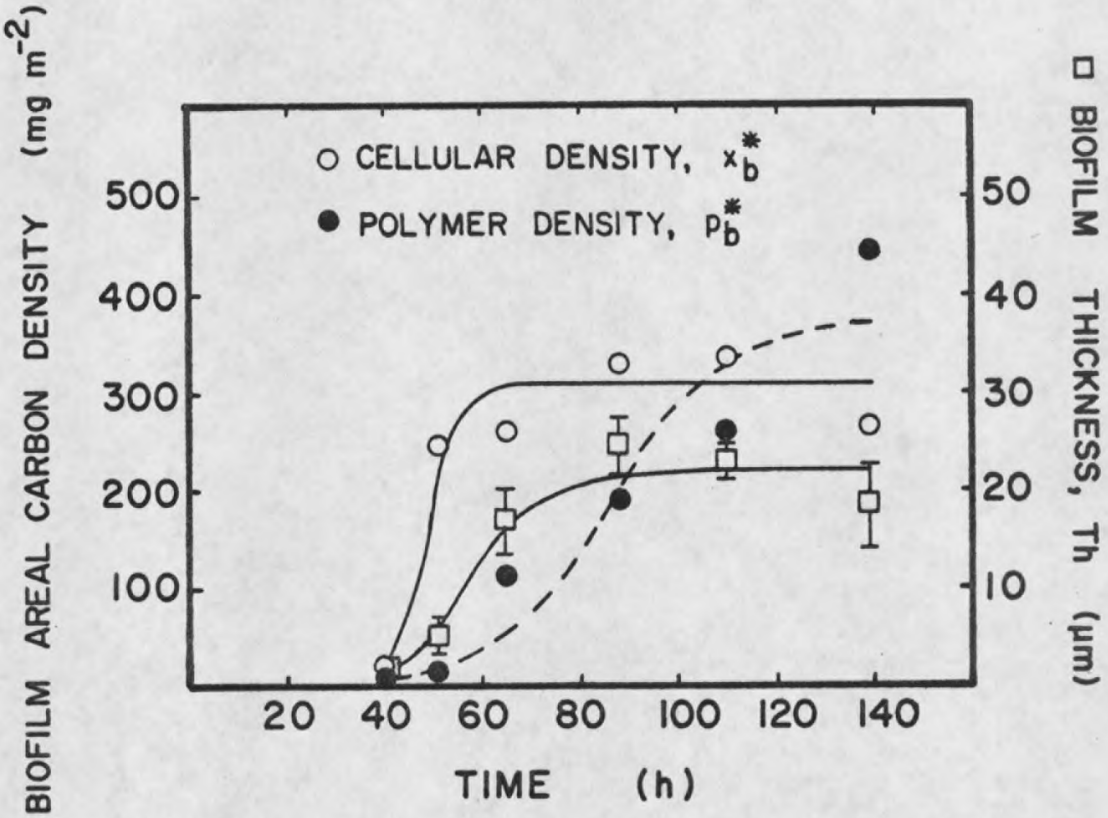

Figure 9. Typical Experimental Progression of Biofilm Componer (Data From AR Experiment 6; Carbon Data Points Repr sent One Sample From One AR, Thickness Data Points Represent Mean ± Standard Deviation of One Thickne Determination From One AR; Curves Represent Time Smoothed Data).

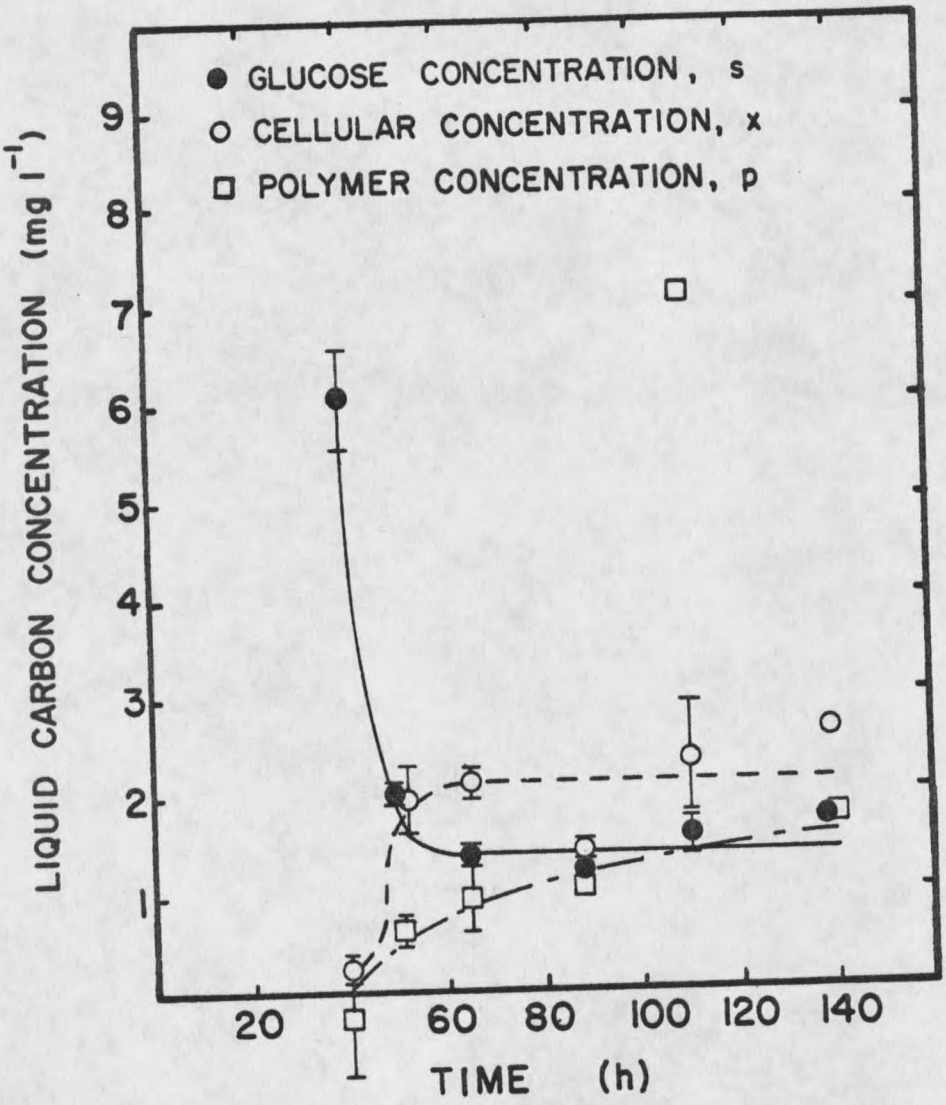

Figure 10. Typical Experimental Progression of Liquid Phase Components During a Biofilm Experiment (Data From AR Experiment 6; Each Data Point Represents The Mean $\pm$ Standard Deviation of Two Samples, One Sample From Each of Two AR's; Curves Represent Time Smoothed Data).

Cellular carbon and polymer carbon in the liquid phase (Figure 10) are produced due to the detachment of cells and polymer from the AR surfaces. The concentrations of these components increase in proportion to their corresponding biofilm densities (Figure 9 and 10).

The experiment illustrated in Figures 9 and 10 was conducted at an influent glucose carbon concentration of 9.6 ± 0.4 mg/l. The effect of different influent glucose concentration on reproduction and polymer formation is shown in Figures 11 and 12. These figures indicate that at low influent glucose (1.9 and 3.8 mg/l glucose carbon) the biofilm is composed of more polymer carbon than cellular carbon, whereas at higher influent glucose (9.6 and 16.7 mg/l glucose carbon) cellular carbon usually dominated.

Mass Conservation Equations

The variations in cellular, polymer, and glucose carbon presented in the previous section are analyzed most meaningfully using the mass balance approach. The conservation equations which are required to apply this approach are developed in this section and are based on carbon mass.

Chemostat Equations

Cellular carbon. A mass balance across a chemostat for cellular carbon can be written as follows:

$$V\frac{dx}{dt} = F(x_i - x) + \mu x V \qquad (3)$$

net rate of cellular carbon accumulation	net rate of cellular input by flow	rate of cellular reproduction

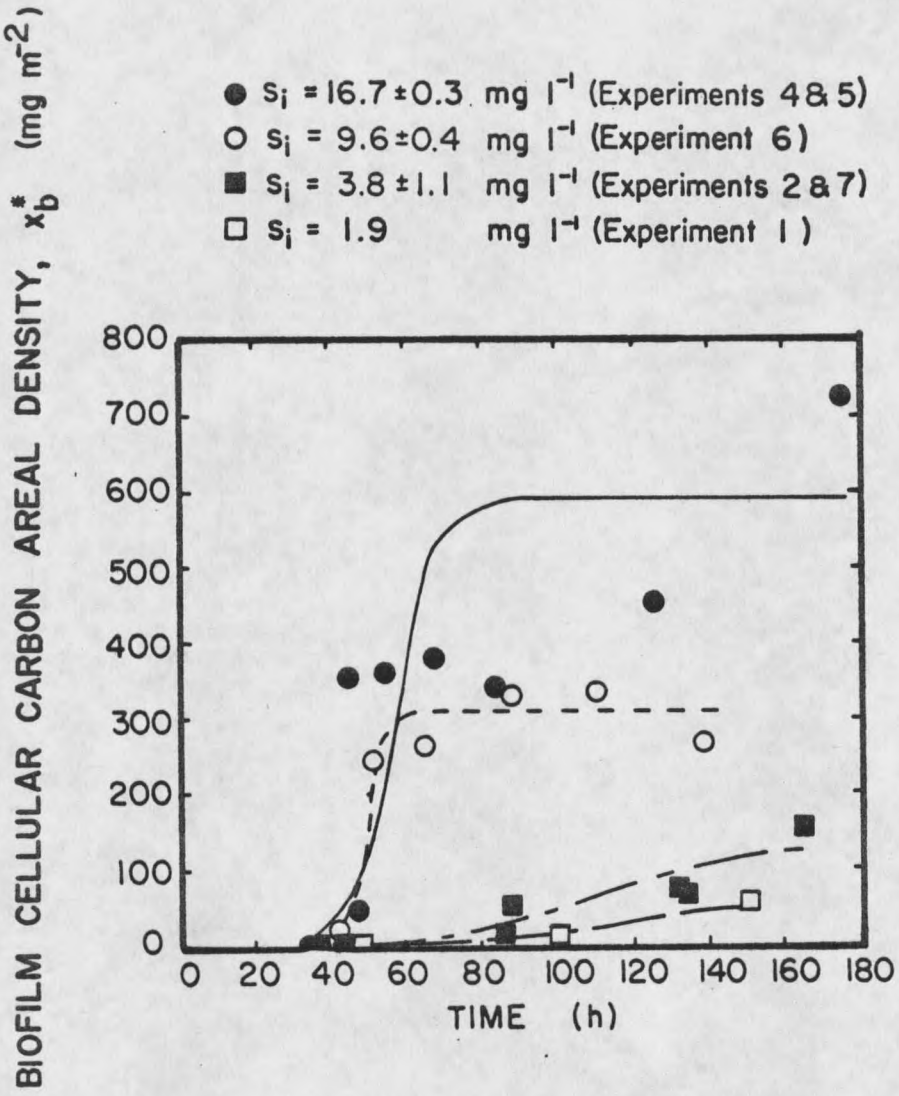

Figure 11. Effect of Influent Glucose Concentration on Biofilm Cellular Carbon Areal Density (Each Data Point Represents One Sample From One AR, Curves Represent Time Smoothed Data).

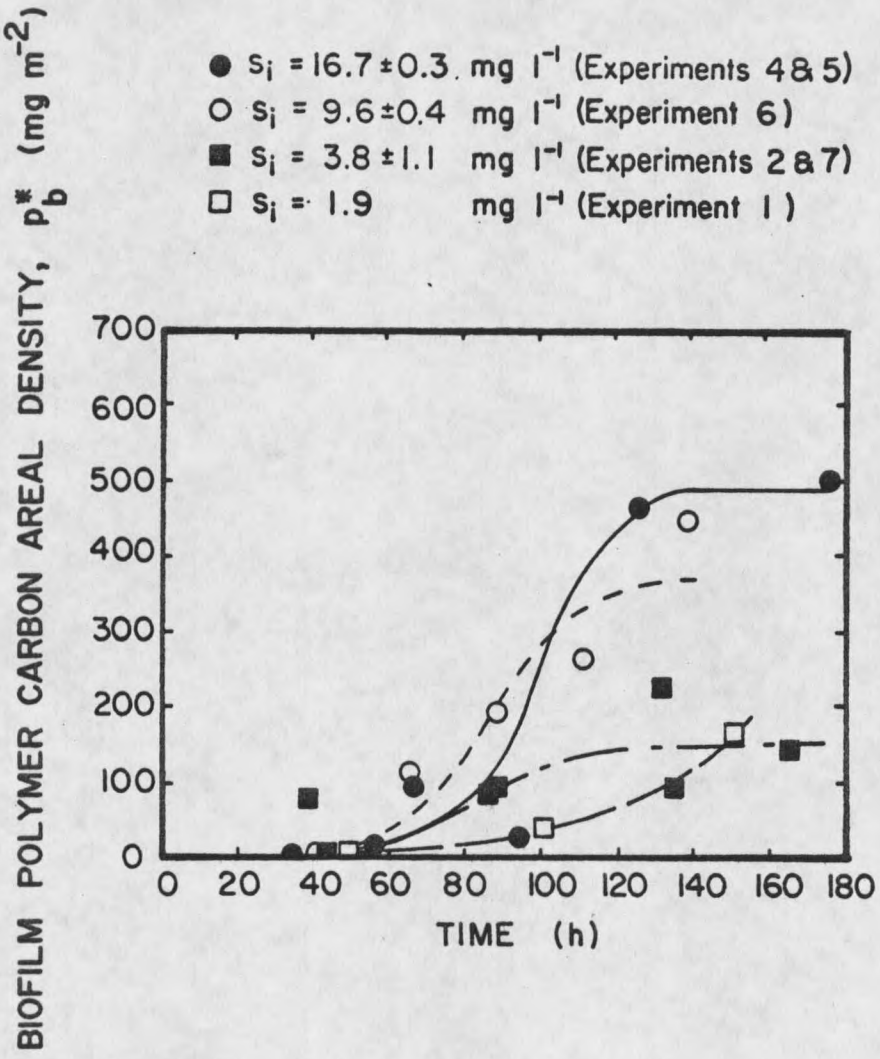

Figure 12. Effect of Influent Glucose Concentration on Biofilm Polymer Carbon Areal Density (Each Data Point Represents One Sample From One AR, Curves Represent Time Smoothed Data).

where

V	= liquid volume	(L^3)
x	= cellular carbon concentration	$(M_x L^{-3})$
t	= time	(t)
F	= volumetric flowrate of the reactor feed	$(L^3 t^{-1})$
x_i	= influent cellular carbon concentration	$(M_x L^{-3})$
μ	= specific cellular growth rate	(t^{-1})

Since all chemostat measurements were made under steady state conditions the net accumulation term, V dx/dt, equals zero. The influent cellular carbon concentration was also equal to zero (sterilized feed solutions). Incorporating these conditions, equation (3) can be simplified as follows:

$$F \bar{x} = \mu \bar{x} V \qquad (4)$$

where

$\bar{x}$	= steady state cellular carbon concentration	$(M_x L^{-3})$

Dividing both sides of equation (4) by V and noting the F/V is equal to the dilution rate, D, equation (4) can be simplified:

$$D = \mu \qquad (5)$$

This is a familiar result for chemostat reactors indicating that specific cellular growth rate is equal to chemostat dilution rate.

Polymer carbon. A mass balance across a chemostat on polymer carbon can

be written as follows:

$$V \frac{dp}{dt} = F (p_i - p) + r_p \times V \qquad (6)$$

net rate of polymer carbon accumulation = net rate of polymer input by flow + rate of polymer formation

where

p = polymer carbon concentration $(M_p L^{-3})$

p_i = influent polymer carbon concentration $(M_p L^{-3})$

r_p = specific polymer formation rate $(M_p M_x^{-1} t^{-1})$

Chemostat experiments were sampled only under steady state conditions (i.e., d/dt = 0). Influent polymer carbon concentration was zero. Therefore, equation (6) can be simplified:

$$F \bar{p} = r_p \bar{x} V \qquad (7)$$

where

$\bar{p}$ = steady state polymer carbon concentration $(M_p L^{-3})$

Dividing both sides of equation (7) by V and substituting the Luedeking-Piret equation for r_p (equation 2), the chemostat polymer balance can be rewritten:

$$D \bar{p} = k \mu \bar{x} + k' \bar{x} \qquad (8)$$

where

k = growth-associated polymer formation rate coefficient $(M_p M_x^{-1})$

k' = nongrowth-associated polymer formation rate coefficient $(M_p M_x^{-1} t^{-1})$

Glucose carbon. A mass balance across a chemostat on glucose carbon can be written as follows:

$$V\frac{ds}{dt} = F(s_i - s) - \frac{\mu x V}{Y_{x/s}} - \frac{k\mu x V + k' x V}{Y_{p/s}} \quad (9)$$

net rate of glucose carbon accumulation	net rate of glucose input by flow	rate of glucose removal for cellular reproduction	rate of glucose removal for polymer formation

where

s = glucose carbon concentration $(M_s L^{-3})$

s_i = influent glucose carbon concentration $(M_s L^{-3})$

$Y_{x/s}$ = cellular carbon yield coefficient $(M_x M_s^{-1})$

$Y_{p/s}$ = polymer carbon yield coefficient $(M_p M_s^{-1})$

Applying the steady state condition and dividing both sides of equation (9) by V, the chemostat glucose balance can be written:

$$D(s_i - \bar{s}) = \frac{\mu \bar{x}}{Y_{x/s}} + \frac{k\mu \bar{x} + k' \bar{x}}{Y_{p/s}} \quad (10)$$

where

$\bar{s}$ = steady state glucose carbon concentration $(M_s L^{-3})$

Annular Reactor Equations

Biofilm cellular carbon. A mass balance for the accumulation of cellular carbon in the biofilm can be written as follows:

$$A \frac{dx_b^*}{dt} = R_{xb} A - R_{dx} A \qquad (11)$$

net rate of cellular carbon accumulation in the biofilm	=	rate of cellular reproduction in the biofilm	-	rate of cellular detachment from the biofilm

where

A	=	reactor surface area	(L^2)
x_b^*	=	cellular carbon areal density in the biofilm	$(M_x L^{-2})$
R_{xb}	=	cellular carbon reproduction rate in the biofilm	$(M_x L^{-2} t^{-1})$
R_{dx}	=	cellular carbon detachment rate from the biofilm	$(M_x L^{-2} t^{-1})$

Defining a biofilm specific cellular growth rate, μ_b, as

$$R_{xb} = \mu_b x_b^* \qquad (12)$$

where

μ_b = specific cellular growth rate in the biofilm (t^{-1})

the biofilm cellular carbon balance (equation 11) can be rewritten:

$$A \frac{dx_b^*}{dt} = \mu_b x_b^* A - R_{dx} A \qquad (13)$$

Biofilm polymer carbon. A mass balance for the accumulation of polymer carbon in the biofilm can be written as follows:

$$A \frac{dp_b^*}{dt} = R_{pb} A - R_{dp} A \qquad (14)$$

net rate of polymer carbon accumulation in the biofilm	=	rate of polymer formation in the biofilm	-	rate of polymer detachment from the biofilm

where

p_b^* = polymer carbon areal density in the biofilm ($M_p L^{-2}$)

R_{pb} = polymer carbon formation rate in the biofilm ($M_p L^{-2} t^{-1}$)

R_{dp} = polymer carbon detachment rate from the biofilm ($M_p L^{-2} t^{-1}$)

Defining biofilm polymer formation rate coefficients, k_b and k_b' as

$$R_{pb} = k_b \mu_b x_b^* + k_b' x_b^* \qquad (15)$$

where

k_b = growth-associated polymer formation rate coefficient in the biofilm ($M_p M_x^{-1}$)

k_b' = nongrowth-associated polymer formation rate coefficient in the biofilm ($M_p M_x^{-1} t^{-1}$)

the biofilm polymer carbon balance (equation 14) can be rewritten:

$$A \frac{dp_b^*}{dt} = (k_b \mu_b x_b^* + k_b' x_b^*) A - R_{dp} A \qquad (16)$$

Liquid cellular carbon. A mass balance across an AR on liquid cellular carbon can be written as follows:

$$V\frac{dx}{dt} = F(x_i - x) + R_{dx}A + \mu x V \quad (17)$$

net rate of cellular carbon accumulation in the liquid	net rate of cellular input by flow	rate of cellular detachment from the biofilm	rate of cellular reproduction in the liquid

Influent cellular carbon concentration in this study was equal to zero. Furthermore, the AR's were operated at a 10 minute hydraulic retention time so that cellular reproduction was essentially limited to cellular carbon in the biofilm. Incorporating these conditions and dividing both sides of equation (17) by V, the AR liquid cellular carbon balance can be rewritten:

$$\frac{dx}{dt} = -D\,x + \frac{R_{dx}A}{V} \quad (18)$$

Liquid polymer carbon. A mass balance across an AR on liquid polymer carbon can be written as follows:

$$V\frac{dp}{dt} = F(p_i - p) + R_{dp}A + r_p x V \quad (19)$$

net rate of polymer carbon accumulation in the liquid	net rate of polymer input by flow	rate of polymer detachment from the biofilm	rate of polymer formation in the liquid

Influent polymer carbon concentration in this study was equal to zero. Furthermore, due to the 10 minute AR hydraulic retention time and the fact that the mass of cellular carbon in the liquid was substantially less than the mass of cellular carbon in the biofilm, liquid polymer carbon formation is assumed negligible. Incorporating these conditions and dividing both sides of equation (19) by V, the AR liquid polymer carbon balance can be rewritten:

$$\frac{dp}{dt} = -D\,p + \frac{R_{dp}\,A}{V} \qquad (20)$$

Glucose carbon. A mass balance across an AR on glucose carbon can be written as follows:

$$V\frac{ds}{dt} = F\,(s_i - s) - \frac{\mu_b\,x_b^*\,A}{Y_{xb/s}} - \frac{k_b\,\mu_b\,x_b^*\,A + k'\,x_b^*\,A}{Y_{pb/s}} \qquad (21)$$

net rate of glucose carbon accumulation in the liquid	net rate of glucose input by flow	rate of glucose removal for cellular reproduction in the biofilm	rate of glucose removal for polymer formation in the biofilm

where

$Y_{xb/s}$ = cellular carbon yield coefficient in the biofilm $(M_x M_s^{-1})$

$Y_{pb/s}$ = polymer carbon yield coefficient in the biofilm $(M_p M_s^{-1})$

Note that glucose removal terms for liquid phase reproduction and polymer formation have not been included in the substrate balance since they were assumed to be negligible in the preceding sections.

Equation time smoothing. To facilitate analysis of the rate terms which appear in the AR mass balances, AR experimental data are time smoothed (e.g., Figures 9, 10, 11 and 12) using the logistics equation:

$$Z = \frac{Z_o\,e^{ct}}{1-(\frac{Z_o}{Z_m})(1-e^{ct})} \qquad (22)$$

where

$Z = x_b^*$, p_b^*, x, p, or $(s_i - s)$

Z_o = Z at time t=0

Z_m = steady state or maximum value of Z

c = rate constant

The rate of change of Z can be described by the following:

$$\frac{dZ}{dt} = c\,Z - \frac{c\,Z^2}{Z_m} \tag{23}$$

For additional information on the time smoothing of AR experimental data see Appendix H.

Cellular Reproduction

Equations (5) and (13) are the mass balance equations which account for cellular reproduction in the chemostat and annular reactors. The specific growth rates which appear in these equations, μ and μ_b, are evaluated in this section.

Specific Cellular Growth Rate in the Chemostats

Figure 13 is a plot of the chemostat cellular specific growth rate, μ, vs steady state glucose carbon concentration, $\bar{s}$. The hyperbolic form of the relation indicates that cellular reproduction can be described by saturation growth kinetics and that μ can be mathematically related to $\bar{s}$ by the Monod (1949) equation for specific growth rate:

$$\mu = \frac{\mu_{max}\, s}{k_s + s} \tag{1}$$

where

μ_{max} = maximum cellular specific growth rate (t^{-1})

k_s = saturation constant $(M_s L^{-3})$

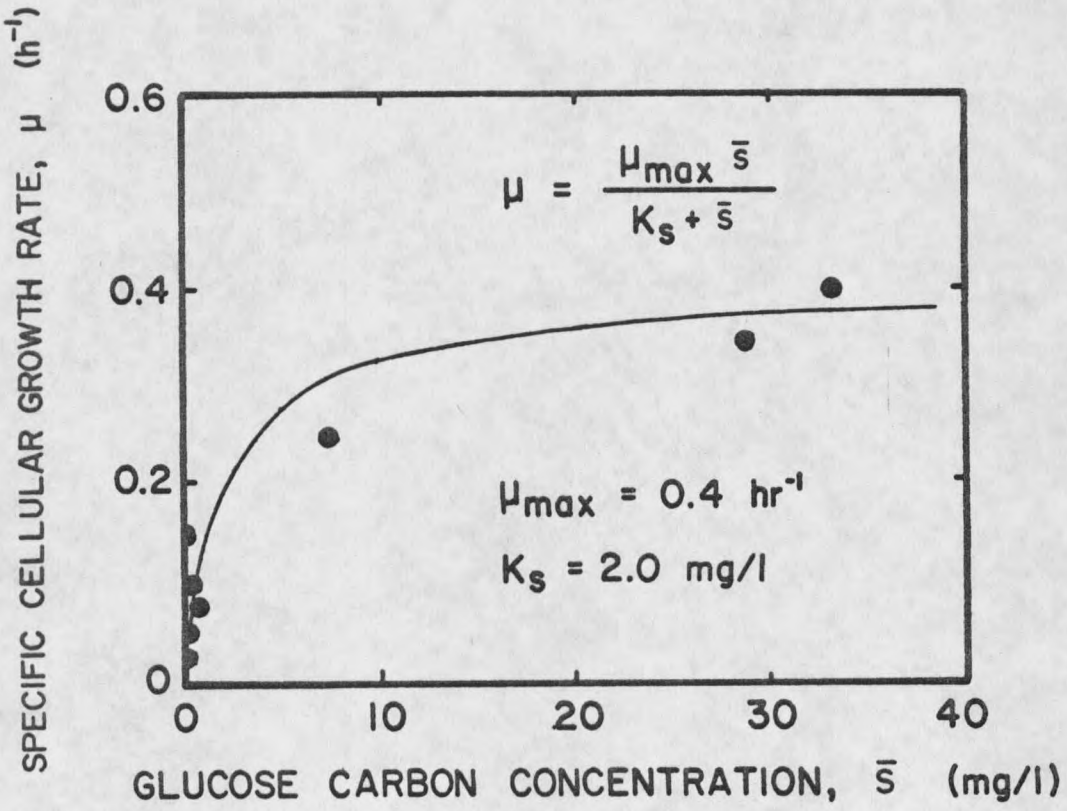

Figure 13. Specific Cellular Growth as a Function of Steady State Glucose Carbon Concentration (Each Point Represents the Mean of Two Samples, One Sample From Each of Two Chemostats).

Equation 1 can be linearized as follows to obtain a relation which can be used to calculate μ_{max} and k_s:

$$\frac{s}{\mu} = \frac{s}{\mu_{max}} + \frac{k_s}{\mu_{max}} \qquad (24)$$

or, since $\mu = D$ (equation 5),

$$\frac{s}{D} = \frac{s}{\mu_{max}} + \frac{k_s}{\mu_{max}} \qquad (25)$$

Equation (25) indicates that a plot of s/D vs s should yield a straight line with slope equal to $1/\mu_{max}$ and intercept equal to k_s/μ_{max}. Figure 14 is a plot of $\bar{s}/D$ vs $\bar{s}$ for the data obtained in this study. A least squares linear regression on the data in Figure 14 (MSU Statistics Library, Program MREGRESS) yields a slope ± 95% confidence interval equal to 2.5 ± 0.2 h (μ_{max} = 0.40 ± 0.03 h^{-1}) and an intercept ± 95% confidence interval equal to 5.1 ± 2.8 mg glucose carbon h/l (k_s = 2.0 ± 1.1 mg glucose carbon/l). The solid line drawn through the data points in Figure 13 corresponds to equation (1) using the above values for μ_{max} and k_s.

Specific Cellular Growth Rate in the Biofilm

Figure 15 is a plot of the biofilm specific cellular growth rate, μ_b, vs AR glucose carbon concentration. μ_b was calculated by rearranging equation (12) as follows:

$$\mu_b = \frac{R_{xb}}{x_b^*} \qquad (12)$$

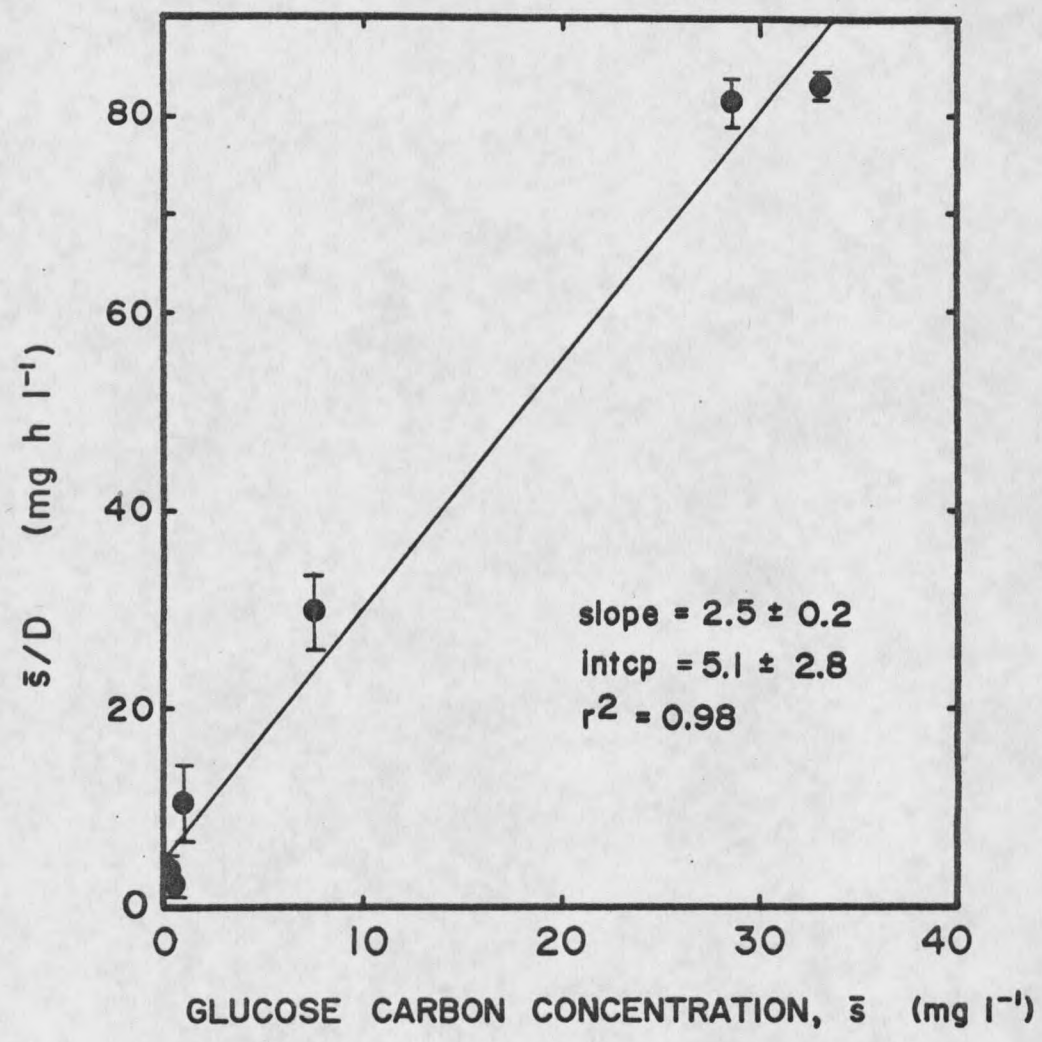

Figure 14. Determination of μ_{max} and k_s from the Chemostat Experiments (Each Point Represents Mean ± Standard Deviation of Two Samples, One Sample from Each of Two Chemostats).

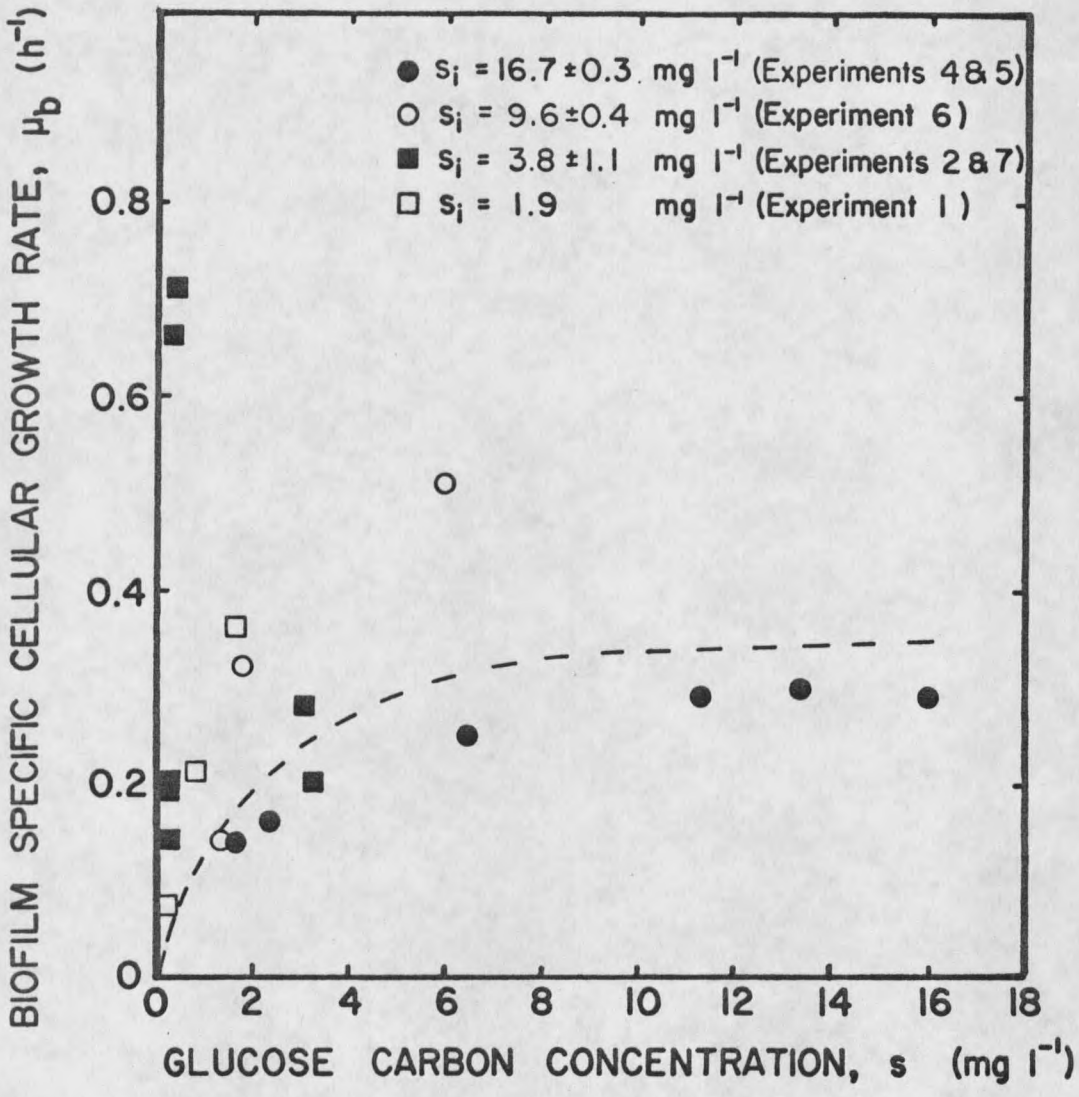

Figure 15. Biofilm Specific Cellular Growth Rate as a Function of Glucose Carbon Concentration (Time Smoothed Data).

Figure 15 suggests that with the exception of a few data points biofilm cellular reproduction may also be described by saturation growth kinetics. Figure 16 is a combination of the chemostat specific growth rate data (Figure 13) with the biofilm specific growth rate data (Figure 15). This figure suggests there is not a significant difference between the two sets of data and that μ_{max} ($0.40 \pm 0.03\ h^{-1}$) and k_s (2.0 ± 1.1 mg/l) determined from the chemostat experiments also adequately describe the majority of the biofilm data.

Polymer Formation

Equations (8) and (16) are the mass balance equations which account for polymer formation in the chemostat and annular reactors. The rate coefficients which describe polymer formation in these equations, k and k' (equation 8), and k_b and k_b' (equation 16), are evaluated in this section.

Polymer Formation Rate Coefficients in the Chemostats

The chemostat growth- and nongrowth-associated polymer formation rate coefficients, k and k', are evaluated by linearizing the chemostat polymer balance, equation (8) as follows:

$$\frac{D\,\bar{p}}{\bar{x}} = k\,\mu + k' \qquad (8)$$

or since $\mu = D$ (equation 5)

$$\frac{D\,\bar{p}}{\bar{x}} = k\,D + k' \qquad (8)$$

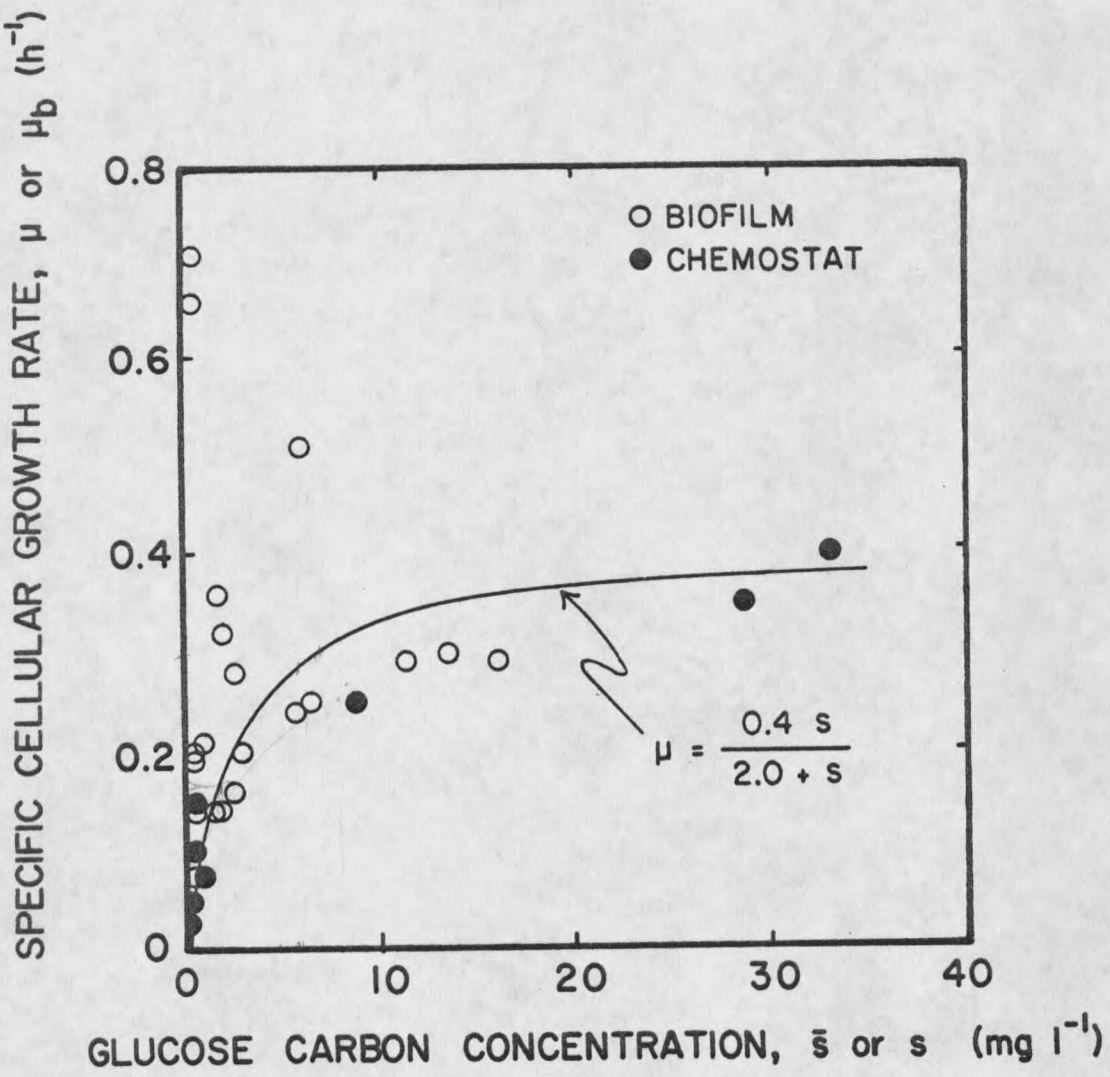

Figure 16. Combination of Chemostat and Biofilm Specific Growth Rate.

Figure 17 is a plot of $\frac{D\,\bar{p}}{\bar{x}}$ vs D. The slope (0.36 ± 0.44 mg polymer carbon/mg cellular carbon) is equal to k ± 95% confidence interval and the intercept (0.03 ± 0.10 mg polymer carbon/mg cellular carbon h) is equal to k' ± 95% confidence interval.

Polymer Formation Rate Coefficients in the Biofilm

The biofilm growth- and nongrowth-associated polymer formation rate coefficients, k_b and k_b', are evaluated by linearizing equation (15) as follows:

$$\frac{R_{pb}}{x_b^*} = k_b \mu_b + k_b' \qquad (15)$$

Figure 18 is a plot of R_{pb/x_b^*} vs μ_b. This figure suggests that the rate constants k_b and k_b' should be determined for each influent substrate concentration. Performing 3 separate linear regressions on the data (slopes = k_b, intercepts = k_b') Table 9 is constructed. The straight lines shown in Figure 18 correspond to the regression data listed in Table 9.

Cellular and Polymer Yield Coefficients

Equations (10) and (21) account for glucose utilization in the chemostat and annular reactors. The stoichiometric ratios which describe the extent of glucose utilization in these equations, $Y_{x/s}$, $Y_{p/s}$, $Y_{xb/s}$, and $Y_{pb/s}$, are evaluated in this section.

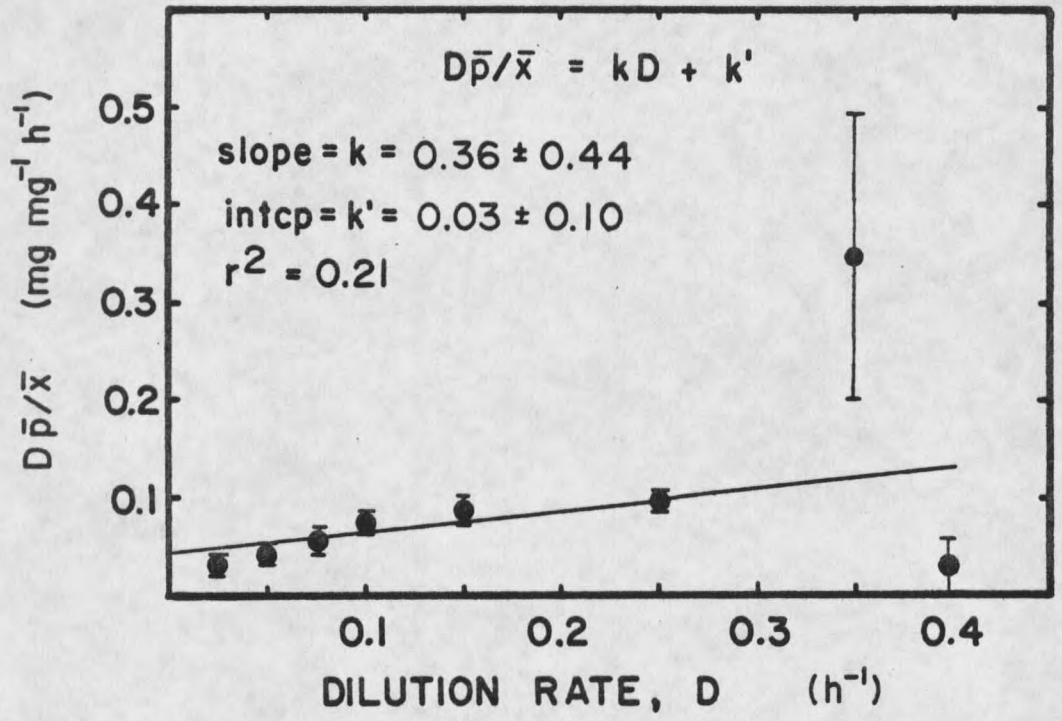

Figure 17. Determination of Growth- and Nongrowth- Associated Polymer Formation Rate Coefficients (Each Data Point Represents the Mean ± Standard Deviation of Two Samples, One Sample From Each of Two Chemostats).

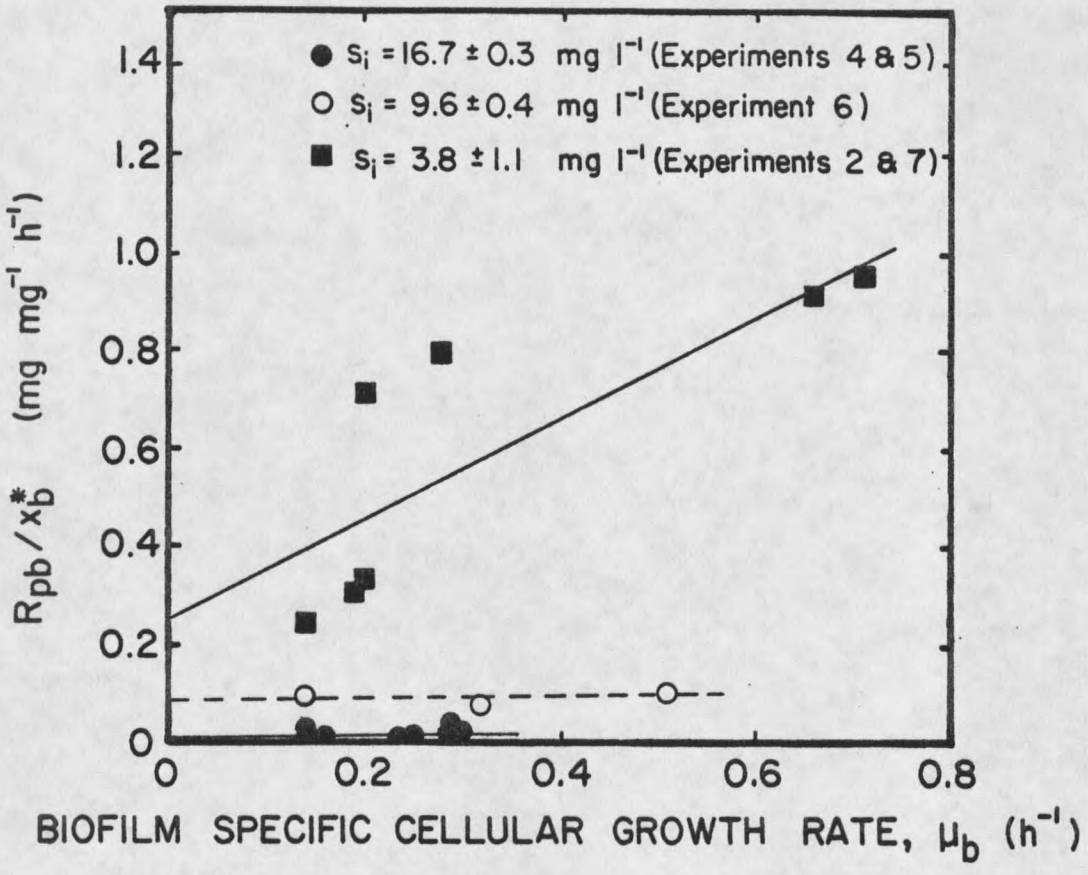

Figure 18. Determination of Biofilm Growth- and Nongrowth-Associated Polymer Formation Rate Coefficients (Time Smoothed Data).

TABLE 9

Biofilm Growth- and Nongrowth-Associated Polymer Formation Rate Coefficients

Exp #	Influent Glucose Carbon Concentration, s_i (mg/l)	Biofilm Growth-Associated Rate Coefficient, k_b (mg polymer carbon/mg cellular carbon)	Biofilm Nongrowth-Associated Rate Coefficient, k'_b (mg polymer carbon/mg cellular carbon h)
2 & 7	3.8 ± 1.1	1.0 ± 0.86[a]	0.25 ± 0.36[a]
6	9.6 ± 0.4	0.01 ± 0.14[a]	0.09 ± 0.04[a]
4 & 5	16.7 ± 0.3	0.02 ± 0.13[a]	0.01 ± 0.03[a]

[a] 95% confidence interval

Yield Coefficients in the Chemostats

The chemostat cellular and polymer yield coefficients, $Y_{x/s}$ and $Y_{p/s}$, are evaluated by rearranging the chemostat glucose balance (equation 10) as follows:

$$\frac{D\ (s_i - \bar{s})}{\bar{x}} = \mu\ (\frac{1}{Y_{x/s}} + \frac{k}{Y_{p/s}}) + \frac{k'}{Y_{p/s}} \qquad (10)$$

Defining a specific glucose removal rate, r_g:

$$r_g = \frac{D\ (s_i - \bar{s})}{\bar{x}} \qquad (26)$$

and substituting D for μ (equation 5), equation (10) can be rewritten as follows:

$$r_g = D\ (\frac{1}{Y_{x/s}} + \frac{k}{Y_{p/s}}) + \frac{k'}{Y_{p/s}} \qquad (27)$$

Figure 19 is a plot of r_g vs D. A least squares linear regression (MSU Statistical Library, program MREGRESS) on the data gives a slope $(1/Y_{x/s} + k/Y_{p/s})$ ± 95% confidence interval equal to 3.5 ± 0.53 mg glucose carbon/mg cellular carbon and an intercept $(k'/Y_{p/s})$ ± 95% confidence interval equal to 0.06 ± 0.12 mg glucose carbon/mg cellular carbon h. Using the previously obtained values for k and k', $Y_{p/s}$ and $Y_{x/s}$ are calculated as follows:

$$Y_{p/s} = \frac{0.03}{0.06} = 0.50 \text{ mg polymer carbon/mg glucose carbon}$$

$$Y_{x/s} = (3.5 - \frac{0.36}{0.50})^{-1} = 0.36 \text{ mg cellular carbon/mg glucose carbon}$$

95% confidence intervals for $Y_{p/s}$ and $Y_{x/s}$ are 1.8 mg polymer carbon/mg glucose carbon and 0.39 mg cellular carbon/mg glucose carbon,

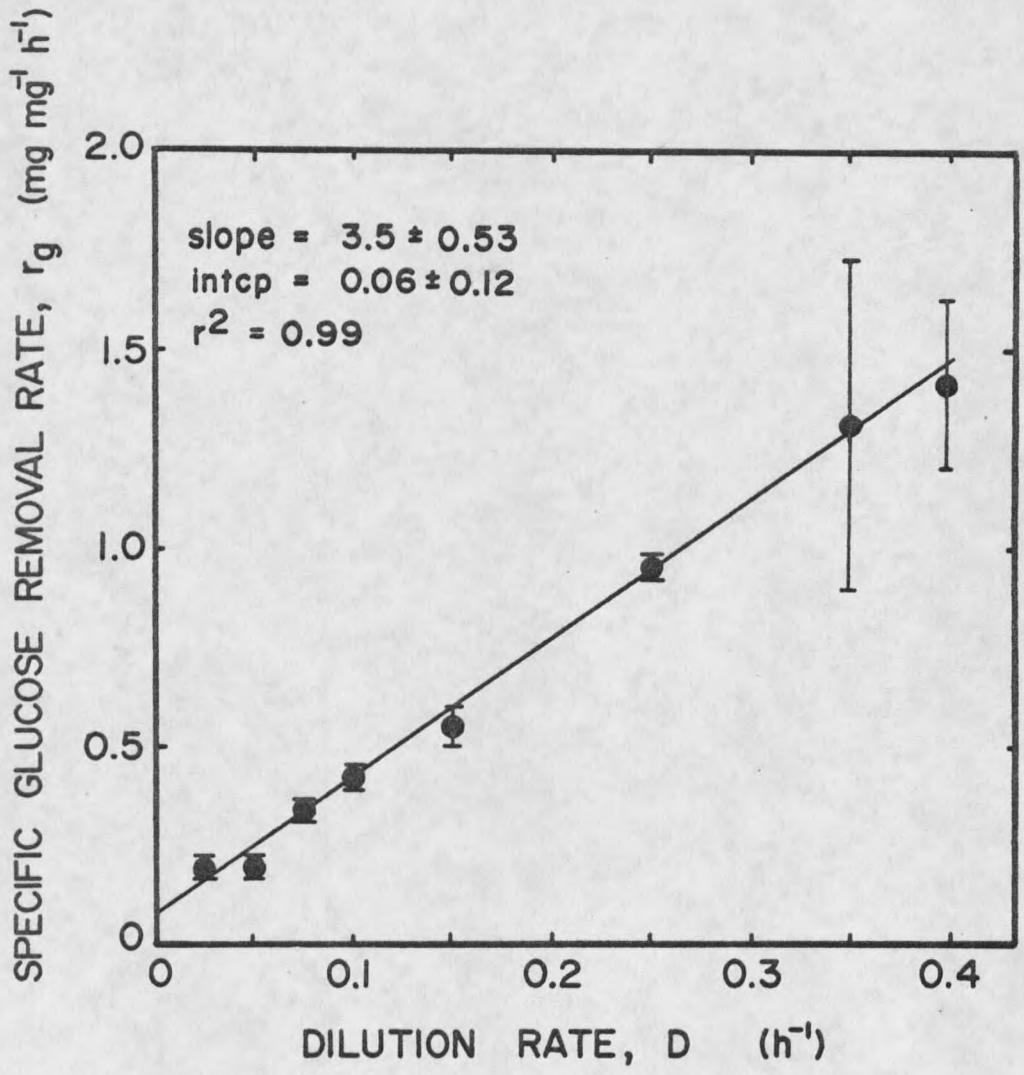

Figure 19. Determination of Chemostat Cellular and Polymer Yield Coefficients (Each Data Point Represents the Mean ± Standard Deviation of Two Samples, One From Each of Two Chemostats).

respectively (see Appendix I for confidence interval calculations).

Yield Coefficients in the Biofilm

The biofilm cellular and polymer yield coefficients, $Y_{xb/s}$ and $Y_{pb/s}$, are evaluated by rearranging the biofilm glucose balance (equation 21) as follows:

$$\frac{F\,(s_i - s) - V\,\frac{ds}{dt}}{x_b^* A} = \mu_b\left(\frac{1}{Y_{xb/s}} + \frac{k_b}{Y_{pb/s}}\right) + \frac{k_b'}{Y_{pb/s}} \qquad (21)$$

Defining a biofilm specific glucose removal rate, r_{gb}:

$$r_{gb} = \frac{F\,(s_i - s) - V\,\frac{ds}{dt}}{x_b^* A} \qquad (28)$$

equation (21) can be rewritten as follows:

$$r_{gb} = \mu_b\left(\frac{1}{Y_{xb/s}} + \frac{k_b}{Y_{pb/s}}\right) + \frac{k_b'}{Y_{pb/s}} \qquad (29)$$

Figure 20 is a plot of r_{gb} vs μ_b. A linear regression on the data gives a slope $(1/Y_{xb/s} + k_b/Y_{pb/s})$ ± 95% confidence interval equal to 4.6 ± 2.9 mg glucose carbon/mg cellular carbon and an intercept $(k'/Y_{pb/s})$ ± 95% confidence interval equal to 0.27 ± 0.90 mg glucose/mg cellular carbon h. Using the values obtained for k_b and k_b' (Table 9), $Y_{xb/s}$ and $Y_{pb/s}$ are calculated as shown above for the chemostat yields. The values of $Y_{xb/s}$ and $Y_{pb/s}$ are given in Table 10. The calculations for the $Y_{xb/s}$ and $Y_{pb/s}$ 95% confidence intervals are given in Appendix I.

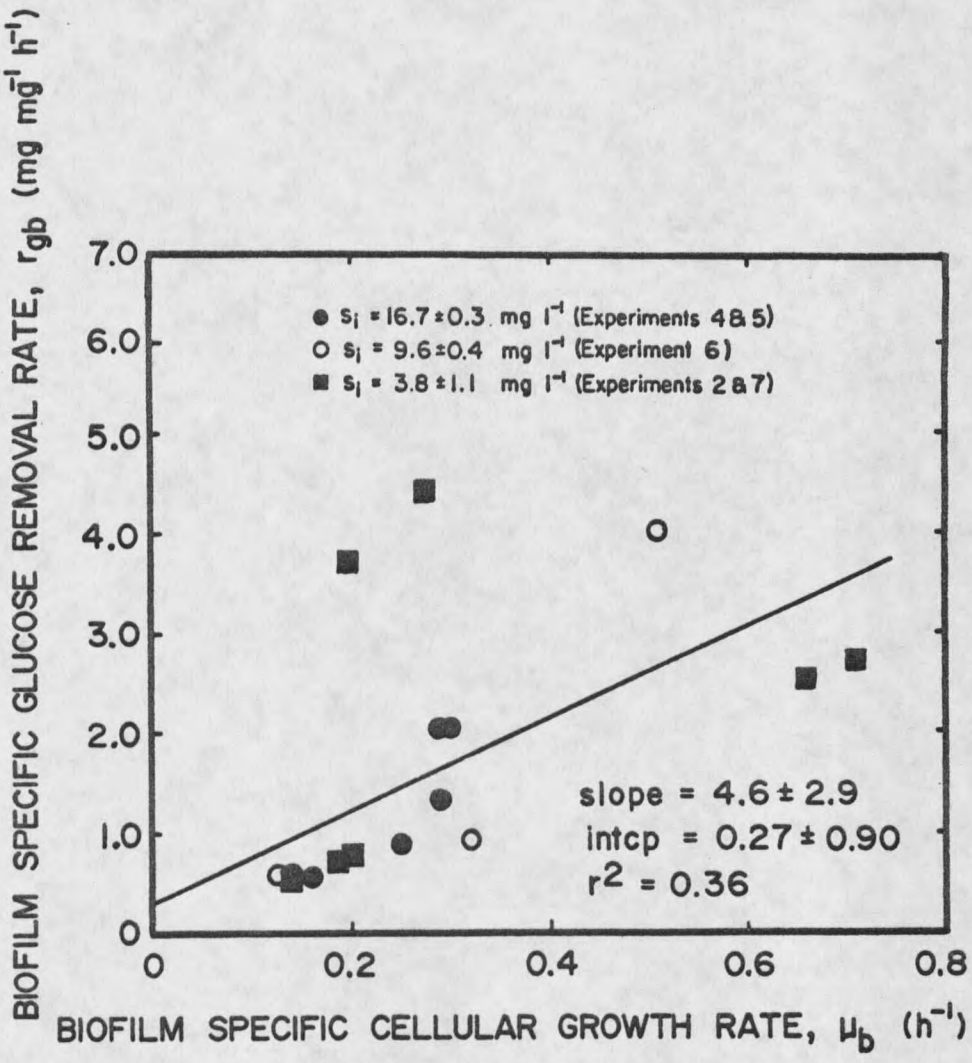

Figure 20. Determination of Biofilm Cellular and Polymer Yield Coefficients (Time Smoothed Data).

TABLE 10

Biofilm Cellular and Polymer Yield Coefficients

Exp #	Influent Glucose Carbon Concentration, s_i (mg/l)	Cellular Carbon Yield Coefficient, $Y_{xb/s}$ (mg cellular carbon/ mg glucose carbon)	Polymer Carbon Yield Coefficient, $Y_{pb/s}$ (mg polymer carbon/ mg glucose carbon)
2 & 7	3.8 ± 1.4	0.29 ± 0.44[a]	0.93 ± 3.5[a]
6	9.6 ± 0.4	0.22 ± 0.14[a]	0.33 ± 1.1[a]
4 & 5	16.7 ± 0.3	0.24 ± 0.29[a]	0.04 ± 0.18[a]

[a] 95% confidence intervals

Electron Photomicrographs

The formation of extracellular polymer by Ps. aeruginosa in this study was visually documented by a series of electron photomicrographs prepared at the end of AR experiment 6. Three of these electron photographs are shown in Photomicrographs 1, 2, and 3.

Photomicrograph 1 is a transmission electron micrograph of the biofilm at the end of AR Experiment 6. Although this photo illustrates a severely condensed version of the biofilm, the micrograph does suggest that the Ps. aeruginosa cells were uniformily distributed through the biofilm.

Photomicrographs 2 and 3 are scanning electron micrographs of the biofilm at the end of AR Experiment 6. These photos more graphically illustrate the extent of extracellular polymer formation than does the corresponding transmission electron micrograph (Photomicrograph 1).

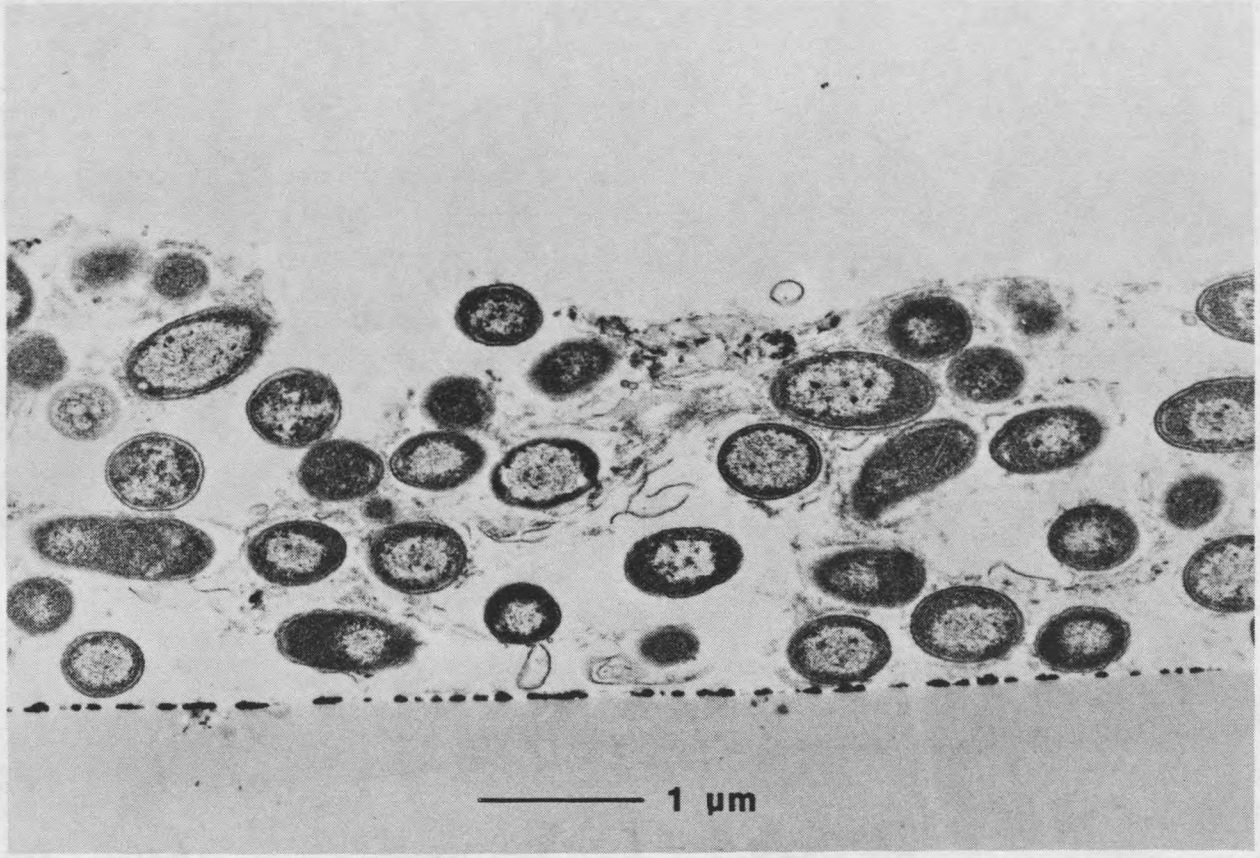

Photomicrograph 1. Transmission Electron Photomicrograph of AR Experiment 6 Biofilm. Scope Magnification Equals 7,000x, Bar Represents 1 µm.

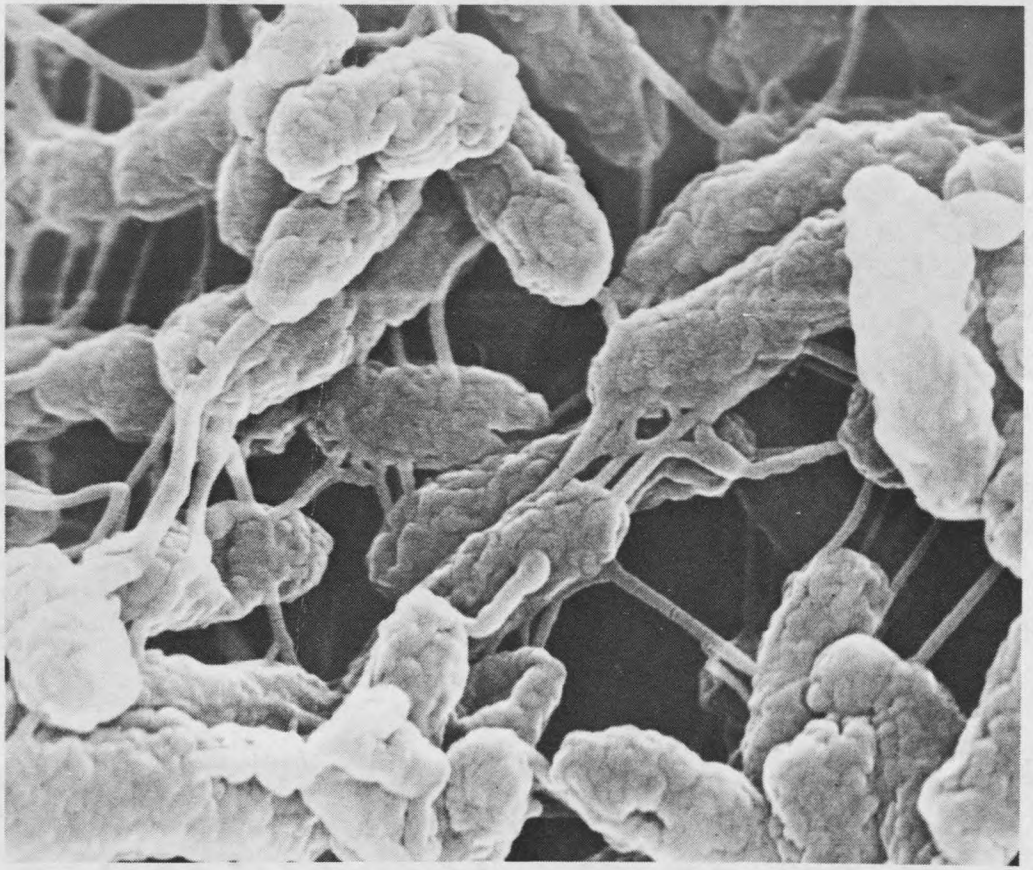

Photomicrograph 2. Scanning Electron Photomicrograph of AR Experiment 6 Biofilm. Scope Magnification Equals 30,000x, Bar Represents 0.5 µm.

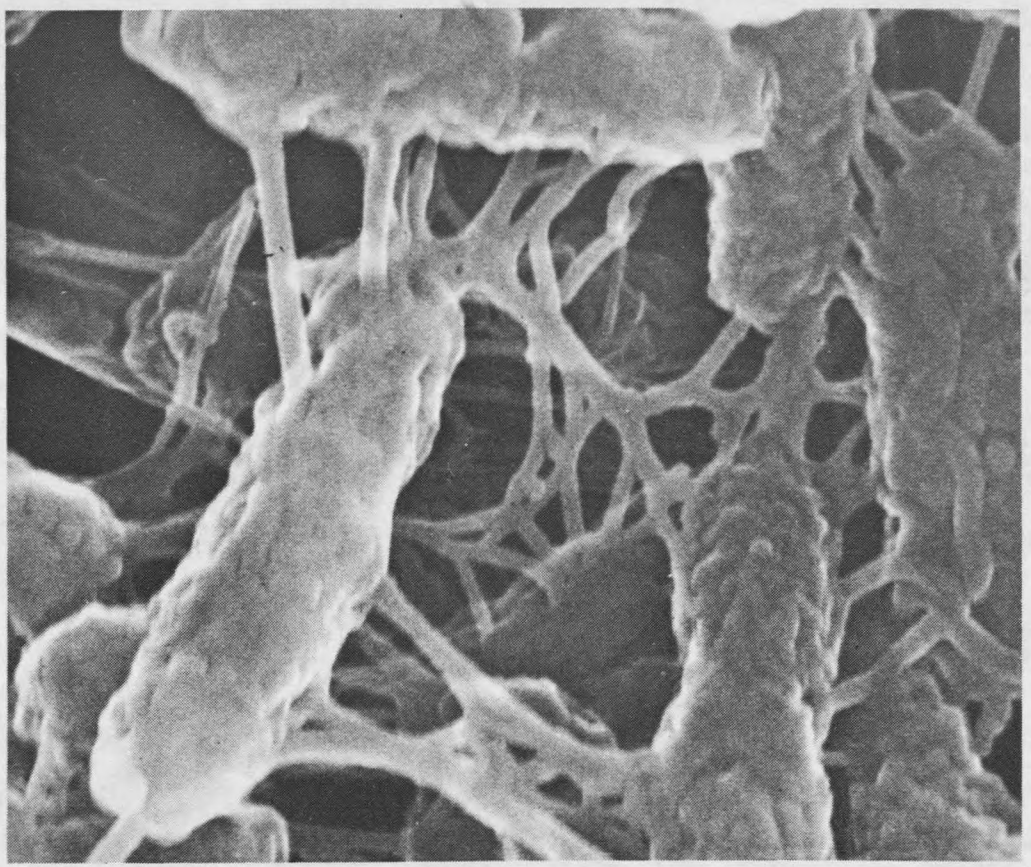

Photomicrograph 3. Scanning Electron Photomicrograph of AR Experiment 6 Biofilm. Scope Magnification Equals 50,000x, Bar Represents 0.5 µm.

DISCUSSION

In this the discussion portion of this manuscript, results from the previous chapter will be analyzed and discussed in relation to their importance to biofilm development. Comparisons will be made with the literature and comments will be provided concerning the importance and relevance of the results obtained.

The opening section of this discussion will consider biofilm substrate diffusion. Subsequent sections discuss Ps. aeruginosa cellular reproduction and extracellular polymer formation. The kinetics of these processes will be discussed first followed by consideration of reaction stoichiometry.

Substrate Diffusion

The literature suggests that diffusional resistances in biofilms can be significant. Since substrate is required for the processes of cellular reproduction and extracellular polymer formation, the diffusion of substrate into the biofilm is of primary importance. Therefore, this section will discuss substrate diffusion in the annular reactors. Diffusional resistance in the dispersed growth chemostats is considered negligible due to the homogeneous and completely-mixed nature of chemostat reactors.

Glucose is the rate limiting reactant in this study, nutrients and oxygen are assumed to be in excess. The following diffusion and reaction processes are of concern:

1. Glucose diffusion from the bulk liquid to the fluid-biofilm interface
2. Glucose diffusion within the biofilm
3. Biochemical reaction (glucose utilization) within the biofilm

Liquid Phase Diffusion

The transport of glucose from the bulk liquid to the fluid-biofilm interface can be represented by the following equation:

$$N = k_L (s - s_s) \tag{30}$$

where

N =	glucose flux to the surface	$(M_s L^{-2} t^{-1})$
k_L =	mass transfer coefficient	(Lt^{1})
s =	glucose concentration in the bulk liquid	$(M_s L^{-3})$
s_s =	glucose concentration at the biofilm surface	$(M_s L^{-3})$

Assuming that glucose accumulation at the biofilm surface is insignificant, the amount of glucose transported to the surface must equal the amount of glucose consumed by the biofilm. This equality can be written as follows:

$$R_g A = N A \tag{31}$$

where

R_g = glucose removal rate $(M_s L^{-2} t^{-1})$

$$= \frac{D}{A} (s_i - s) - \frac{ds}{A\, dt} \tag{32}$$

Lamotta (1976b) has investigated liquid phase diffusion and identified two limiting regimes depending on the magnitude of the mass transfer coefficient. When k_L is large, glucose concentration at the biofilm surface is essentially the same as in the bulk liquid. Under these conditions, liquid phase diffusional resistance is negligible and the rate of the overall removal (R_g) is determined by the kinetics of the internal diffusion-reaction process.

However, when the mass transfer coefficient is small, glucose concentration at the biofilm surface can be substantially lower than in the bulk liquid. Under these conditions, liquid phase diffusional resistance is significant and the rate of the overall removal (R_g) is determined by the rate of glucose transport to the surface.

The transition from significant to negligible liquid phase diffusional resistance can be achieved by increasing fluid velocity at the biofilm surface (Maier, et al., 1967; Kornegay and Andrews, 1967; Lamotta, 1976b; Trulear, 1980). Hence an experiment (AR experiment 8) was conducted to experimentally define the range of fluid velocities in which liquid phase diffusional resistance in the AR is negligible. The results of this experiment are plotted in Figure 21 and suggest that liquid phase diffusional resistance is negligible for rotational speeds greater than 175 rpm (93.5 cm/sec) since R_g reaches a maximum value in this region. The results shown in Figure 21 were obtained by developing a mature biofilm at 200 rpm, changing the rotational speed to one of the test speeds, and determining the glucose removal after a 1 hour tran-

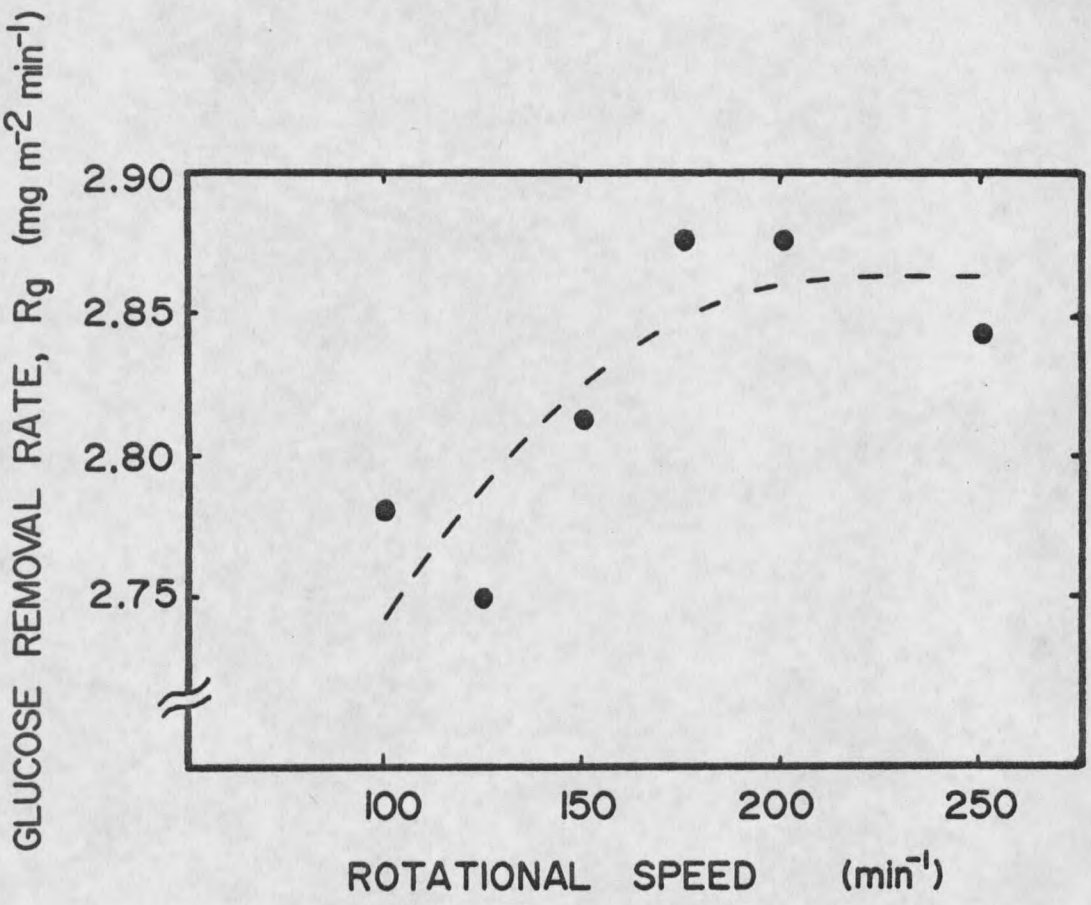

Figure 21. Results of Liquid Phase Diffusion Experiment (AR Experiment 8).

sition period. A detailed description of the experimental procedure is given in Appendix J.

All AR experiments in this study were run at a rotational speed of 200 rpm, hence liquid phase diffusional resistance is assumed negligible.

Biofilm Diffusion Equations

Simultaneous diffusion and reaction within biofilms has been studied extensively by Atkinson and co-workers (Atkinson and Daoud, 1970; Atkinson and Davies, 1974). Figure 22 shows the conceptual basis for the Atkinson model. Note that the bulk glucose concentration, s, is assumed uniform up to the fluid-biofilm interface, i.e., liquid phase diffusional resistance is negligible.

According to the Atkinson model, the flux of substrate into a biofilm is given by:

$$N_b = \lambda \frac{\mu_{max}\, x_b\, Th\, s}{Y_{x/s}\,(k_s + s)} \qquad (33)$$

where

N_b	=	glucose flux into the biofilm	$(M_s L^{-2} t^{-1})$
λ	=	effectiveness factor, the ratio of the actual flux to the flux that would occur if the entire biofilm were fully penetrated at concentration s, $0 < \lambda \leq 1$	(dimensionless)
μ_{max}	=	maximum specific cellular growth rate	(t^{-1})
x_b	=	cellular carbon density in the biofilm	$(M_x L^{-3})$
Th	=	biofilm thickness	(L)
s	=	glucose concentration in the liquid	$(M_s L^{-3})$

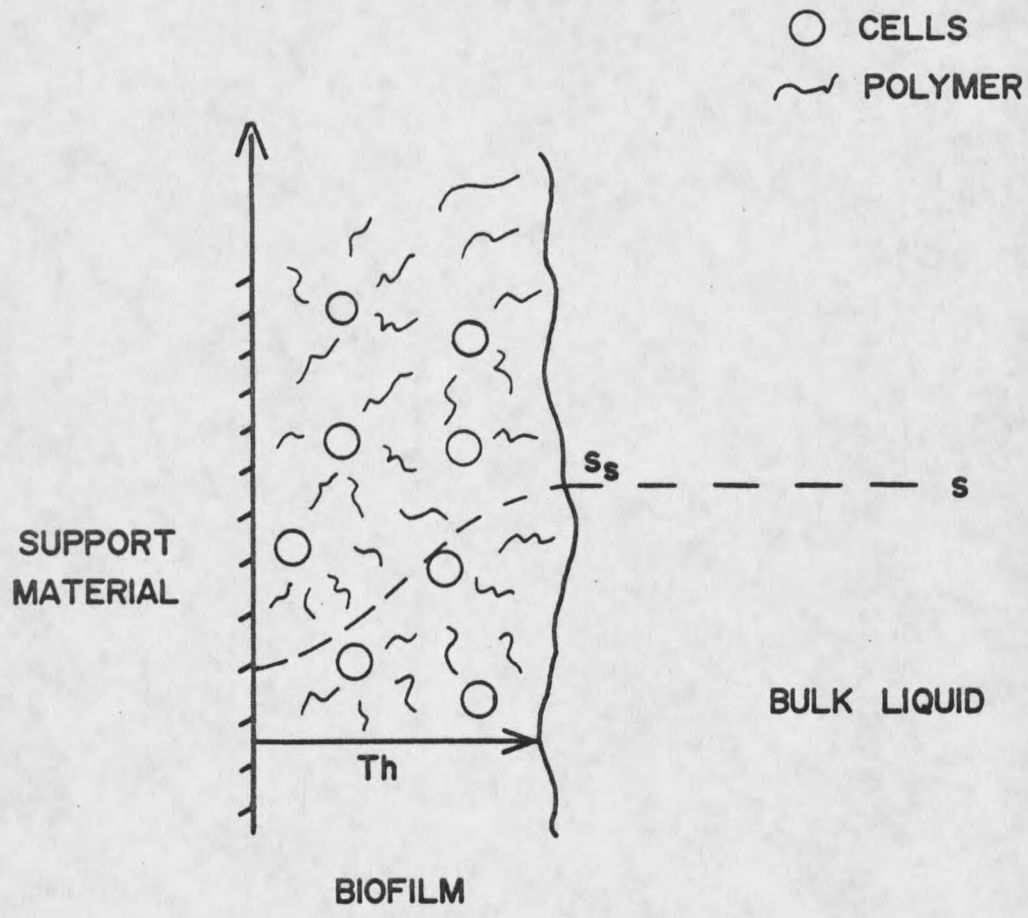

Figure 22. Conceptual Basis for the Atkinson Biofilm Diffusion Model.

$Y_{x/s}$ = cellular carbon yield coefficient ($M_x M_s^{-1}$)

k_s = saturation coefficient ($M_s L^{-3}$)

λ is a measure of the relative importance of biofilm diffusional resistance in controlling the internal diffusion-reaction process and is defined as follows using dimensionless variables:

a) predominantly reaction-controlled region

$$\lambda = 1 - \frac{\tanh k_2 \, Th}{k_2 \, Th} \left(\frac{\phi}{\tanh \phi} - 1 \right) \quad ; \quad \phi \leq 1$$

b) predominantly diffusion-controlled region

$$\lambda = \frac{1}{\phi} - \frac{\tanh k_2 \, Th}{k_2 \, Th} \left(\frac{1}{\tanh \phi} - 1 \right) \quad ; \quad \phi \geq 1$$

where

$\phi = \dfrac{k_2 \, Th}{(1 + 2 \, k_3 \, s)^{\frac{1}{2}}}$ = Thiele modulus (dimensionless)

$k_2 = \left(\dfrac{\mu_{max} \, x_b}{Y_{x/s} \, k_s \, D_e} \right)^{\frac{1}{2}}$ (L^{-1})

D_e = effective diffusion coefficient of glucose in the biofilm ($L^2 t^{-1}$)

$k_2 \, Th$ = dimensionless thickness (dimensionless)

$k_3 = 1/k_s$ ($L^3 M_s^{-1}$)

$k_3 \, s$ = dimensionless substrate concentration (dimensionless)

The Atkinson model assumes that growth coefficients determined from dispersed growth cultures (μ_{max}, k_s, $Y_{x/s}$) are valid for biofilm growth. This assumption has also been made by Rittman and McCarty (1980, 1981)

in their modeling work. Evidence supporting this assumption has not been presented in the literature.

Equation (33) of the Atkinson model can be rearranged to obtain an expression which is useful for calculating specific cellular growth rate in the biofilm. Rewriting equation (33), the rearrangement is as follows:

$$N_b = \lambda \frac{\mu_{max}\, x_b\, Th\, s}{Y_{x/s}\,(k_s + s)} \qquad (33)$$

Multiplying both sides of equation (33) by $Y_{x/s}/x_b Th$ results in the following:

$$\frac{Y_{x/s}\, N_b}{x_b\, Th} = \lambda \frac{\mu_{max}\, s}{k_s + s} \qquad (t^{-1})$$

The left side of this equation is equal to specific cellular growth rate in the biofilm, μ_b. Substituting,

$$\mu_b = \lambda \frac{\mu_{max}\, s}{k_s + s} \qquad (34)$$

Biofilm Diffusion and Specific Cellular Growth Rate in the Biofilm

Results obtained in this study suggest that based on liquid phase substrate concentration, specific cellular growth rate in the biofilm (μ_b) is not significantly different than specific cellular growth rate in dispersed growth chemostat culture (μ). In equation form this relation is expressed as follows:

$$\mu_b = \mu = \frac{\mu_{max}\, s}{k_s + s} \qquad (35)$$

Comparison of this equation with equation (34) obtained from the Atkinson model indicates that the only condition under which these two equations are equal is for the condition of negligible biofilm diffusional resistance (i.e., $\lambda = 1$).

The extent of biofilm diffusional resistance in this study can be demonstrated by calculating λ for each AR experiment. Since the Atkinson model does not explicitly account for polymer formation, the Atkinson rate coefficient k_2 is redefined as follows:

$$k_2 = \left(\left(\frac{\mu_{max} X_b}{k_s D_e}\right)\left(\frac{1}{Y_{x/s}} + \frac{k}{Y_{p/s}} + \frac{k'}{\mu_{max} Y_{p/s}}\right)\right)^{\frac{1}{2}} \quad (L^{-1})$$

Figure 23 is a plot of λ for the biofilm experiments. The biofilm experimental data used to calculate λ are shown in Figures 24, 25 and 26. It is apparent from the data in Figure 23 that biofilm diffusional resistance in this study was minimal and that glucose carbon concentration in the biofilm was not significantly different from glucose carbon concentration in the bulk liquid.

This result is contrary to results in the literature since biofilm diffusional resistance is usually reported to be significant. An explanation for the apparent disagreeement between results reported in this and other studies is obtained by consideration of biofilm thickness and cellular density in the biofilm.

Maximum biofilm thickness in this study was usually in the range of 30 μm (Figure 25). Cellular carbon density in the biofilm never exceeded 30 mg/cm^3 (Figure 26). Table 11 lists biofilm thickness and biofilm density values reported in biofilm diffusion literature. It is

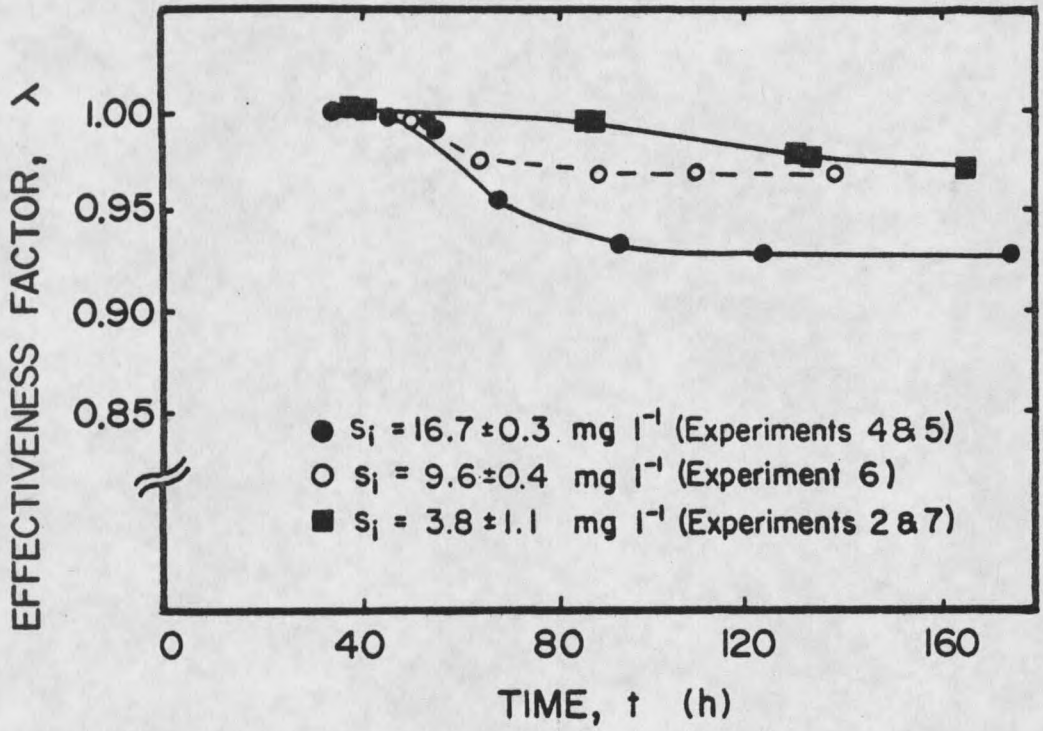

Figure 23. Change in Effectiveness Factor With Time.

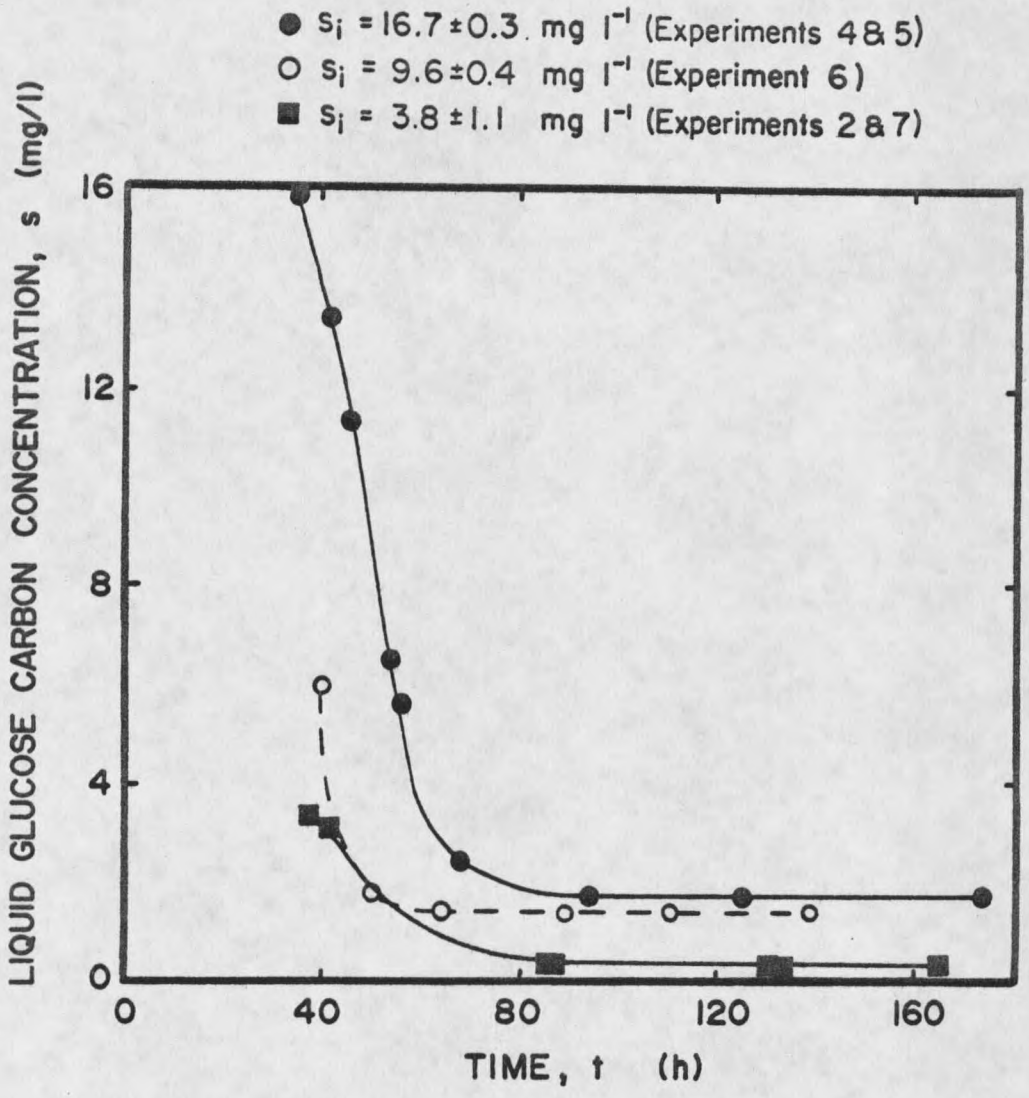

Figure 24. Change in Glucose Carbon Concentration With Time (Time Smoothed Data).

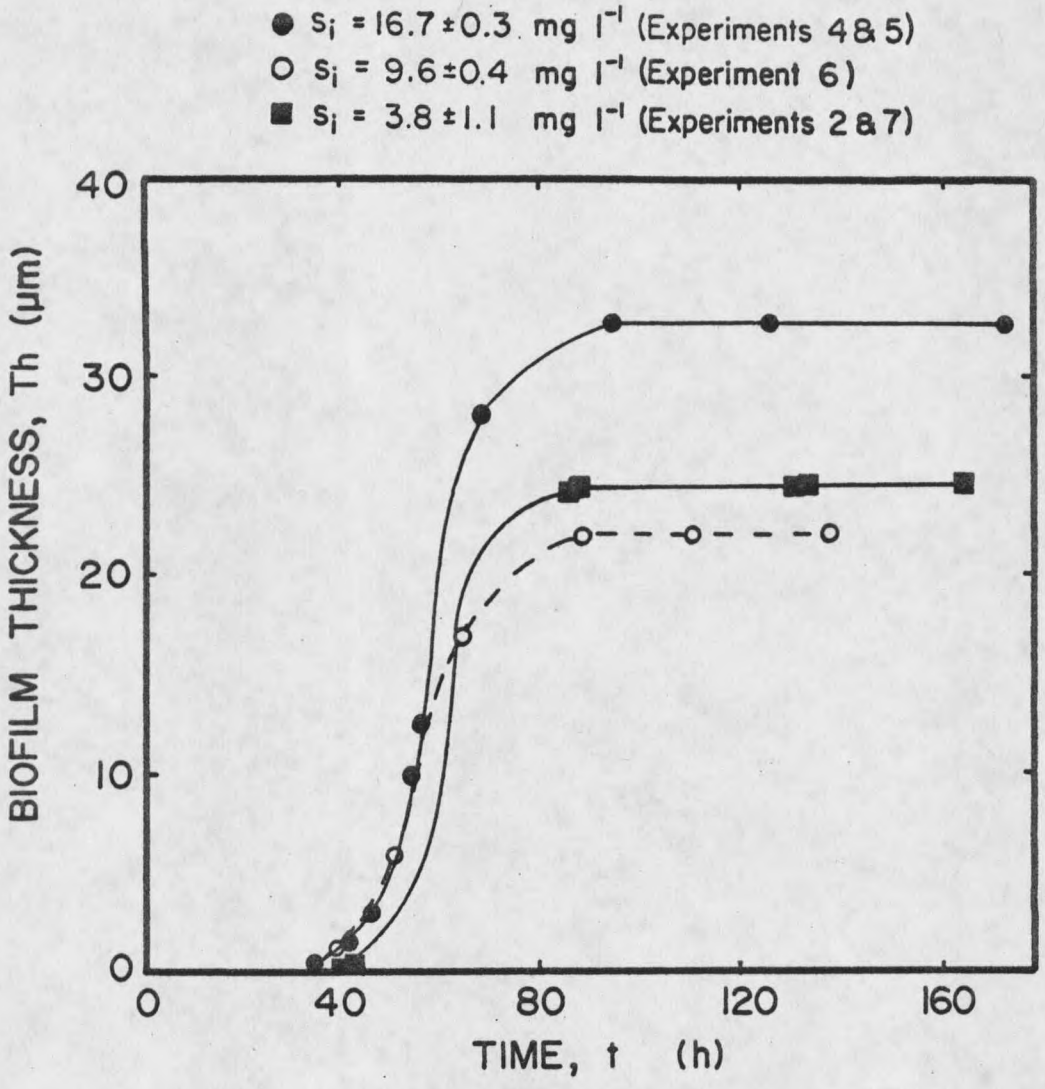

Figure 25. Change in Biofilm Thickness With Time (Time Smoothed Data).

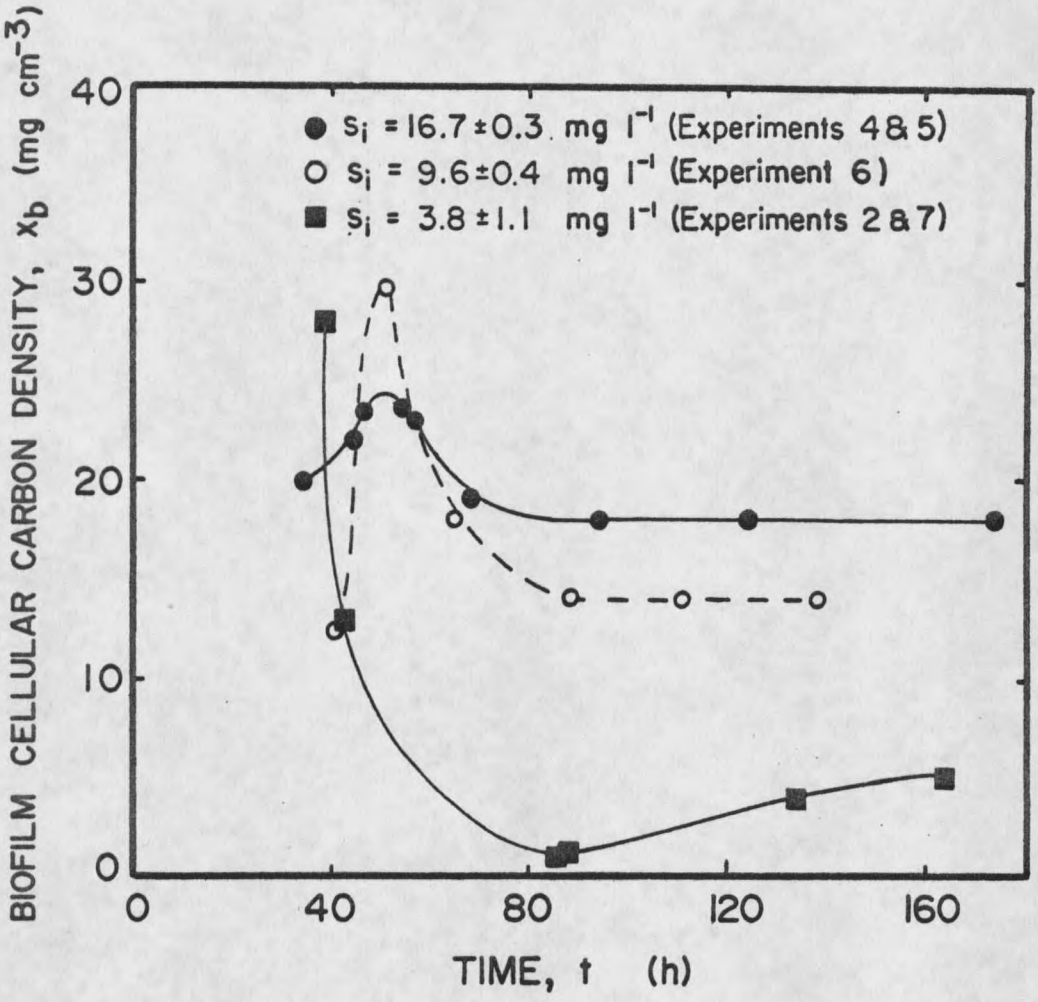

Figure 26. Change in Biofilm Cellular Carbon Density With Time (Cellular Carbon Density Calculated Using Time Smoothed Data in Figures 11 and 25).

TABLE 11

Biofilm Thickness and Biofilm Density Reported in Biofilm Diffusion Literature

Biofilm Thickness (μm)	Biofilm Density (mg/cm^3)	Type of Biofilm	Reference
160 - 210	66 - 130[a]	A	Kornegay and Andrews (1967)
30 - 1300	20 - 105[a]	B	Hoehn and Ray (1973)
150 - 580	42 - 109[a]	C	Williamson and McCarty (1976)
2 - 583	-	B	Lamotta (1976a)
100	40[b]	A	Rittman and McCarty (1978)
119 - 226	2.5[c]	B	Rittman and McCarty (1980)
0 - 125	2.5[c]	B	Rittman and McCarty (1981)
10 - 124	10 - 65[a]	B	Trulear and Characklis (1982)

a total mass density (total dry mass per wet volume)
b volatile mass density (volatile dry mass per wet volume)
c cellular carbon mass density (cellular carbon mass per wet volume)

A steady state, heterotrophic, mixed culture
B heterotrophic, mixed culture
C steady state, nitrifying, dual culture

apparent from the data in Table 11 that the majority of the biofilms in these studies were considerably thicker and denser than the biofilms observed in this study. These factors undoubtedly contribute to the differences in biofilm diffusional resistance between this and other studies.

Two additional points should be made. First, the majority of the literature have not distinguished between cellular and total density in the biofilm. Hence biofilm diffusional resistance may have been overestimated in many of these studies due to an unrealistic representation of cellular density in the biofilm.

Secondly, this is the only study which has used pure culture biofilms. Hence the species composition of the biofilms was defined and remained constant with time. In mixed culture biofilms, species population shifts are known to occur (Marshall, 1976; Corpe, 1978; Trulear and Characklis, 1982), however the effect of such changes on biofilm diffusion is not known and hence has not been accounted for in previous diffusion studies.

Extracellular Polymer Formation

Extracellular polymer formation by the Ps. aeruginosa strain used in this study depends on both the growth rate of the organism and on the quantity of Ps. aeruginosa present, i.e., extracellular polymer formation is both growth- and nongrowth-associated. These results agree with data reported by Mian et al. (1978) which also indicate growth- and nongrowth-associated polymer formation by Ps. aeruginosa.

Polymer Formation Rate Coefficients

Growth- and nongrowth-associated polymer formation rate coefficients determined in this study are reported in Table 12 along with coefficients from the Mian et al. (1978) study. Data used to calculate the Mian et al. coefficients are shown in Figure 27. Figure 17 illustrates the corresponding chemostat data from this investigation.

The data in Table 12 and Figures 17 and 27 indicate that extracellular polymer formation in the Mian et al. (1978) study was significantly greater than extracellular polymer formation in this investigation. The Mian et al. data were collected under nitrogen limitation in an effort to maximize extracellular polymer formation. Furthermore, influent glucose concentration in the Mian et al. study was greater than two orders of magnitude higher than influent glucose concentration used in this study (Table 12). These differences in substrate solution, in addition to possible differences in Ps. aeruginosa strain, undoubtedly contribute to the higher degree of polymer formation observed in the Mian et al. study.

Effect of Glucose Concentration

The observed differences in the polymer formation rate coefficients from this study suggest that influent glucose concentration has a significant influence on Ps. aeruginosa extracellular polymer formation. Growth environment (dispersed vs attached) may also exert an influence, however, it is felt that glucose concentration has a greater influence since the chemostat polymer formation rate coefficients are within the range of the biofilm rate coefficients (Table 12).

TABLE 12

Growth- and Nongrowth-Associated Polymer Formation Rate Coefficients

Reactor and Exp # or Reference	Influent Glucose Carbon Concentration, s_i (mg/l)	Growth-Associated Rate Coefficient, k or k_b (mg polymer carbon/ mg cellular carbon)	Nongrowth-Associated Rate Coefficient, k' or k'_b (mg polymer carbon/ mg cellular carbon h)
Chemostat 1-8	36.8 ± 2.3	0.36 ± 0.44[a]	0.03 ± 0.10[a]
AR 2 & 7	3.8 ± 1.1	1.0 ± 0.86[a]	0.25 ± 0.36[a]
AR 6	9.6 ± 0.4	0.01 ± 0.14[a]	0.09 ± 0.04[a]
AR 4 & 5	16.7 ± 0.3	0.02 ± 0.13[a]	0.01 ± 0.03[a]
Mian et al. (1978)	20.5[b]	3.29	0.12

[a] 95% confidence interval

[b] gm/l instead of mg/l

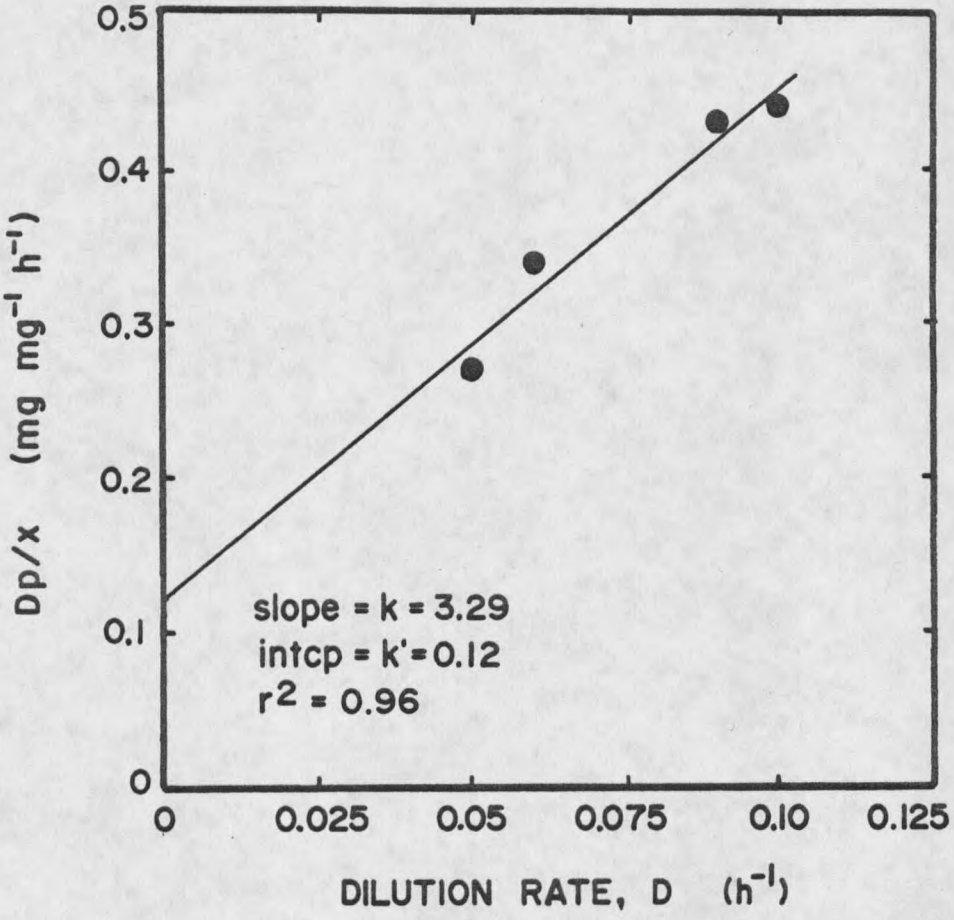

Figure 27. Determination of Growth- and Nongrowth-Associated Polymer Formation Rate Coefficients for Mian et al. (1978).

Reference to Figures 11, 12, and 24 suggests that, in addition to influent glucose concentration, reactor glucose concentration may also have an influence on Ps. aeruginosa extracellular polymer formation. These figures indicate that at high glucose concentration, polymer formation was minimal. However at low glucose concentration, polymer formation was significant and usually resulted in polymer carbon areal density exceeding cellular carbon areal density.

Since influent glucose concentration determines reactor glucose concentration, it is not clear whether the apparent effect of influent concentration may actually be due to reactor glucose concentration. In either case, the relation between glucose concentration and extracellular polymer formation is not clearly understood.

It is apparent that Ps. aeruginosa extracellular polymer formation increases at low glucose, however further research is required to fully understand the trends observed.

Cellular and Polymer Yield Coefficients

Stoichiometric Model

The cellular and polymer yield coefficients determined in this study are based on the following stoichiometric model:

$$\alpha \text{ glucose carbon} \rightarrow \beta \text{ cellular carbon} \qquad (36)$$

$$\kappa \text{ glucose carbon} \rightarrow \omega \text{ polymer carbon} \qquad (37)$$

where α, β, κ, and ω are stoichiometric coefficients defined as follows:

α = cellular glucose distribution coefficient (dimensionless)

β = inverse of cellular yield coefficient, $Y_{x/s}^{-1}$ ($M_s M_x^{-1}$)

κ = polymer glucose distribution coefficient (dimensionless)

ω = inverse of polymer yield coefficient, $Y_{p/s}^{-1}$ ($M_s M_p^{-1}$)

α and κ represent the fraction of glucose carbon utilized by the cell for cellular reproduction and extracellular polymer formation, respectively. β ($Y_{x/s}^{-1}$) and ω ($Y_{p/s}^{-1}$) represent the quantity of cellular and polymer carbon formed per unit quantity of glucose carbon utilized for either cellular reproduction or extracellular polymer formation. Diagrammatically, these coefficients can be illustrated as follows:

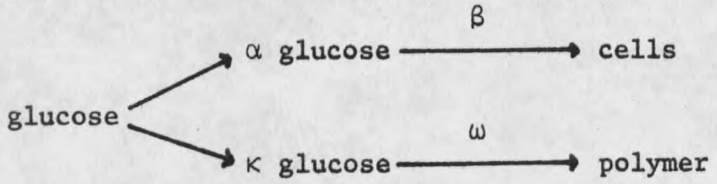

where $\alpha + \kappa = 1$

Cellular Yield Coefficients

Table 13 contains the cellular yield coefficients determined in this study along with Ps. aeruginosa yield coefficients reported in the literature. The literature yield coefficients were all determined from dispersed growth batch cultures and are based on suspended solids concentration. Since a distinction between cellular and extracellular "solids" was not made in the literature studies, the literature yield coefficients tend to be higher than the cellular yield coefficients obtained in this study.

TABLE 13

Pseudomonas aeruginosa Cellular Yield Coefficients

Reactor and Exp #	Cellular Yield Coefficient, $Y_{x/s}$ or $Y_{xb/s}$ (mg cellular carbon/ mg glucose carbon)	Literature Yield Coefficient (mg cellular carbon/ mg glucose carbon)	Reference
Chemostat 1-8	0.36 ± 0.39[a]	-	-
AR 2 & 7	0.29 ± 0.44[a]	-	-
AR 6	0.22 ± 0.14[a]	-	-
AR 4 & 5	0.24 ± 0.29[a]	-	-
-	-	0.54[b]	Mackechnie and Dawes (1969)[c]
-	-	0.49[b]	Mano and Dawes (1969)[c]
-	-	0.33[b]	Ribbons (1969)[c]

[a] 95% confidence intervals

[b] calculated assuming 0.5 mg cellular carbon/mg dry mass and 0.4 mg glucose carbon/mg glucose (see METHODS)

[c] references reported by Payne (1970)

The cellular yield coefficients determined in this study suggest that cellular yield in the chemostat experiments is slightly higher than cellular yield in the biofilm experiments. However, the small differences in chemostat and biofilm cellular yield are considered insignificant due to the experimental errors (Table 13) inherent in the determination of these coefficients.

Polymer Yield Coefficients

The polymer yield coefficients determined in this study are shown in Table 14. Polymer yield for Ps. aeruginosa has not been reported previous to this study. Mian et al. (1978) also studied extracellular polymer formation by Ps. aeruginosa but only report the polymer conversion efficient, η. η is defined as follows:

$$\eta = \frac{\text{polymer formed}}{\text{total glucose consumed}} \qquad (38)$$

Polymer conversion efficiency is an "apparent" yield since it does not account for glucose consumed for cellular reproduction. Polymer yield as defined in this study is a more fundamental stoichiometric coefficient since it is based on glucose consumed solely for polymer formation.

Table 15 contains polymer conversion efficiencies reported in the Mian et al. (1978) study along with conversion efficiencies from this study. These data indicate that η from the Mian et al. study generally exceeded η from this study. As discussed previously, differences in extracellular polymer formation between this and the Mian et al. study

TABLE 14

Pseudomonas aeruginosa Polymer Yield Coefficients

Reactor and Exp #	Influent Glucose Concentration, s_i (mg/l)	Polymer Yield Coefficient, $Y_{p/s}$ or $Y_{pb/s}$ (mg polymer carbon/ mg glucose carbon)
Chemostat 1-8	36.8 ± 2.3	0.50 ± 1.8[a]
AR 2 & 7	3.8 ± 1.1	0.93 ± 3.5[a]
AR 6	9.6 ± 0.4	0.33 ± 1.1[a]
AR 4 & 5	16.7 ± 0.3	0.04 ± 0.18[a]

[a] 95% confidence interval

TABLE 15

Pseudomonas aeruginosa Polymer Conversion Efficiencies

Reference	Reactor and Exp #	Polymer Conversion Efficiency, η (mg polymer carbon/ mg total glucose carbon)
Mian *et al.* (1978)[a]	-	0.61 ± 0.06[c]
Mian *et al.* (1978)[b]	-	0.33
-	Chemostat 1-8	0.17 ± 0.07[c]
-	AR 2 & 7	0.34 ± 0.10[c]
-	AR 6	0.13 ± 0.08[c]
-	AR 4 & 5	0.01 ± 0.01[c]

[a] nitrogen limited chemostat, D = 0.05 - 0.10 h^{-1}

[b] carbon limited chemostat, D = 0.05

[c] 95% confidence interval

are attributed to differences in substrate solution and to possible differences in Ps. aeruginosa strain.

Data from this study (Table 14) indicate that there is an effect of experimental conditions on polymer yield coefficient. This is consistent with variations discussed previously for the growth- and nongrowth-associated polymer formation rate coefficients.

The wide variation in the polymer yield coefficients is not understood, particularily the extremely low value obtained in AR experiment 4-5. Since extracellular polymer composition was not determined, some of the variation in polymer yield may be indicative of variations in extracellular polymer composition.

The literature indicates that under laboratory conditions, mucoid strains of Ps. aeruginosa frequently mutate to non-mucoid forms (Govan, 1975; Mian et al., 1978; Costerton, 1981). Non-mucoid colonies were not detected in the biofilm experiments of this study. Hence the wide variations in polymer yield are not attributed to Ps. aeruginosa mutation. Non-mucoid Ps. aeruginosa colonies were occasionally detected during chemostat experiments. Whenever this occurred the experiments were considered contaminated and were repeated (see METHODS).

Cellular and Polymer Distribution Coefficients

The cellular and polymer glucose distribution coefficients, α and κ, can be determined by rearranging equations (36) and 37) as follows:

$$\alpha = \frac{\text{cellular carbon produced}}{Y_{x/s} \cdot \text{total glucose carbon utilized}} \qquad (36)$$

$$\kappa = \frac{\text{polymer carbon produced}}{Y_{p/s} \cdot \text{total glucose carbon utilized}} \quad (37)$$

These equations are expressed separately for the chemostat and AR reactors as follows:

a. chemostat reactors

$$\alpha_c = \frac{\bar{x}}{Y_{x/s}(s_i - \bar{s})} \quad (40)$$

$$\kappa_c = \frac{\bar{p}}{Y_{p/s}(s_i - \bar{s})} \quad (41)$$

b. annular reactors

$$\alpha_b = \frac{R_{xb}}{Y_{xb/s}(r_{gb} \quad x_b^*)} \quad (42)$$

$$\kappa_b = \frac{R_{pb}}{Y_{pb/s}(r_{gb} \quad x_b^*)} \quad (43)$$

Figure 28 is a plot of the ratio κ/α as a function of specific cellular growth rate for the chemostat experiments and for three of the biofilm experiments. This figure indicates that the fraction of glucose distributed by Ps. aeruginosa for extracellular polymer formation and cellular reproduction is not constant and that the ratio of κ/α appears to be related to specific cellular growth rate. This suggests that κ and α are under some level of "physiological control" and that these stoichiometric coefficients change depending on the physiological state of Ps. aeruginosa.

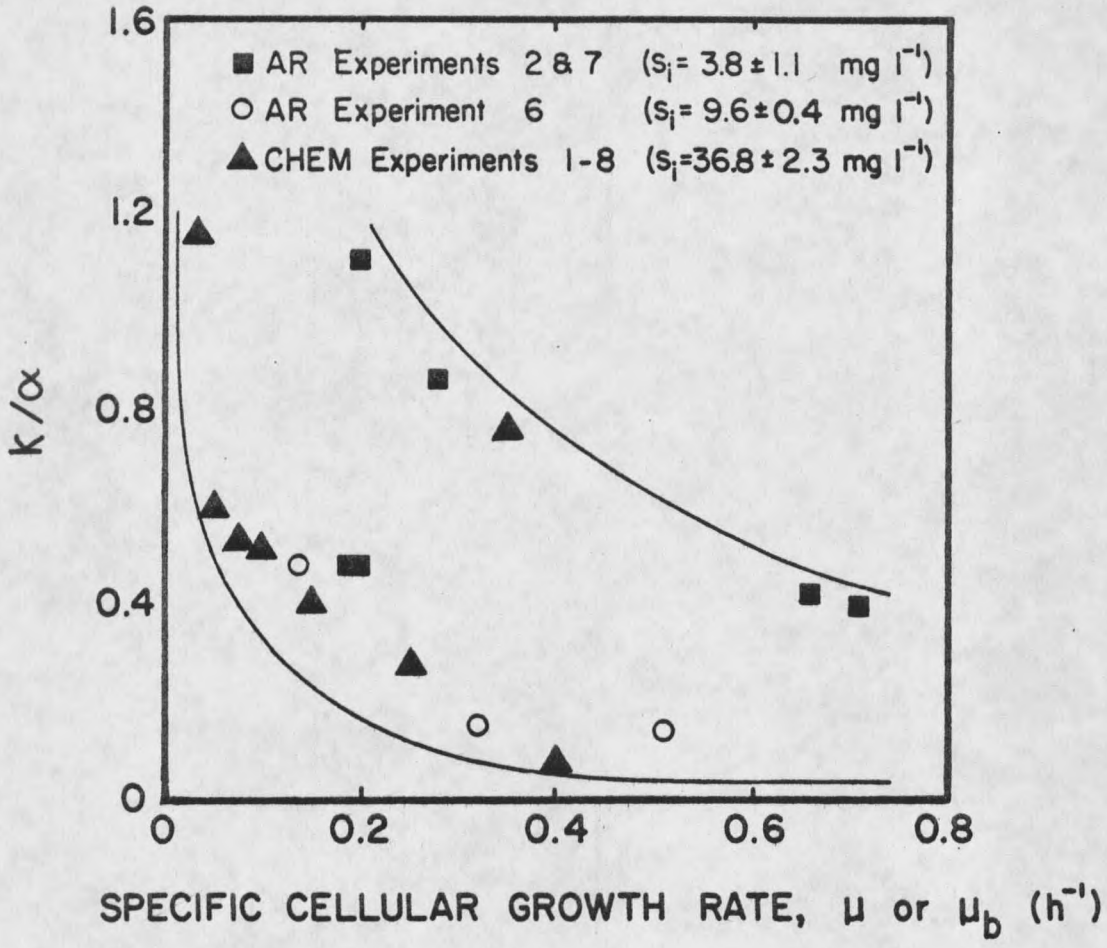

Figure 28. Ratio of Polymer and Cellular Distribution Coefficients as a Function of Specific Cellular Growth Rate.

The apparent relation between κ/α and specific cellular growth rate suggest that at low growth rate (i.e., low glucose concentration), a greater proportion of the available glucose is used for extracellular polymer formation than for cellular reproduction. Whereas at high growth rate (i.e., high glucose concentration), a greater proportion of the glucose is used for cellular reproduction.

It is interesting to speculate whether these results are also true for other extracellular polymer forming organisms which are usually found in biofilm communities. As discussed in the second chapter of this manuscript, biofims are frequently found in low nutrient environments. Since biofilms are composed primarily of extracellular polymer material the trend presented in Figure 28 may also be applicable to other organisms commonly found in biofilms.

CONCLUSIONS

The purpose of this study was to investigate the kinetics and stoichiometry of cellular reproduction and extracellular polymer formation in the development of biofilms.

Based on pure culture experiments with Ps. aeruginosa, the following conclusions are derived:

1. Ps. aeruginosa cellular reproduction follows Monod-type saturation kinetics.
2. Monod coefficients determined from dispersed growth chemostat reactors (μ_{max} and k_s) also describe the rate of Ps. aeruginosa cellular reproduction in biofilms.
3. The stoichiometry of Ps. aeruginosa cellular reproduction in dispersed growth chemostat reactors is not significantly different from the stoichiometry of Ps. aeruginosa cellular reproduction in biofilms.
4. Substrate diffusional resistance in Ps. aeruginosa biofilms (biofilm thickness less than 35 μm) is negligible. Hence, biofilm substrate concentration is not significantly different from substrate concentration in the bulk liquid phase.
5. Ps. aeruginosa extracellular polymer formation is growth- and nongrowth-associated, i.e., the rate and extent of extracellular polymer formation depend on both the growth

rate of the organism and on the quantity of Ps. aeruginosa present.

6. Rate and stoichiometric coefficients which describe Ps. aeruginosa extracellular polymer formation in dispersed growth chemostat reactors do not agree with corresponding coefficients which describe extracellular polymer formation by Ps. aeruginosa in biofilms.

7. The relative contributions of cellular reproduction and extracellular polymer formation to overall biofilm development depend on the growth rate of Ps. aeruginosa. At low growth rates (low substrate concentration), extracellular polymer formation contributes most significantly and the resulting biofilm is composed primarily of extracellular polymer. However at high growth rates (high substrate concentration), cellular reproduction contributes most significantly to the overall development and the resulting biofilm is composed of more cellular carbon than extracellular carbon.

RECOMMENDATIONS

A relatively simple methodology has been developed for quantitatively studying cellular reproduction and extracellular polymer formation in biofilms. Results obtained indicate that the relative importance of reproduction and polymer formation in the overall development of a biofilm strongly depend on the growth rate of the organism present.

Since the experiments reported herein were conducted solely with Ps. aeruginosa, similar studies need to be conducted to determine the effect of growth rate on the polymer-forming characteristics of other organisms commonly found in biofilms. The effect of different substrates should also be investigated.

Results from further studies could have important practical applications, particularly in the area of biofilm control.

As discussed in the first chapter of this manuscript, the most common method of controlling biofilm development is through periodic chlorination. However, the use of chlorine for biofilm control has come under increasingly critical environmental scrutiny due to harmful effects of chlorine and its reaction products when introduced into natural ecosystems.

Since biofilms are commonly found in systems characterized by low nutrient conditions, the results from this study suggest that a more environmentally acceptable method of biofilm control may be achieved by

developing control strategies directed towards controlling extracellular polymer formation. However, prior to investigating practical applications such as control strategy, the broad range applicability of the results obtained in this study must first be determined using biofilm organisms other than Ps. aeruginosa and substrate components other than glucose.

REFERENCES CITED

REFERENCES CITED

1. Atkinson, B., and Daoud, I.S., "Diffusion Effects Within Microbial Films," Transactions, Institution of Chemical Engineers, Vol. 48, 1970, pp. T245-T254.

2. Atkinson, B., and Davies, I.J., "The Overall Rate of Substrate Uptake by Microbial Films. Part I - A Biological Rate Equation," Transactions, Institute of Chemical Engineers, Vol 52, 1974, pp. 248-259.

3. Baier, R.E., "Applied Chemistry at Protein Interfaces," Applied Chemistry at Protein Interfaces, R.E. Baier, ed., American Chemical Society, Advances in Chemistry Series 145, Washington, D.C., 1975, pp. 1-25.

4. Baier, R.E., and Depalma, V.A., "Microfouling of Metallic and Coated Metallic Flow Surfaces in Model Heat Exchanger Cells," Calspan Corporation Report, Buffalo, NY, 1977.

5. Brock, T.D., Biology of Microorganisms, 3rd edition, Prentice Hall, Inc., Englewood Cliffs, NJ, 1979, p. 44.

6. Bryers, J.D., "Rates of Initial Biofouling in Turbulent Flow Systems," Ph.D. Dissertation, Rice University, Houston, TX, 1980.

7. Buchanan, R.E., and Gibbons, N.E., Bergey's Manual of Determinative Bacteriology, 8th edition, The Williams and Wilkins Co., Baltimore, 1974, pp. 221-222.

8. Characklis, W.G., "Microbial Reaction Rate Expressions," Journal of the American Society of Civil Engineering-Sanitary Engineering Division, Vol. 104, No. EE3, June 1978, pp. 531-534.

9. Characklis, W.G., "Fouling Biofilm Development: A Process Analysis," Biotechnology and Bioengineering, Vol. 23, 1981, pp. 1923-1960.

10. Characklis, W.G., and Dydek, S.T., "The Influence of Carbon-Nitrogen Ratio on the Chlorination of Microbial Aggregates," Water Research, Vol. 10, 1976, pp. 515-522.

11. Characklis, W.G., Nimmons, M.J., and Picologlou, B.F., "Influence of Fouling Biofilms on Heat Transfer," J. Heat Transfer Eng., Vol. 3, No. 1, 1981, pp. 23-37.

12. Clark, D.J., "Regulation of Deoxyribonucleic Acid Replication and Cell Division in *Escherichia coli*, Journal of Bacteriology, Vol. 96, 1968, pp. 1214-1224.

13. Corpe, W.A., "An Acidic Polysaccharide Produced by a Primary Film-Forming Marine Bacterium," Developments in Industrial Microbiology, Vol. 11, 1970, pp. 402-412.

14. Corpe, W.A., "Ecology of Microbial Attachment and Growth on Solid Surfaces," Proc. Microbiology of Power Plant Effluents, R.M. Gerhold, ed., University of Iowa, Iowa City, IA, 1978, pp. 57-66.

15. Costerton, J.W., "*Pseudomonas aeruginosa* in Nature and Disease," Proc. *Pseudonomas aeruginosa* International Symposium, L.D. Sabath, ed., Boston, MA, 1979, pp. 15-24.

16. Costerton, J.W., and Geesey, G.G., "Microbial Contamination of Surfaces," Surface Contamination, Vol. 1, K.L. Mittal, ed., Plenum Publishing Corp., New York, 1979, pp. 211-221.

17. Costerton, J.W., Geesey, G.G., and Cheng, K.J., "How Bacteria Stick," Scientific American, Vol. 238, No. 1, Jan. 1978, pp. 86-95.

18. Costerton, J.W., Irvin, R.T., and Cheng, K.J., "The Bacterial Glycocalyx in Nature and Disease," Ann. Rev. Microbiol., 1981, pp. 299-324.

19. Dharmarajan, R., Unpublished Results, 1981.

20. Doetsch, R.N., and Cook, T.M., Introduction to Bacteria and Their Ecology, University Park Press, Baltimore, 1973.

21. Evans, L.R., and Linker, A., "Production and Characterization of the Slime Polysaccharide of *Pseudomonas aeruginosa*," Journal of Bacteriology, Vol. 116, No. 2, Nov. 1973, pp. 915-924.

22. Fletcher, M., and Floodgate, G.D., "An Electron-microscopic Demonstration of an Acidic Polysaccaride in the Adhesion of a Marine Bacterium to Solid Surfaces," Journal of General Microbiology, Vol. 74, 1973, pp. 325-334.

23. Geesey, G.G., "Microbial Exopolymers: Ecological and Economic Considerations," ASM News, Vol. 48, No. 1, 1982, pp. 9-14.

24. Geesey, G.G., Mutch, R., Costerton, J.W., and Green, R.B., "Sessile Bacteria: An Important Component of the Microbial Population in Small Mountain Streams," Limnol. Oceanogr., Vol. 23, No. 6, Nov. 1978, pp. 1214-1223.

25. Govan, J.R.W., "Mucoid Strains of *Pseudomonas aeruginosa*: The Influence of Culture Medium on the Stability of Mucus Production," Journal Medical Microbiology, Vol. 8, 1975, pp. 513-522.

26. Grady, C.P.L., Jr., "Modeling of Biological Fixed Films-A State of the Art Review," Proc. First International Conference on Fixed-Film Biological Processes, April 20-23, 1982, Kings Island, OH, pp. 90-118.

27. Haack, T.K., and McFeters, G.A., "Nutritional Relationships Among Microorganisms in a Epilithic Biofilm Community," Microbial Ecology, Vol. 8, 1982, pp. 115-126.

28. Harremoës, P., "Biofilm Kinetics," Water Pollution Microbiology, Vol. 2, R. Mitchell, ed., John Wiley and Sons, New York, 1978, pp. 71-190.

29. Harris, N.P., and Hansford, G.S., "A Study of Substrate Removal in a Microbial Film Reactor," Water Research, Vol, 10, 1976, pp. 935-943.

30. Hobbie, J.E., Daley, R.J., and Jasper, S., "Use of Nuclepore Filters for Counting Bacteria by Fluorescence Microscopy," Applied and Environmental Microbiology, Vol. 33, No. 5, May 1977, pp. 1225-1228.

31. Hoehn, R.C., and Ray, A.D., "Effects of Thickness on Bacterial Film," Journal of the Water Pollution Control Federation, Vol. 45, Nov. 1973, pp. 2302-2320.

32. Howell, J.A., and Atkinson, B., "Sloughing of Microbial Film in Trickling Filters," Water Research, Vol. 10, 1976, pp. 307-315.

33. Iverson, W.P., "Biological Corrosion," Advances in Corrosion Science and Technology, Vol. 2, M. Fontana and R.W. Staehle, eds., Plenum Press, New York, 1972.

34. Jenkins, D., "Activated Sludge Floc Structure and Its Relation to Process Performance," National Science Foundation Final Report, Project No. CME-7684422, Department Civil Engineering, University of California, Berkley, CA, July 1980.

35. Klimek, J., and Ollis, D.F., "Extracellular Microbial Polysaccharides: Kinetics of *Pseudomonas* sp., *Azotobacter vinelandii*, and *Aureobasidium pullulans* Batch Fermentations,"

Biotechnology and Bioengineering, Vol. 22, 1980, pp. 2321-2342.

36. Kornegay, B.H., and Andrews, J.F., "Characteristics and Kinetics of Biological Film Reactors," Federal Water Pollution Control Administration Final Report, Research Grant WP-01181, Department of Environmental Systems Engineering, Clemson University, Clemson, SC, 1967.

37. Lamotta, E.J., "Kinetics of Growth and Substrate Uptake in a Biological Film System" Applied and Environmental Microbiology, Vol. 31, No. 2, Feb. 1976a, pp. 286-293.

38. Lamotta, E.J., "External Mass Transfer in a Biological Film Reator," Biotechnology and Bioengineering, Vol. 18, 1976b, pp. 1359-1370.

39. Loeb, G.I., and Neihof, R.A., "Marine Conditioning Films," Applied Chemistry at Protein Interfaces, R.E. Baier, ed., American Chemical Society, Advances in Chemistry Series 145, Washington, D.C., 1975, pp. 319-335.

40. Luedeking, R., and Piret, E.L., "A Kinetic Study of the Lactic Acid Fermentation-Batch Processes at Controlled pH," J. of Biochemical and Microbiological Technology and Engineering, Vol. 1, No. 4, 1959, pp. 393-412.

41. Luria, S.E., "The Bacterial Protoplasm: Composition and Organization," The Bacteria, Vol. 1, I.C. Gunsalus and R.Y. Stainer, eds., Academic Press Inc., New York, 1960.

42. Mackechnie, I., and Dawes, E.A., "An Evaluation of the Pathways of Metabolism of Glucose, Gluconate, and 2-Oxogluconate by *Pseudomonas aeruginosa* by Measurement of Molar Growth Yields," Journal of General Microbiology, Vol. 55, 1969, pp. 341-349.

43. Maier, W.J., Behn, V.C., and Gates, C.D., "Simulation of the Trickling Filter Process," Journal of the American Society of Civil Engineering-Sanitary Engineering Division, Vol. 93, Aug. 1967, pp. 91-112.

44. Marshall, K.C., Interfaces in Microbial Ecology, Harvard University Press, Cambridge, MA, 1976.

45. Marshall, K.C., Stout, R., and Mitchell, R., "Mechanism of the Initial Events in the Sorption of Marine Bacteria to Surfaces," Journal of General Microbiology, Vol. 68, 1971, pp. 337-348.

46. Matin, A., Grootjans, A., and Hogenhuis, H., "Influence of Dilution Rate on Enzymes of Intermediary Metabolism in Two Freshwater Bacteria Grown in Continuous Culture," Journal of General Microbiology, Vol. 94, 1976, pp. 123-130.

47. Mian, F.A., Jarman, T.R., and Righelato, R.C., "Biosynthesis of Exopolysaccaride by *Pseudomonas aeruginosa*," Journal of Bacteriology, Vol. 134, May 1978, pp. 418-422.

48. Monod, J., "The Growth of Bacterial Cultures," Annual Review of Microbiology, Vol. 3, 1949, pp. 371-394.

49. Payne, W.J., "Energy Yields and Growth of Heterotrophs," Annual Review of Microbiology, Vol. 24, C.E. Clifton, ed., Annual Reviews Inc., Palo Alto, CA, 1970, pp. 17-51.

50. Picologlou, B.F., Zelver, N., and Characklis, W.G., "Biofilm Growth and Hydraulic Performance," Journal of the American Society of Civil Engineering-Hydraulics Division, Vol. 106, No. HY5, May 1980, pp. 733-746.

51. Rittman, B.E., and McCarty, P.L., "Variable Order Model of Bacterial Film Kinetics," Journal of the American Society of Civil Engineering-Environmental Engineering Division, Vol. 104, No. EE5, Oct. 1978, pp. 889-900.

52. Rittman, B.E., and McCarty, P.L., "A Model of Steady State Biofilm Kinetics," Biotechnology and Bioengineering, Vol. 22, No. 11, 1980, pp. 2343-2357.

53. Rittmann, B.E., and McCarty, P.L., "Substrate Flux into Biofilms of any Thickness," Journal of the American Society of Civil Engineering-Environmental Engineering Division, Vol. 107, No. EE4, Aug. 1981, pp. 831-848.

54. Roels, J.A., and Kossen, N.W.F., "On the Modeling of Microbial Metabolism," Progresses in Industrial Microbiology, M.J. Bull, ed., Vol. 14, 1978, pp. 95-203.

55. Sanders, W.M., 3rd, "The Relationship Between the Oxygen Utilization of Heterotrophic Slime Organisms and the Wetted Perimeter," Ph.D. Dissertation, The Johns Hopkins University, Baltimore, MD, 1964.

56. Sanders, W.M., 3rd, Bungay, H.R., 3rd, and Whalen, W.J., "Oxygen Microprobe Studies of Microbial Slime Films," Chemical Engineering Symposium Series, Vol. 67, No. 107, 1970, pp. 69-74.

57. Shehata, T.E., and Marr, A.G., "Effect of Nutrient Concentration on the Growth of *Escherichia coli*," Journal of Bacteriology, Vol. 107, No. 1, July 1971, pp. 210-216.

58. Stanier, R.Y., Adelberg, E.A., and Ingraham, J.L., The Microbial World, 4th ed., Prentice Hall, Inc., Englewood Cliffs, NJ, 1976.

59. Tam, K.T., and Finn, R.K., "Polysaccharide Formation by a *Methylomonas*," Extracellular Microbial Polysaccharides, P.A. Sandford and A. Laskin, eds., American Chemical Society, Symposium Series 45, Washington, D.C., 1977, pp. 58-80.

60. Tomlinson, T.G., and Snaddon, D.H.M., "Biological Oxidation of Sewage by Films of Microorganisms," International Journal of Air and Water Pollution, Vol. 10, 1966, pp. 865-881.

61. Trulear, M.G., and Characklis, W.G., "Dynamics of Biofilm Processes," Journal of The Water Pollution Control Federation, Vol. 54, No. 9, Sept. 1982, pp. 1288-1300.

62. Weiss, R.M., and Ollis, D.F., "Extracellular Microbial Polysaccharides. I. Substrate, Biomass, and Product Kinetic Equations for Batch Xanthan Gum Fermentation," Biotechnology and Bioengineering, Vol. 22, 1980, pp. 859-873.

63. Williams, A.G., and Wimpenny, J.W.T., "Exopolysaccharide Production by *Pseudomonas* NCIB11264 Grown in Continuous Culture," Journal of General Microbiology, Vol. 104, 1978, pp. 47-57.

65. Zelver, N., "Biofilm Development and Associated Energy Losses in Water Conduits," M.S. Thesis, Rice University, Houston, TX, 1979.

66. Zobell, C.E., "The Effect of Solid Surfaces Upon Bacterial Activity," Jounal of Bacteriology, Vol. 46, 1943, pp. 39-56.

APPENDICES

APPENDIX A

NOTATION

A	Reactor Surface Area	(L^2)
AR	Annular Reactor	
c	Time Smoothing Rate Constant	(t^{-1})
D_e	Effective Diffusion Coefficient of Glucose Within the Biofilm	(L^2t^{-1})
F	Volumetric Flowrate	(L^3t^{-1})
k	Growth-Associated Polymer Formation Rate Coefficient	$(M_pM_x^{-1})$
k'	Nongrowth-Associated Polymer Formation Rate Coefficient	$(M_pM_x^{-1}t^{-1})$
k_b	Biofilm Growth-Associated Polymer Formation Rate Coefficient	$(M_pM_x^{-1})$
k_b'	Biofilm Nongrowth-Associated Polymer Formation Rate Coefficient	$(M_pM_x^{-1}t^{-1})$
k_L	Mass Transfer Coefficient	(Lt^{-1})
k_s	Saturation Coefficient	(M_sL^{-3})
k_2	Atkinson Rate Coefficient	(L^{-1})
k_3	Atkinson Rate Coefficient	$(L^3M_s^{-1})$
N	Glucose Flux to the Biofilm Surface	$(M_sL^{-2}t^{-1})$
N_b	Glucose Flux into the Biofilm	$(M_sL^{-2}t^{-1})$
p	Polymer Carbon Concentration	(M_pL^{-3})

p_b	Biofilm Polymer Carbon Density	$(M_p L^{-3})$
p_i	Influent Polymer Carbon Concentration	$(M_p L^{-3})$
$\bar{p}$	Steady State Polymer Carbon Condentration	$(M_p L^{-3})$
p_b^*	Biofilm Polymer Carbon Areal Density	$(M_p L^{-2})$
R_g	Glucose Removal Rate	$(M_s L^{-2} t^{-1})$
R_p	Polymer Formation Rate	$(M_p L^{-3} t^{-1})$
r_g	Specific Glucose Removal Rate	$(M_s M_x^{-1} t^{-1})$
r_{gb}	Biofilm Specific Glucose Removal Rate	$(M_s M_x^{-1} t^{-1})$
r_p	Specific Polymer Formation Rate	$(M_p M_x^{-1} t^{-1})$
R_{dp}	Polymer Carbon Detachment Rate From the Biofilm	$(M_p L^{-2} t^{-1})$
R_{dx}	Cellular Carbon Detachment Rate From the Biofilm	$(M_x L^{-2} t^{-1})$
R_{pb}	Polymer Carbon Formation Rate in the Biofilm	$(M_p L^{-2} t^{-1})$
R_{xb}	Cellular Carbon Reproduction Rate in the Biofilm	$(M_x L^{-2} t^{-1})$
s	Glucose Carbon Concentration	$(M_s L^{-3})$
s_i	Influent Glucose Carbon Concentration	$(M_s L^{-3})$
s_s	Glucose Carbon Concentration at the Biofilm Surface	$(M_s L^{-3})$
$\bar{s}$	Steady State Glucose Carbon Concentration	$(M_s L^{-3})$
t	Time	(t)
Th	Biofilm Thickness	(L)
TOC_b	Biofilm Total Organic Carbon Concentation	$(M_c L^{-3})$
TOC_{soln}	Liquid Solution Total Organic Carbon Concentration	$(M_c L^{-3})$
V	Reactor Liquid Volume	(L^3)

x	Cellular Carbon Concentration	$(M_x L^{-3})$
x_b	Biofilm Cellular Carbon Density	$(M_x L^{-3})$
x_i	Influent Cellular Carbon Concentration	$(M_x L^{-3})$
$\bar{x}$	Steady State Cellular Carbon Concentration	$(M_x L^{-3})$
x_b^*	Biofilm Cellular Carbon Areal Density	$(M_x L^{-2})$
$Y_{p/s}$	Polymer Carbon Yield Coefficient	$(M_p M_s^{-1})$
$Y_{x/s}$	Cellular Carbon Yield Coefficient	$(M_x M_s^{-1})$
$Y_{pb/s}$	Biofilm Polymer Carbon Yield Coefficient	$(M_p M_s^{-1})$
$Y_{xb/s}$	Biofilm Cellular Carbon Yield Coefficient	$(M_x M_s^{-1})$
α	Cellular Glucose Distribution Coefficient	(dimensionless)
β	Inverse of Cellular Yield Coefficient, $Y_{x/s}^{-1}$	$(M_s M_x^{-1})$
η	Polymer Conversion Efficiency	$(M_p M_s^{-1})$
κ	Polymer Glucose Distribution Coefficient	(dimensionless)
λ	Effectiveness Factor	(dimensionless)
μ	Specific Cellular Growth Rate	(t^{-1})
μ_b	Biofilm Specific Cellular Growth Rate	(t^{-1})
μ_{max}	Maximum Cellular Specific Growth Rate	(t^{-1})
Φ	Thiele Modulus	(dimensionless)
ω	Inverse of Polymer Yield Coefficient, $Y_{p/s}^{-1}$	$(M_s M_p^{-1})$

APPENDIX B

AR MIXING STUDY

A mixing study was conducted in the annular reactors using leuco crystal violet dye. Each AR behaves as a continuously stirred tank reactor (CSTR) at 200 rpm as illustrated in Figure 29. The following equation applies for an ideal CSTR:

$$c/c_i = e^{-t/td}$$

where

c	= reactor dye concentration	(ML^{-3})
c_i	= initial dye concentration	(ML^{-3})
t	= time	(t)
t_d	= mean residence time	(t)

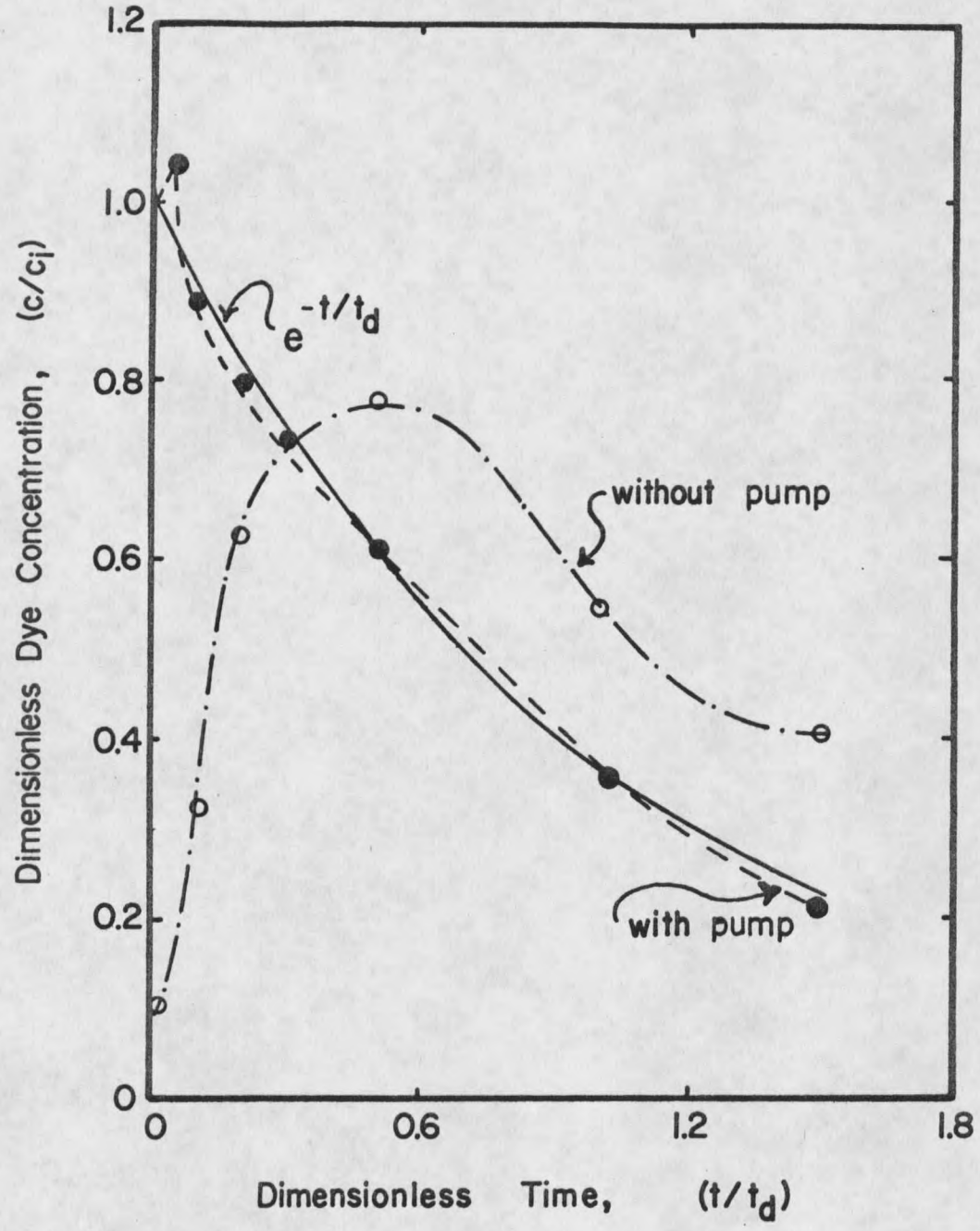

Figure 29. Annular Reactor Mixing Study. At t=0 Dye Was Injected Into the Reactor and the Decay Monitored.

APPENDIX C

AGAR PLATE RECIPES

Glucose-Micronutirent Agar (GMN)

80 mg glucose (200 mg/l final concentration)

micronutrients

6 gm agar

Dissolve glucose in distilled water and dilute to 100 cm^3. In a second container, dissolve micronutrients (see Table 6 for appropriate proportions) plus agar and dilute to 300 cm^3 using distilled water. Autoclave solutions separately. When finished combine solutions and pour into sterile plates.

Trypticase Soy-Yeast Extract Agar (TSY)

13.75 gm trypticase soy broth with dextrose

5.0 gm lactose

1.5 gm yeast extract

7.5 gm agar

Dissolve first three ingredients in 400 cm^3 distilled water. Add agar and dilute to 500 cm^3 total volume.

APPENDIX D

PROCEDURE MODIFICATIONS FOR SIGMA 510 GLUCOSE ANALYSIS

1. For glucose concentrations between 2.5 and 100 mg/l, make six standards - 2.5, 5.0, 10.0, 25.0, 50,0, and 100.0 mg/l glucose. Use 0.5 cm^3 standard and 0.5 cm^3 undiluted sample for analysis.
2. For glucose concentrations between 0.5 and 25 mg/l, make seven standards - 0.5, 1.0, 2.5, 5.0, 10.0, 15.0. and 25 mg/l glucose. Use 1.5 cm^3 standard and 1.5 cm^3 undiluted sample for analysis.
3. Prepare linear calibration curves from standards and determine sample concentrations.

APPENDIX E

API 20E IDENTIFICATION SYSTEM

Name - API 20E System for the Identification of *Enterobacteriaceae* and Other Gram Negative Bacteria

Company - Analylab Products
Division of Ayerst Laboratories, Inc.
200 Express Street
Planiveiw, NY 11803

Components - 23 standard biochemical tests, 3 complimentary test, analytical profile index (numerical data base)

Abbreviated Procedure - a) inoculate reagent strip
b) add reagents
c) incubate for 24 to 48 hours
d) read results and compare with numerical data base to determine identification

APPENDIX F

CHEMOSTAT EXPERIMENTAL DATA

D	= dilution rate	(h^{-1})
CHEM #	= chemostat reactor number	
cc	= cell count	(#/cm^3)
CD	= cell dimensions	(μm)
s_i	= influent glucose carbon concentration	(mg/l)
s	= glucose carbon concentration	(mg/l)
x	= cellular carbon concentration	(mg/l)
p	= polymer carbon concentration	(mg/l)

Chemostat Experiments

D	CHEM #	CC $x10^{-8}$	CD	s_i	s	x	p
0.025	1	0.840	1.48 x	36.3	0.1	4.0	4.5
	2	1.20	0.59	37.0	0.1	5.7	11.0
0.050	1	1.95	1.57 x	33.4	0.2	10.2	7.3
	2	1.38	0.60	30.2	0.2	7.2	7.0
0.075	1	1.60	1.66 x	38.3	0.6	8.8	7.3
	2	1.52	0.60	38.3	1.0	8.4	5.2
0.10	1	1.58	1.75 x	36.4	0.4	9.5	6.7
	2	1.61	0.61	42.2	0.4	9.7	7.1
0.15	1	1.83	1.93 x	39.9	0.3	12.1	6.2
	2	1.46	0.61	38.2	0.3	9.7	5.7
0.25	1	0.936	2.29 x	36.0	6.9	7.9	3.1
	2	0.900	0.63	37.5	8.1	7.6	2.8
0.35	1	0.192	2.65 x	36.8	28.0	1.9	2.6
	2	0.207	0.64	35.3	29.1	2.1	5.1
0.40	1	0.096	2.83 x	37.4	33.0	1.1	0.1
	2	0.063	0.65	35.6	33.4	0.7	0.0

APPENDIX G

ANNULAR REACTOR EXPERIMENTAL DATA

t	= time	(h)
R #	= reactor number	
LPCC	= liquid phase cell count	(#/cm^3)
CD	= cell dimensions	(μm)
s	= glucose carbon concentration	(mg/l)
x	= cellular carbon concentration	(mg/l)
p	= polymer carbon concentration	(mg/l)
BCC	= biofilm cell count	(#/cm^2)
x_b^*	= biofilm cellular carbon areal density	(mg/m^2)
p_b^*	= biofilm polymer carbon areal density	(mg/m^2)
Th	= biofilm thickness (reported as mean ± standard deviation)	(μm)

AR Experiment 1

Liquid Phase Data

t	LPCC $x10^{-6}$	CD	s	x	p
48	0.356	1.64 x 0.53	0.4	0.02	-
75	1.07	1.64 x 0.53	1.6	0.05	-
100	6.80	1.64 x 0.53	1.1	0.29	-
125	2.11	1.64 x 0.53	0.2	0.09	-
150	2.39	1.64 x 0.53	0.4	0.10	-

Biofilm Data

t	BCC $x10^{-7}$	CD	x_b^*	p_b^*	Th
48	0.066	1.54 x 0.54	0.3	8.8	-
100	2.39	1.54 x 0.54	9.9	32.6	15.1 ± 5.8
150	12.9	1.54 x 0.54	53.4	161.8	51.1 ± 11.6

AR Experiment 2

Liquid Phase Data

t	LPCC $x10^{-7}$	CD	s	x	p
38	1.10	1.61 x 0.59	1.5	0.6	0.8
62	1.51	1.61 x 0.59	1.0	0.8	0.7
86	1.37	1.61 x 0.59	0.3	0.7	2.3
109	0.987	1.61 x 0.59	0.4	0.5	1.7
134	2.98	1.61 x 0.59	0.2	1.5	3.6
165	2.19	1.61 x 0.59	0.4	1.1	1.2

Biofilm Data

t	BCC $x10^{-7}$	CD	x_b^*	p_b^*	Th
38	0.581	1.54 x 0.53	2.3	76.3	-
86	2.39	1.54 x 0.53	9.6	80.9	24.3 ± 7.9
134	15.6	1.54 x 0.53	62.4	91.4	35.7 ± 7.9
165	38.2	1.54 x 0.53	152.9	139.8	27.4 ± 5.8

AR Experiment 3

Liquid Phase Data

t	LPCC $x10^{-6}$	CD	s	x	p
36	1.40	1.60 x 0.52	3.5	0.1	0.9
60	14.0	1.60 x 0.52	1.0	0.6	1.4
84	7.70	1.60 x 0.52	0.5	0.3	0.5
108	14.0	1.60 x 0.52	0.5	0.6	1.1
132	2.90	1.60 x 0.52	0.4	0.1	0.7

Biofilm Data

t	BCC $x10^{-7}$	CD	x_b^*	p_b^*	Th
36	0.430	1.75 x 0.50	1.4	12.3	-
84	2.00	1.75 x 0.50	8.1	105.8	18.3 ± 1.1
132	2.30	1.75 x 0.50	9.3	146.2	17.2 ± 1.8

AR Experiment 4

Liquid Phase Data

t	R#	LPCC $x10^{-7}$	CD	s	x	p
43	1	1.29	2.00 x 0.75	8.0	1.3	0.0
43	2	1.31	2.00 x 0.75	8.1	1.4	-1.6
55	1	7.49	2.00 x 0.70	3.4	7.0	-0.7
55	2	9.21	2.00 x 0.75	3.6	8.8	-1.6
68	1	7.65	2.00 x 0.70	3.4	7.1	-
68	2	8.20	1.75 x 0.70	2.7	7.2	-1.4
94	1	5.44	1.63 x 0.75	2.5	4.5	0.7
94	2	3.26	1.63 x 0.75	-	2.7	-
125	1	7.51	1.75 x 0.70	1.6	5.8	-
125	2	5.76	1.75 x 0.70	1.8	4.6	0.3
175	1	3.86	1.75 x 0.70	1.8	3.0	-0.6

Biofilm Data

t	R	BCC $x10^{-8}$	CD	x_b^*	p_b^*	Th
43	1	3.38	2.00 x 0.75	351.8	28.0	7.3 ± 6.7
	2	3.41	2.00 x 0.75	354.8	-32.9	11.4 ± 10.3
55	1	3.47	1.75 x 0.70	294.1	35.9	12.7 ± 8.9
68	2	5.37	1.75 x 0.70	379.2	91.0	25.3 ± 3.4
79	1	5.71	1.88 x 0.75	336.0	24.8	32.2 ± 4.7
125	2	9.62	1.60 x 0.60	453.3	471.7	29.8 ± 3.1
175	1	19.2	1.50 x 0.50	723.1	499.3	36.0 ± 13.1

AR Experiment 5

Liquid Phase Data

t	LPCC $x10^{-6}$	CD	s	x	p
34	0.250	2.00 x 0.75	16.0	0.03	2.8
47	1.59	2.00 x 0.75	14.0	0.16	-0.1
54	4.10	2.00 x 0.75	9.4	0.42	-0.6

Biofilm Data

t	BCC $x10^{-7}$	CD	x_b^*	p_b^*	Th
34	0.069	1.75 x 0.75	0.7	4.3	-
47	4.32	2.00 x 0.75	44.0	10.3	0.4
54	41.8	2.00 x 0.75	426.1	-103.2	1.6

AR Experiment 6

Liquid Phase Data

t	R#	LPCC $\times 10^{-7}$	CD	s	x	p
40	1	0.220	2.00 x 0.75	5.7	0.2	0.1
40	2	0.232	2.00 x 0.75	6.4	0.2	-0.7
51	1	2.06	1.75 x 0.70	1.8	1.6	0.6
51	2	2.47	2.00 x 0.75	2.1	2.2	0.5
65	1	2.92	1.75 x 0.70	1.4	1.9	1.1
65	2	3.62	1.75 x 0.70	1.3	2.3	0.7
88	1	2.25	1.50 x 0.60	1.1	1.3	1.0
88	2	2.57	1.75 x 0.60	1.2	1.5	-
110	1	3.55	1.63 x 0.65	1.7	2.7	-
110	2	2.84	1.63 x 0.65	1.4	1.9	7.1
139	1	3.40	1.50 x 0.60	1.7	2.6	1.7

Biofilm Data

t	R#	BCC $\times 10^{-8}$	CD	x_b^*	p_b^*	Th
40	2	0.180	2.00 x 0.75	18.7	6.7	1.5 ± 0.5
51	1	3.08	1.75 x 0.70	244.0	12.2	4.8 ± 1.4
65	2	4.07	1.63 x 0.65	259.2	110.6	16.9 ± 3.1
88	1	6.17	1.60 x 0.60	328.3	189.9	24.6 ± 3.0
110	2	6.45	1.55 x 0.60	332.5	259.5	22.8 ± 2.2
139	1	7.65	1.50 x 0.50	265.6	443.3	18.3 ± 4.4

AR Experiment 7

Liquid Phase Data

t	LPCC $x10^{-7}$	CD	s	x	p
43	0.310	1.75 x 0.62	2.6	0.2	-0.5
88	1.70	1.75 x 0.67	0.7	1.1	0.3
131	1.50	1.75 x 0.62	0.5	0.9	-0.1

Biofilm Data

t	BCC $x10^{-7}$	CD	x_b^*	p_b^*	Th
43	0.710	1.57 x 0.57	3.3	7.7	0.2
88	10.0	1.57 x 0.57	47.1	89.2	15.8 ± 3.4
131	14.0	1.57 x 0.57	67.3	218.1	19.4 ± 1.5

AR Experiment 8

Rotational Speed (rpm)	s
200	0.48
100	0.60
150	0.56
200	0.48
125	0.64
175	0.48
225	0.52

APPENDIX H

CONSTANTS FOR LOGISTICS EQUATION

EXP	Biofilm Cellular Carbon			Biofilm Polymer Carbon			Biofilm Thickness		
	c	$x^*_{b_o}$	$x^*_{b_m}$	c	$p^*_{b_o}$	$p^*_{b_m}$	c	Th_o	Th_m
1	0.059	1.0	53.4	0.03	8.77	800.0	0.042	1.5	100.0
2 & 7	0.05	2.8	140.0	0.08	3.9	149.8	0.247	0.10	24.5
4 & 5	0.202	7.0	588.2	0.12	0.2	485.5	0.186	0.35	32.7
6	0.30	18.7	308.8	0.087	6.7	375.0	0.16	1.5	21.9

EXP	Glucose Removal			Liquid Phase Cellular Carbon			Liquid Phase Polymer Carbon		
	c	$(s_i-s)_o$	$(s_i-s)_m$	c	x_o	x_m	c	p_o	p_m
1	0.048	0.2	1.6	0.07	0.015	0.16	0.059	1.0	53.4
2 & 7	0.115	0.5	3.5	0.162	0.02	0.86	0.077	0.083	1.5
4 & 5	0.157	1.4	15.7	0.22	0.03	4.12	0.045	0.01	0.13
6	0.316	3.6	8.2	0.34	0.2	2.1	see below[a]		

[a] $p = kt^m$ $k = 0.203$ $m = 0.45$

APPENDIX I

CELLULAR AND POLYMER YIELD CONFIDENCE INTERVAL CALCULATIONS

Confidence intervals for cellular and polymer yield coefficients were calculated using the following formula:

$$CI_q = q\left(\left(\frac{CI_a}{a}\right)^2 + \left(\frac{CI_b}{b}\right)^2\right)^{1/2}$$

where

CI_q = confidence interval

$q = a/b$

$$CI_d = (e^2 + f^2)^{1/2}$$

where

$d = e-f$

APPENDIX J

DESCRIPTION OF SUBSTRATE DIFFUSION EXPERIMENT

A mature biofilm was developed at 200 rpm with an influent glucose carbon concentration of 3.7 mg/l. The rotational speed was changed at random to one of the test speeds (100, 125, 150, 175, 200, with 225 rpm tested last). Sixty minutes after changing the rotational speed glucose removal was determined. The rotational speed was then returned to 200 rpm for a 10 minute period to eliminate any biofilm which may have accumulated during the 60 minute test period. This procedure was repeated until each of the test speeds had been tested.